Design, Physico- Chemical Characterization and Bioactivity Studies of Hybrid Nanostructured Titanium Surfaces for Enhanced Osseointegration

Dissertation presented to the

Department of Biochemistry and Molecular Biology

University of the Basque Country (UPV/EHU), Bilbao for the

degree of Doctor in Molecular Biology and Biomedicine

Presented by

Danijela Gregurec

Thesis Supervisor: Dr. Sergio E. Moya

University Tutor: Prof. Félix M. Goñi

eman ta zabal zazu

Universidad del País Vasco Euskal Herriko Unibertsitatea

Leioa, 2016

Acknowledgments

It is my pleasure to acknowledge the individuals who in one way or another had a significant role in past few years of my studies and motivated my development as a scientist.

Firstly, I would like to express my sincere appreciation to my supervisor, Dr. Sergio Enrique Moya, for all his support and understanding in research but in life too, for giving me freedom and encouraging me throughout my study and research.

I am thankful to Prof. Luis Liz-Marzán for all his support, but mostly for believing in me and giving me opportunity to realize my study in an exceptional situation.

Big thanks to present and former group members for spicing up stimulating and productive lab environment with music and laughter. Thanks to all of you for being motivating colleagues and good friends; Dr. Guocheng Wang, Dr. Nikolaos Politakos, Dr. Marija Kosutic, Dr. Richard Murray, Eleftheria Diamanti, Joseba Irigoyen Otamendi, María Echeverría Igartua, Ane Escobar Fernández, Elena Rojas Darceles, Angel Martinez and Tanja Luedtke.

The work presented in this thesis along with the other studies I was involved in trough past two and half years lead to expansion of my knowledge. For this I am grateful to my collaborators. First, I want to thank to Dr. Luis Yate and Dr. Fernando López-Gallego for enjoyable collaboration within CIC biomaGUNE that resulted in remarkable studies. Thanks to Dr. Omar Azzaroni and Dr. Waldemar Marmisollé as well to the rest of the Azzaroni group from INIFTA I had a pleasant and constructive stay in Argentina. I want to thank to Dr. Mihaela Delcea and Dr. Ricardo H. Pires from ZIK HIKE for productive stay in Germany. Thanks to Prof. Didier Astruc and Dr. Roberto Ciganda from University of Bordeaux for involving me into outstanding and rewarding research. I want to thank to Dr. Lars Dahne from Surflay for successful work in cooperative project.

My big thank you is devoted to people that created environment of a family during my stay in San Sebastian. Thanks to Katarzyna Brzezicka for all the care and for making me smile every day. Thanks to Marta Gallego Gonzalez to take care of me as mother would. Thanks to Dr. Sonia Serna for patient support.

Another big thank you is to Dr. Marco Marradi and Dr. Luca Salassa that made my stay more cheerful but moreover stimulated my scientific enthusiasm.

The work at CIC biomaGUNE was more pleasant with the kind help of the administration and patient assistance of David and Mikel from IT. I also wish to thank to all the platforms and CIC biomaGUNE personnel I closely worked with for all the help.

I acknowledge the University of the Basque Country for help in organization of my thesis defense, especially thanks to Prof. Miguel Trueba Conde.

I gratefully acknowledge the funding sources that made my PhD work possible. I was funded by the Spanish Ministry of Economy and partially by the Marie Curie Seventh Framework Programme.

Rijeci ne mogu izraziti moju zahvalu ljudima koji su bili, iako daleko, blizu mene podrskom i ljubavi ovih zadnjih godina.

Veliko hvala mojoj obitelji za svu ljubav i podrsku na mojem putu prema doktoru znanosti. Hvala mama, hvala tata, hvala braco i hvala baka.

Jos jedno veliko hvala Goranu na velikoj podrsci, strpljenju i razumjevanju tjekom mog istrazivackog rada.

Kristini, Mariji, Igoru, Petri, Lari i Luciji hvala na velikoj ljubavi i vjeri tijekom ovog iznmnog razdoblja u mom zivotu.

Universidad del País Vasco Euskal Herriko Unibertsitatea

NAZIOARTEKO BIKAINTASUN CAMPUSA
CAMPUS DE EXCELENCIA INTERNACIONAL

AUTHORISATION OF THE THESIS TUTOR

FOR ITS PRESENTATION

Prof. Félix M. Goñi in his capacity as Tutor of the Doctoral Thesis: *Design, physico-chemical characterization and bioactivity studies of hybrid nanostructured titanium surfaces for enhanced osseointegration* completed within the Doctoral Programme Biología Molecular y Biomedicina by the PhD student Ms.Danijela Gregurec, and supervised by Dr. Sergio E. Moya hereby authorises the presentation of the aforementioned Doctoral Thesis, given that it fulfils the conditions necessary for its viva.

In _____on ____of _____, _____

THE THESIS TUTOR

Félix M. Goñi

Signed: _____

AUTHORISATION OF THE DOCTORAL PROGRAMME'S ACADEMIC COMMISSION

The Academic Commission of the Doctoral Programme in Biología Molecular y Biomedicina during its meeting held on 25th of January, 2016, agreed to authorise the presentation of the Doctoral Thesis entitled: *Design, physico- chemical characterization and bioactivity studies of hybrid nanostructured titanium surfaces for enhanced osseointegration* supervised by Dr. Sergio E. Moya and presented by Ms. Danijela Gregurec and registered with the Department Bioquímica y Biología Molecular.

In _____on ____of _____, _____

THE COORDINATOR OF THE DOCTORAL PROGRAMME

Miguel Angel Trueba Conde

Signed: _____

eman ta zabal zazu

Universidad del País Vasco | Euskal Herriko Unibertsitatea

NAZIOARTEKO BIKAINTASUN CAMPUSA
CAMPUS DE EXCELENCIA INTERNACIONAL

DEPARTMENT AUTHORISATION

The Board of the Department Bioquímica y Biología Molecular during its meeting held on ___ of _____, _____ agreed to authorise the processing of the Doctoral Thesis entitled: *Design, physico- chemical characterization and bioactivity studies of hybrid nanostructured titanium surfaces for enhanced osseointegration* supervised by Dr. Sergio E. Moya and presented by Ms. Danijela Gregurec to this Department.

In_____, on ___of_____, _____

APPROVED BY THE DEPARTMENT DIRECTOR AND DEPARTMENT SECRETARY

José Luis Nieva Escandón

Signed: _____

Helena Ostolaza Etxabe

Signed.: _____

Universidad del País Vasco Euskal Herriko Unibertsitatea | NAZIOARTEKO BIKAINTASUN CAMPUSA CAMPUS DE EXCELENCIA INTERNACIONAL

PHD DEGREE CERTIFICATE
DOCTORAL THESIS VIVA CERTIFICATE

PhD STUDENT MS. **Danijela Gregurec**

TITLE OF THE THESIS: **Design, physico- chemical characterization and bioactivity studies of hybrid nanostructured titanium surfaces for enhanced**

After having witnessed the completion of the viva by the author and their response to any objections and/or suggestions made, the Panel appointed by the Postgraduate Commission of the University of the Basque Country to examine the Doctoral Thesis indicated above, meeting on the indicated date, agreed _____ to award the following grade:
unanimously or by majority vote

DISTINCTION / MERIT / PASS / FAIL

Viva language(s) (in the event of there being more than one language, please specify the percentage of the thesis defended in each):

Spanish _____

Basque _____

Others (specify which and the corresponding percentage) _____

In _____on _____of _____, _____

CHAIRPERSON, SECRETARY,

Signed: Signed:

Dr. _____ Dr: _____

MEMBER 1, MEMBER 2, MEMBER 3,

Signed: Signed: Signed:

Dr. _____Dr._____Dr._____

PHD STUDENT

Danijela Gregurec

Signed_____

List of figures

Introduction

Chapter 1 Materials and methods

Chapter 2 Nb-C nanocomposite coatings for enhanced hard tissue implants

Chapter 3 Biopolymer coatings for improved titanium implant surfaces

Chapter 4 Superior osseo- activity on TiO_2 via polymer brush- strontium coatings

Chapter 5 Refining the surface topography of titanium: A chemical approach

Tables

Equations

Abstract

This PhD thesis is focused on the development of hybrid titanium- based surfaces with improved bioactivity for bone forming cells. Four different approaches for the modification of titanium surface are presented in the thesis, with the potential to be applied to currently used implant surfaces, enhancing and establishing a bone ingrowth onto the implant surface.

Alongside the enhanced cell activity, some surfaces showed extended action on the mineralization ability of osteoblast cells, thus could lead to rapid bone tissue formation. The overall aim of this work is to contribute to the biomaterials scientific community with new approaches for the nanoscale engineering of titania that can lead to an enhanced osseointegration and help to overcome implant rejections and inflammations.

One of the key challenges in the engineering of orthopedic implants is to “bioactivate” their surface. Carbon films have attracted much attention in biomedical fields due to biocompatibility and low wearing capacity. However, they are bioinert and thus unsuitable for bioactive use in orthopedic implant substrates. We have employed non-reactive magnetron sputtering to produce amorphous carbon, a-C films and utilize biocompatible niobium (Nb) to alter the surface chemistry and nanotopography of the a-C films with the purpose of bioactivating carbon coated surfaces implants. The nanocomposite films (Nb-C) formed by the addition of Nb into the a-C films possess enhanced mechanical properties regarding nanohardness, Young´s modulus and super-elastic recovery.

It is of special interest that preosteoblasts cells cultured on the Nb-C films have enhanced adhesion and upregulated alkaline phosphatase (ALP) activity, compared to those cultured on the bare carbon and on TiO_2 films. This improvement is ascribed to the combined effects of the changes in surface chemistry and the refinement of the nanotopography caused by the addition of Nb.

Recently, interest has raised in the so called biological approach to enhance the performance of implants. We have also modified the surface of titania (TiO_2) with a self-assembled and chemically crosslinked biopolymer film. The biopolymer film is made from naturally occurring polymers, alginate and collagen. The biopolymer coated titania closely mimics the bone extracellular matrix regarding bio-morphology and mechanical properties.

The biopolymer coatings are prepared using the layer by layer technique and crosslinked by carbodiimide chemistry to obtain a stable and compact structure. Alginate- collagen coatings display fibrillar morphology with an apparent fiber diameter of ~50 nm and lengths ranging from a few hundred nanometers to ~3 μm, mimicking therefore, the extracellular matrix of the bone in fiber length and extent. Atomic force spectroscopy revealed a Young's modulus of a few kPa for the films, which matches the mechanical properties of naturally occurring collagen fibers. Osteoblast cells showed enhanced adhesion on the coated surface compared to the bare titania, and a superior biological activity in means of mineralization of the alginate-terminated coating that interfaces the cells in biological fluids.

Strontium, an essential element in bone remodeling cycle, has large perspectives for application in therapies for bone- related diseases and replacements. However, its use is limited since oral application with effective dose induces a toxic response and unwilled side effects. We have incorporated strontium onto the surface of titania through complexation with carboxylic groups from polyacrylic acid (PAA) polymer brushes, synthesized from the surface of the titania. This approach can help to overcome the drawbacks of strontium treatment, by restricting the presence of strontium at the site of implantation and consequently its bioaction to the cells in direct contact with the titanium surface.

We have for the first time to our knowledge, applied polymer brushes bound to titania with the scope of entrapping strontium for enhanced osseoactivity of biomaterials. The concentration of strontium can be varied through the grafting density of PAA to the titania surface. At higher grafting density brushes offer more carboxyl groups for Sr binding. Initial adhesion of osteoblast was superior on these structures compared to bare TiO_2. Moreover, these coatings showed ability to promote bone tissue mineralization in dependence of the strontium concentration. The synergistic effect of the polymer coating enhancing biocompatibility and the osseoactive strontium is confirmed with increased ALP and osteocalcin, the main components of the mineralized extracellular matrix (ECM).

Titanium osseointegration, the bone- implant binding process, largely depends on the texture of titanium. It is enhanced on surfaces containing nano and micro features, that mimic the texture of extracellular matrix. We have applied alkaline etching of titanium alloys to refine the surface texture of titanium producing defined micro and

nanotopographical cues. The resulting morphology depends on mainly time of process and concentration of NaOH. Using longer times and high concentration of NaOH we have been able of producing very rough and irregular topographic features. The reaction of titania with NaOH forms a layer of sodium titanate that we used to incorporate strontium with one of aims of overcoming toxic effects that may come from the alkaline compounds. Furthermore, we have explored the capacity of the surfaces to incorporate bioactive strontium in relation to their morphology. We found that slightly alkaline conditions are more favorable for ion exchange between Na^{+} and Sr^{2+}, resulting in higher amount of Sr^{2+} incorporated in the surface of the modified Ti alloys.

The surface morphology of alloys influences the final amount of Sr^{2+} in the surface; rougher surfaces have higher capacity for Sr^{2+} binding, as they can react more intensely with NaOH, providing more exposed surface area for ion exchange. A preliminary evaluation of bioactivity and biocompatibility with pre-osteoblast cell draws a parallel between morphology of implant substrates and enhanced biological performance as the cells showed a better adherence to the nanostructured surfaces.

Resumen

Esta tesis se centra en el desarrollo de superficies hibridas basadas en titanio con una bioactividad mejorada para aplicaciones en regeneración de tejido óseo. En este trabajo se incluyen cuatro enfoques diferentes para la modificación de las superficies de titanio con potencial para ser utilizadas como implantes, mejorando el crecimiento y la fijación del tejido óseo en la superficie del implante. Además de una mejora en la actividad celular, algunas de las superficies en este estudio mostraron capacidad de mineralización de las células de osteoblastos, con potencial para conducir a una rápida formación del tejido óseo.

Este trabajo tiene como objetivo general el contribuir a la comunidad científica en el área de biomateriales con el desarrollo de nuevos materiales funcionalizados en la nano-escala que podrían ser usados para mejorar la integración ósea y así, superar los posibles rechazos y/o inflamación generadas por los implantes.

Un aspecto clave en la ingeniería de implantes ortopédicos es la de “bioactivar” su superficie. El uso de capas finas de carbono ha atraído una atención considerable en los campos biomédicos debido a su biocompatibilidad y su baja tasa de desgaste. Sin embargo, las capas de carbono son bioinertes y por lo tanto su bioactividad es inapropiada para el uso en implantes ortopédicos. En esta tesis se utilizó la técnica de magnetrón sputtering no-reactivo para producir capas finas de carbono amorfo, a-C, incluyendo el elemento biocompatible niobio (Nb) para alterar la química y nanotopografia de las capas de a-C con el fin de bioactivar la superficie de implantes recubiertos con carbono. Las capas de nanocompuestos de carburo de niobio (Nb-C)

formadas a partir de la incorporación de Nb en las capas de a-C presentaron propiedades mecánicas mejoradas, tales como una relativa alta nanodureza, elevado módulo de Young y una inusual súper elasticidad.

Es especialmente destacable que las células de preosteoblastos cultivadas sobre capas de Nb-C presentaron una adhesión y una actividad de fosfatasa alcalina (ALP, por sus siglas en inglés) mejorada, comparada con las células cultivadas sobre superficies de carbono y TiO_2. Esta mejora se puede asociar a los efectos combinados de cambios en la química superficial y del refinamiento de la nano topografía generado por la incorporación del Nb.

En los últimos años ha crecido el interés por utilizar los así llamados enfoques biológicos para optimizar el desempeño de implantes. En esta tesis se modifico la superficie de la titania (TiO_2) con una multicapa auto-ensamblada de biopolímeros químicamente entrecruzados. La multicapa de biopolímero se fabricó en base a polímeros de origen natural; alginato y colágeno. Se observó que el titanio recubierto con la multicapa biopolímero reproduce de una forma muy cercana a la matriz extracelular del hueso en términos de bio-morfología y propiedades mecánicas. La multicapa se desarrollo mediante la técnica de capa-a-capa y se entrecruzó por medio de química de carbodiimidas para obtener una estructura estable y compacta.

Los recubrimientos de alginato y colágeno mostraron una morfología fibrilar con un diámetro aparente de las fibras de ~50 nm y longitudes que variaron desde unos cientos de nanómetros a unas ~3 μm, imitando por tanto la matriz extracelular del hueso en la longitud y alcance de las fibras. Los análisis de espectroscopia de fuerzas de la capa

revelaron un modulo de Young de unos pocos kPa, el cual concuerda con las propiedades mecánicas de las fibras de colágeno de origen natural.

Las células de osteoblastos mostraron una adhesión mejorada en la superficie polimérica comparada con la superficie de titania sin recubrir, y una actividad biológica superior en términos de la mineralización especialmente con alginato como última capa en la multicapa.

El estroncio, un elemento esencial en el ciclo de remodelación ósea, tiene grandes perspectivas en el desarrollo de terapias para enfermedades relacionadas con los huesos y con reemplazos ortopédicos. Sin embargo, su uso está limitado debido a que su aplicación efectiva mediante administración oral induce una respuesta tóxica y efectos secundarios indeseados. En esta tesis hemos incorporado también estroncio en titanio a través de cepillos poliméricos de acido poliacrílico (PAA), generados in situ a partir de la superficie de titanio. El estroncio forma un complejo con los grupos carboxilato del PAA y queda retenido en el cepillo. Este enfoque puede ayudar a superar los inconvenientes del tratamiento con estroncio, restringiendo su presencia solo a la superficie implantada y consecuentemente su acción a las células que se encuentren en contacto directo con la superficie del implante. Hemos utilizado por primera vez, a nuestro conocimiento, la modificación superficial de titanio con cepillos poliméricos con el fin de capturar estroncio y lograr una mejora en la osteoactividad del biomaterial.

La concentración del estroncio puede ser variada por medio de la densidad de las cadenas en el cepillo de PAA enlazadas a la superficie de titanio. Una mayor densidad de cadenas poliméricas en el cepillo ofrece más grupos carboxilos para acomplejar estroncio La

adhesión inicial de los osteoblastos fue mayor sobre estas estructuras poliméricas comparadas con la superficie de TiO_2 sin recubrir. Además, los cepillos mostraron capacidad para promover la mineralización del tejido óseo en función de la concentración de estroncio. El efecto sinérgico del recubrimiento polimérico aumentando la biomineralización y osteoactividad del estroncio se confirmó con un aumento de la ALP y la osteocalcina, los elementos principales de la matriz extracelular (ECM, por sus siglas en inglés) mineralizada.

La osteointegración en el titanio, el proceso de unión del implante al tejido óseo, depende en gran medida de la textura del titanio. La osteointegración se ve mejorada en superficies con características nano y micro, que simulen la textura de la matriz extracelular. En este trabajo también hemos realizado un decapado alcalino de aleaciones de titanio para refinar su textura superficial produciendo una topografía con detalles en escala micro y nano.

La morfología resultante depende principalmente del tiempo de proceso y la concentración de NaOH utilizado. Empleando tiempos largos y altas concentraciones de NaOH hemos sido capaces de producir superficies rugosas e irregulares. La reacción de titanio con el NaOH forma una capa de titanato de sodio que usamos para incorporar estroncio. El estroncio es un elemento bioactivo, así que exploramos la capacidad de las superficies para incorporar el estroncio en función de su morfología. Encontramos que las condiciones ligeramente alcalinas son más favorables para el intercambio de iones entre el Na^+ y Sr^{2+}, resultando en una incorporación más alta de Sr^{2+} en la superficie de las aleaciones modificadas de Ti. La morfología superficial de las aleaciones antes del decapado influenciaron el contenido final de Sr^{2+} en la superficie. Las superficies más

rugosas tienen una mayor capacidad para incorporar Sr^{2+}, debido a que pueden reaccionar más intensamente con el NaOH, de tal forma que más área queda expuesta para el intercambio de iones.

La evaluación preliminar de la bioactividad y biocompatibilidad con células de pre-osteblastos permite establecer un paralelo entre la morfología de los implantes y un mejor comportamiento biológico en cuanto las células de osteoblastos mostraron una mejor adherencia a las superficies nano estructuradas.

Introduction

Need for implants, state of the art

Bone tissue loss or failure resulting from bone diseases such as arthritis, osteoporosis and bone cancer as well as from physical injuries has become a major health problem, causing an ever-increasing demand for orthopedic implants with an improved activity. Approximately 1 million hip replacements and 250 000 knee replacements are carried out annually worldwide and this number is expected to double between 1999 and 2025.(1) In United States, it is estimated that hip replacements will reach 570 000 surgeries by year 2030, rising by a 174% while knee arthoplasties are expected to rise by a 673% with 3.48 million procedures by that year.(2) The most recent statistical data published by The Organisation for Economic Cooperation and Development (OECD) show an increase in the number of hip and knee replacements in European countries with an average increase of hip replacement by 35% between 2000 and 2013 per country and up to 90% of increase of knee replacement over 10 years.(3) Implant materials are expected to replace the bone and thus have a role to bind to living bone material without soft tissue between. A material is considered osseointegrated when there is an absence of relative motion between the implant and bone.(4) Insufficient osseointegration of implants can result in the premature failure and aseptic loosening of the implants. This limits the lifetime of the implant in the body, causing very often the replacement of the implant. Revision surgery is usually less successful than initial implantation surgery. This inevitably increases the financial burden to the patients and

decreases life expectancy and quality of life for people having hard tissue, bone and teeth diseases. According to data collected in six European countries, hip revision surgeries result in 6.5% implant revisions after five years of initial surgery and 12.9% after ten years of initial implantation.(5) On the other hand, the rate of knee replacement varies from 5.3% revision surgeries in France up to 17% in Portugal.(6) The revision surgery is being more difficult and has low success rate. Since the seventies, with the development of first oral implant surface with micro defined roughness that resulted with minimal trauma and optimal healing period of the bone (7), efforts are still nowadays being directed to improve the quality of the currently used implants.

Titanium biomaterials and osseointegration

A biomaterial is any natural or artificial construct, other than a drug, that is implemented into body for any period of time. The purpose of biomaterials is to act as support or to restore any tissue, organ or function of the body and thus improve the quality of life of individuals.(8) Due to their intended implementation in the body, high requirements are put on biomaterials biocompatibility and integration with minimal risk of infections and rejections. Biocompatibility is a primary requisite for a bio material. For biocompatibility is understood that the material should display no toxicity, non allergenicity and non inflammatory characteristics. Beside biocompatibility, biomaterials have to compile other physical, chemical and mechanical requirements, depending on their targeted implementation in the human body. For orthopaedic or dental implants, there are three major requirements for these materials to successfully

achieve osseointegration and simultaneous biofunctionality: biological, mechanical and morphological compatibility.

Metal based implants, such as stainless steel, are a common choice in orthopaedic implants as they provide stable structural support to the bone. Titanium (Ti) and its alloys (Ti-6Al-4V and Ti-6Al- 7Nb) are well-established orthopaedic and dental implant biomaterials. Titanium is shown to have a closer contact with the bone tissue compared to other metal substrates such as stainless steel and zirconium and it strongly displays a biomechanical compatibility with the bone material.(9, 10) Some of its numerous applications in tissue engineering and regenerative medicine are shown in **Figure 1.**

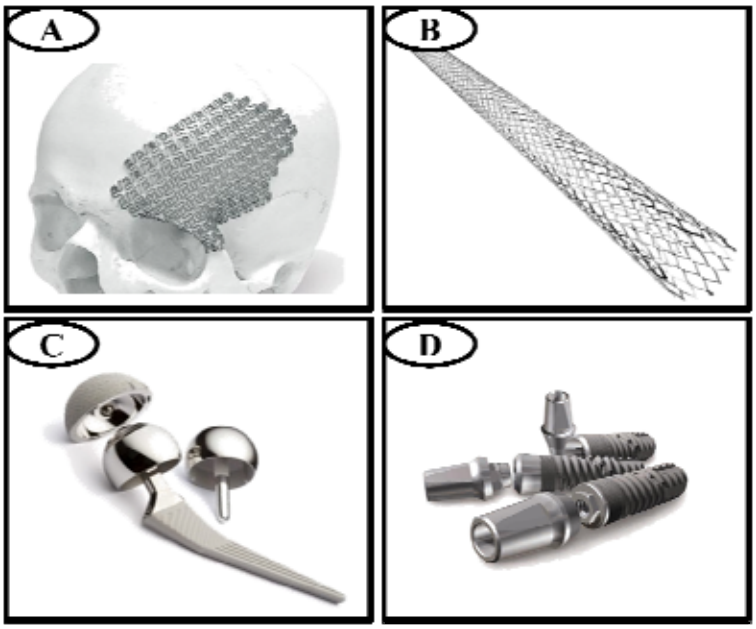

Figure 1. Examples of widely used titanium as implant material as **A** mesh plate for skull replacement, **B** vascular stent, **C** artificial hip joint and **D** screw for dental implant.

These applications include the preparation of vascular stents, dental implants or artificial joints mainly used in hip and knee implant, bone screws and plates in

orthopedic and dental applications as bone implant material. Their spread use is acknowledged to their good mechanical properties, biocompatibility and high corrosion resistance.(1, 11, 12) Biocompatibility and corrosion resistance of titanium mainly arise from the naturally formed protective oxide layer, TiO_2, called titania, which covers the whole titanium surface.(13)

Since the implant is expected to replace or support the bone, it has to imitate the biological environment and mechanical properties of the bone. The mechanical properties considered in the evaluation of the suitability of a biomaterial are elongation, hardness, tensile strength and Young's modulus (E). The Young's modulus, a measure of materials elasticity or stiffness, of the bone hard material lays in the range of tens of GPa.(14) Commercial titanium implant satisfies this requirement till large extent with E of one order of magnitude higher (100-120 GPa).(15)

Even if it particularly satisfies requirements given to implant material, drawback of titanium materials is in displaying poor osseointegration. The failure of titanium to osseointegrate with bone may come from the corrosion if the protective oxide layer includes deformations. Deformations can cause solubility in a host biological environment where metal cations can dissolve and form Lewis acid, thus lower the pH at implant surface. In such lowered pH, physiological chlorine may form HCl attacking bone and result in undesirable tissue response.(16) Bacterial infection and failure of the implant is increased at a low pH environment as this interface lacks a vascular blood supply resulting in immunogenic response. Bacteria growth is favored in acidic conditions, leading to a destructive tissue environment and finally aseptic loosening of the implant.(17)

For the last decade, various approaches have been attempted to provide titanium and its alloys with the ability to improve the bondingto living bone. Commonly used concepts will be addressed in the further text as well an overview on the strategies that endow titanium materials with the most suitable surface for bone cells adhesion and bonding.

Bone forming cells and interaction with their substrate

Bone in the human body is a very dynamic organ, being constantly remodeled in the cycle where osteoblast cells are responsible for formation of a new bone tissue while osteoclast cells are simultaneously resorbing old bone tissue. Osteoblasts, a bone forming cells are depositing a matrix including collagen, calcium and phosphate. Three components give to bone flexibility and rigidity. The matrix deposited by osteoblasts becomes a new layer of bone tissue on which new osteoblast cells adhere and continue with bone remodeling cycle.

Bone cells sense the underlying surface by their cytoskeletal projections such as filopodia and lamellipodia. Once a suitable site is detected, cells will attach to it resulting in the so called “focal adhesion”.

The process leading to the focal adhesion is mediated by an integral membrane protein called integrin, which binds to the actin cytoskeleton inside the cells and the adhesive recognition sequences (e.g. Arginylglycylaspartic acid, RGD) on the underlying substrate surface, as shown in the schematic representation in **Figure 2.**(18)

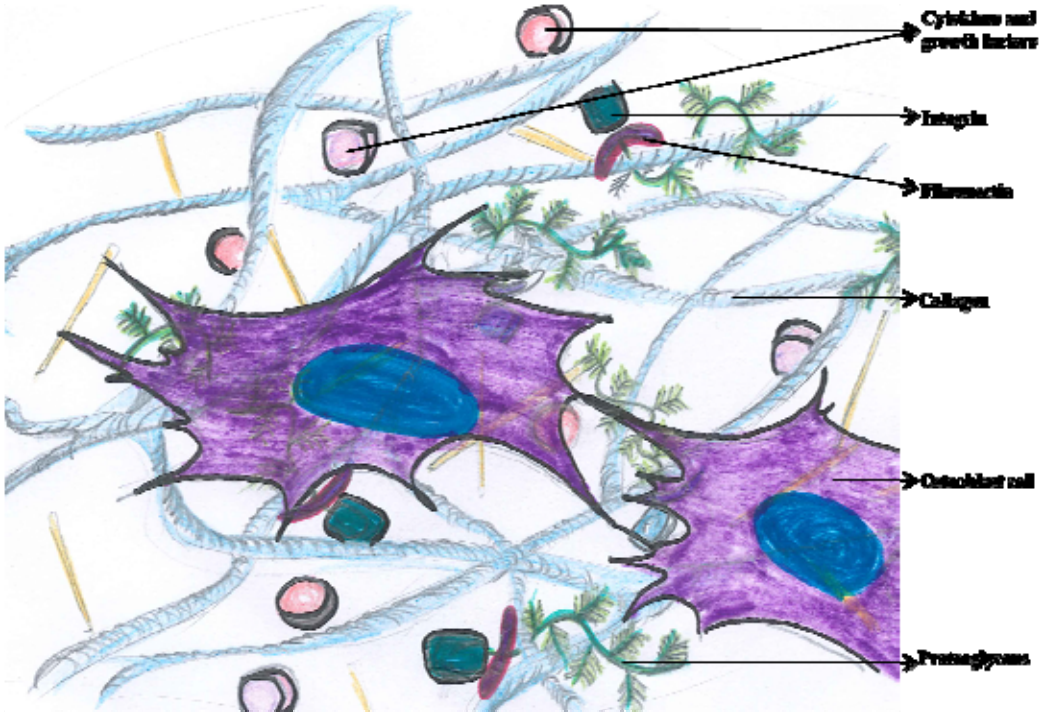

Figure 2. Schematic representation of bone extracellular matrix components. Cytokines and growth factors are signaling molecules for the cells; **Integrin**, receptors for cell-extracellular matrix interactions**; Fibronectin**, the glycoprotein that binds collagen; **Collagen**, the main structural protein of the ECM; **Osteoblasts**, cells that generatebone and **Proteoglycans,** glycosylated proteins that bind growth factors and cytokines.

Therefore, through focal adhesion cells are able to mediate the bidirectional signaling with underlying substrates. The signaling takes place through a mechanotransductive mechanism, leading to molecular cascades regulating transcription factor activity, gene and protein expression, and cell growth and differentiation.(19) Well documented mechanotransducers are stretch-mediated ion channels, primary cilia and integrins.(20-23) The mechano induced intracellular signals regulate cellular response that includes adhesion, proliferation, differentiation and cell spreading.

Surface aspects: nanotopography and bioenvironment

The surface characteristics of titanium regarding morphology, chemistry, bioactivity and mechanics plays a key role in the response of the bone forming cells as the surface of titanium provides the place of contact of the implant with the bone cells and will determine the fate of the cells.(24) In the natural bone environment, functionality and differentiation of osteoblast cells is a response of the mechanical and bio-morphological properties of the extracellular matrix, the substrate to which they are adhering onto. Therefore, the efforts to achieve advantageous bioactive implant surfaces are directed to generate architectures that closely mimic the environment of the natural bone.

The relatively hard hydroxyapatite bone core is covered by an extracellular matrix (ECM), shown schematically in **Figure 2**. This matrix has a hybrid hierarchical mesh structure built of protein fibers, e.g. collagen and elastin, providing a scaffold support abundant with topographical information for the cells. The bone's ECM consists of a large number of micro and nanotopographical features, where the collagen molecules are extending approximately to 300 nm in length and 1.5 nm in width. They can form collagen fibrils with diameters between 260 nm and 410 nm extending for tens of microns in length.(18) The size of the apatite crystals embedded in the collagen fibrils is at the nanoscale level. Crystals have dimensions of around 30- 50 nm in length and 20-25 nm in width.(25) In addition, a large number of nano and submicron pores are featured in the bone ECM structures providing topographical cues to the cells. Beside the chemical and topographical cues, the mechanical response of the matrix in terms of

its stiffness and elasticity has a significant influence for cell activity and function.(26) As cells adhere to a substrate, they closely interact with the ECM by mechanotransduction converting mechanical stimuli to biochemical signals.(27) The local stiffness of ECM that guides the cells is significantly lower than of underlying hard bone, in the range of few kPa.(28, 29) Therefore, ahigh Young's modulus of a biomaterials core will determine its long range implementation and while low E values at its surface will influence the activity of the cells adhering to the material previous to osseointegration.

The surface of the implanted material with its morphological and chemical features will provide the support for cell adhesion and subsequent tissue formation leading to the fixation of the implant to the bone or it will result in an immunogenic response causing the rejection of the implant and infections in the surrounding tissue.(24, 30, 31) Cell adhesion, migration and differentiation can be influenced by modulating the nanoscale topography of the implant substrate, i.e. introducing nano and micro features into the metallic or alloy substrate.(32) Alternatively, the so- called biological approaches can be applied, such as substrate coating with natural polymers. A biological coating becomes more attractive recently because it introduces a biochemical environment closer to the natural one as it will be discussed further in the text.

Strategies for osseointegration enhancement

There are numerous approaches for enhancing implant biocompatibility and long term osseointegration, based on the engineering and modification of the surface nanotopography, chemistry and biology. The use of topographical features at the

nanoscale to manipulate the cell functions to induce new bone formation has attracted great interest in the biomaterials field.

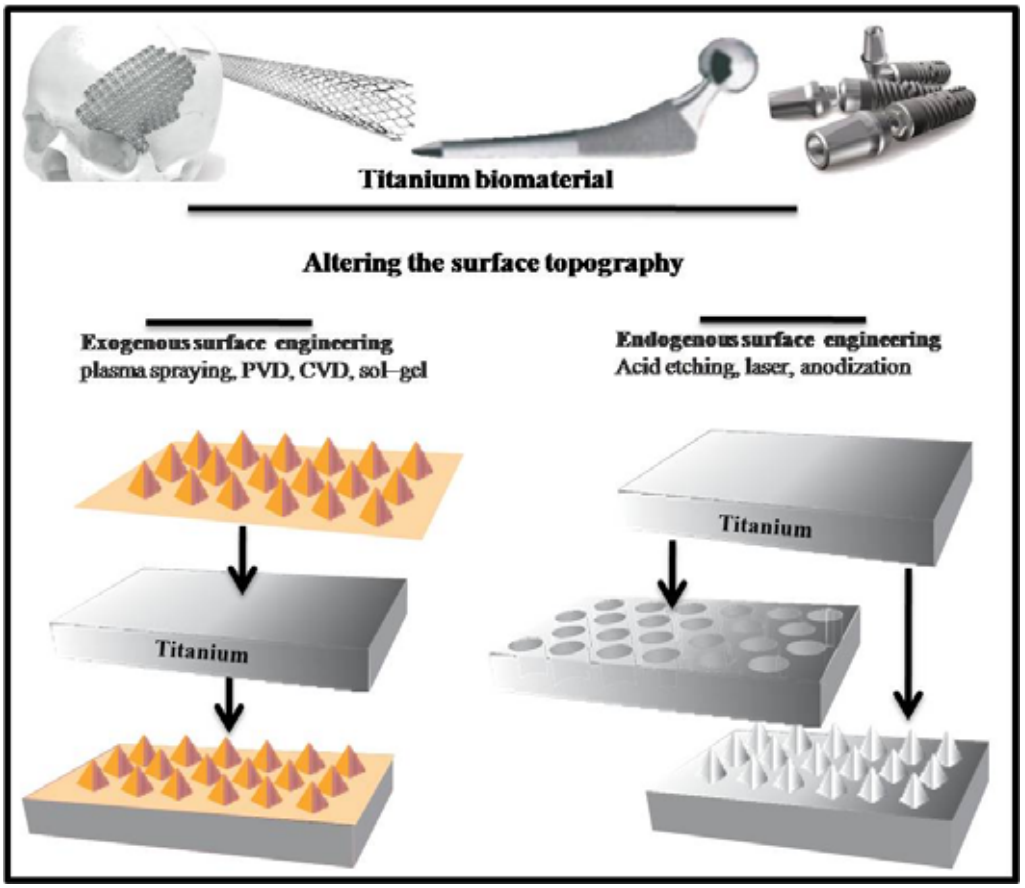

Figure 3. **Scheme of the exogenous and endogenous surface engineering** approaches for refining the surface nanotopography of the implants.

Techniques for surface engineering can be divided into two major categories; 1) "exogenous" where topography is derived from external materials; and 2) "endogenous" by which nanostructured topography is formed *in situ* on the implant surface, as sketched in **Figure 2**. Commonly used techniques to obtain controlled nano and micro

scale features at a surface of titanium are sand-blasting, acid and alkali etching, plasma spraying, electropolishing and anodic oxidation.(33-36)

The endogenous formations techniques can be commonly used to situ generate nanotopographical features without altering the original surface chemistry. However, the surface chemistry can be altered if the processes are specially designed or post-treatments are utilized.

Various nanotopographical features have been produced by these nanofabrication techniques and their effects on the activation of bone cells have been investigated. With use of chemical etching it is possible to produce submicron/nanoscale rough surfaces composed of nanopits, nanocaves and nanopores by controlling the process parameters such as temperature, time or concentration. (37-39) It is also reported that anodization can induce growth of TiO_2 nanotubes on the surface.(40)

The exogenous approaches can include alterations of surface chemistry simultaneously with topography. These are for example coatings with hydroxyapatite and calcium phosphate resulting in crystalline features thus approaching the bone chemical composition.(41, 42) Examples of topographical features obtained by plasma spraying are titania nanograins or Nb_5O_2 nanograins implemented into titania coating.(43, 44) The surfaces can be coated with nanoporous structures by a PEG modified sol-gel technique.(45) Most common approaches for exogenous surface modification are shown schematically in **Figure 4.**

A sub category of “exogenous” surface modification is the so-called biological approach, where the surface of the implant is coated with biological molecules as shown

in **Figure 4 C and D.** This strategy receives a lot of attention recently since it makes possible to mimic the topology of bone ECM as well as its biochemical characteristics.(46)

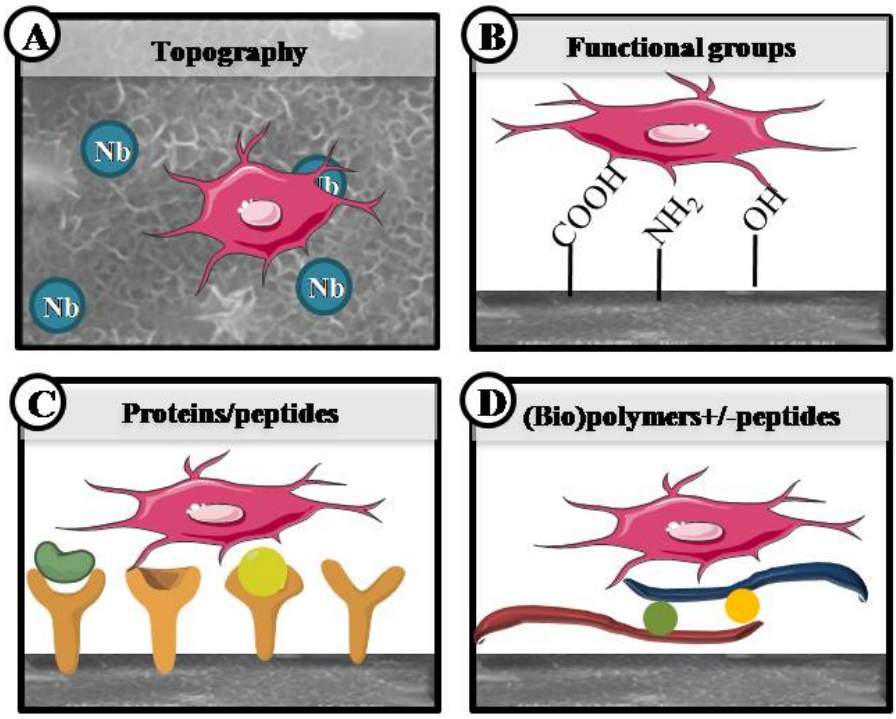

Figure 4: **Examples of exogenous surface modification approaches** for enhancement of osteoblast adhesion and differentiation on titanium. **A)** Surface roughness promoting cell differentiation. **B)** Surface modification with functional groups such as carboxyl or amino enhances protein adsorption and osteoblast differentiation. **C** and **D are biological approaches** where in **C** adsorption of proteins or peptides can be used for integrin mediated cell attachment and in **D** coating with (bio)polymers enables tuning of the surface chemistry and topography. Additionally, biomolecules can be embedded into the polymer coatings.

Coatings based on engineered proteins can be assorted to this category, for example the coating of surfaces with peptide sequences that are offering binding domains for cell binding.(47, 48)

The use of the polymeric coatings has become very popular due to the possibility of tuning elasticity, chemistry and surface cues (**Figure 4 D**). These can be natural or synthetic with each of them having advantages and disadvantages; Natural polymers are biocompatible and bioactive but they have a low mechanical strength and their stability is limited. On the other hand, synthetic polymers are easy to process but lack bioactivity. The bioactivity of synthetic polymers can be enhanced by inclusion of biomolecules.(49)

All the strategies have the common scope of producing structures resembling the bone environment as far as topography, mechanics and bio-chemistry are concerned, thus resulting in a highly bioactive and biocompatible surface for the implant that will interface biological fluids and bone cells in the body.

Coatings with bioactive incorporated elements

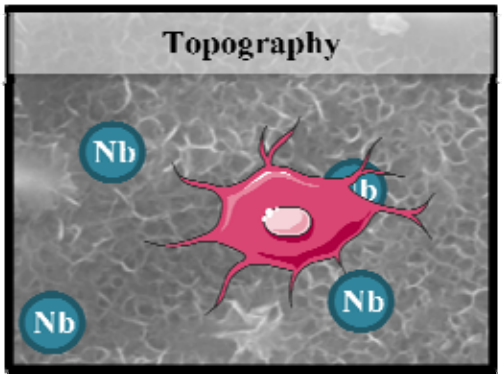

One of the key challenges in the engineering of the orthopaedic implants is the bioactivation of their surface. Beside commonly used titanium, other metals and alloys posses the characteristic required for implant surface, biocompatibility or mechanical strength and material elasticity. The modulation of chemistry and nanotopography on the materials surface may result in bioactive surfaces capable of leading to osseointegration keeping its beneficial mechanical properties beneath the layer of modified surface. Carbon is an example of a material that can be considered

biocompatible, it has good mechanical properties in the sense of a low wearing rate but at the same time it lacks bioactivity due to its inertness. One of the strategies to "bioactivate" the biomaterials surface is implementation of bioactive elements in its surface, simultaneously introducing topographical features mimicking nano and microtopography of the ECM. A "bioactivated" carbon coating on the surface of titanium may create the topographical features and additionally enhance bioactivity of titanium alloy. Importantly, the bioactivation of other material than titanium will help to improve understanding how the materials surface itself influences the initial osteoblasts cell adhesion and proliferation. Therefore, coating the titanium alloys with carbon films that are additionally doped with Nb may well enhance implant surface bioactivity while maintaining core mechanical properties of titanium. The addition of Nb in the carbon film also induces topographic alterations and reduces the corrosion of the underlying titanium substrate.(50) Using this approach, we are able to alter the surface chemistry by incorporating bioactive elements and simultaneously improve mechanical properties of the coating, especially improve resistance of the carbon coating.(32)

Chemical modifications of titanium surface

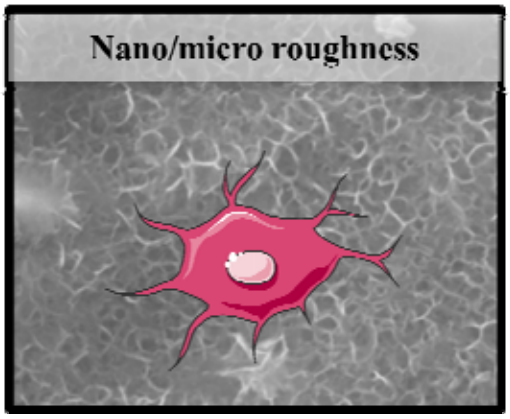

A possible approach to improve the surface topography of titanium is to mimic the bone extracellular matrix characteristics and nano and microscale features. Various micro-topographies have been produced by different methods such as sand-blasting,

machining and thermal spraying, with proven effects on the bone formation and fixation of the implant to the remnant bone.(51) Chemical methods that consider etching of surfaces are simple and cost-effective, showing attractive practicality.(52) However, traditional chemical methods involving applications of strong acids and strong bases inevitably raise safety and eco issues. Additionally, residual acids or bases on the surface are harmful for cells and tissue. It is therefore of great value to develop more applicable, safer and more eco-friendly alternative routes of nanofabrication.

Bio-inspired polymer coatings

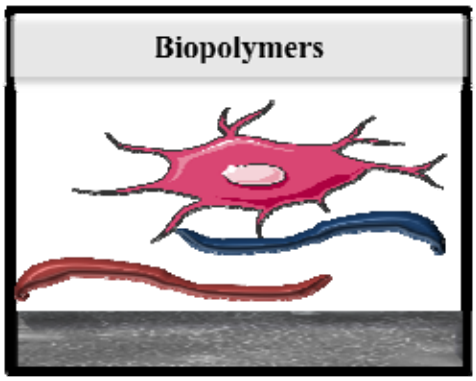

A biological coating based on naturally occurring polymers introduces a biochemical environment closer to the natural ones. In literature we can find several examples of biological coatings For example, it has been shown that a modified hyaluronan coating provides titania surfaces with enhanced release of growth factors for activation of bone regeneration.(53) Also, chitosan covalently bound to titanium alloy promotes cell proliferation and collagen fiber deposition.(54) Collagen and alginate are natural polymers and are approved by the U.S. Food and Drug Administration (FDA) for human use in many types of medical applications. In the last three decades, they are applied for wound dressings, artificial skin and tissue matrices due to their low inflammatory response and good biocompatibility.(55, 56) The two biopolymers are exceptional building blocks for the design of a biological inspired artificial ECM.

Collagen, a main structural protein of the connective tissue, in the form of elongated fibers found in a bone ECM, provides structural and mechanical support to the bone.(57) Alginate is a natural polysaccharide known for its excellent biocompability and for having a degradation rate, which depends on its molecular weight, and when incorporated in tissue scaffolds the degradation rate can be additionally tuned by choosing the proper methodology for scaffold fabrication.(58-60) The combination of these two polymers in a polyelectrolyte multilayer has already shown high stability and biocompatibility to endothelial cells after crosslinking with genipin, which also lead to the improved cell proliferation.(61)

Release of essential minerals implemented into the surface

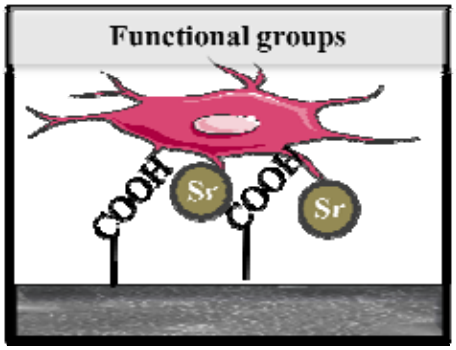

Strontium is one of the important essential trace elements in human body. Its deficiency can lead to poor bone mineralization. Strontium has a beneficial effect on the bone metabolism due to its anabolic and antiresorptive activity, therefore affecting bone formation and resorption.(62) It has been shown to be a promising therapeutic agent to heal bone disease. For example, strontium renalate (SrRan) has been used in clinics for long time to promote bone healing.(63) SrRan, used for osteoporosis contributed to the increase of mechanical fixation of the implants when taken orally. SrRan acts on both, desorption and formation of the bone.(64) However, since 2013 the use of SrRan is restricted due to a high risk of myocardial infarction. The therapeutic effects of strontium used in bone disease healing, as well its

contribution to implant fixation have been clearly proven. Because of the above mentioned properties. Strontium has been incorporated into surface- engineered biomaterials such as bioactive ceramics, for applications in bone tissue engineering, with encouraging results.(65)

There are few possibilities to dope the titanium surface with strontium; by ion exchange with Na ions from sodium titanate, by co sputtering of Sr and Ti and by complexing strontium into titanium surface. For strontium to promote osseointegration it is necessary that the ions are liberated into the biological fluid and then uptaken by the cells. Therefore, strontium has to be incorporated in titanium in a way that enables progressive release in the biological media and cell uptake.

Objectives and aims of the thesis

This PhD thesis is focused on the engineering of titanium surfaces through several approaches with the main goal to develop highly biocompatible and stable titania surfaces with potential to overcome body implant rejections. More specifically, the objectives and aims of this thesis are:

Goal 1

- To explore the ability of Nb-doped carbon films for improving the bioactivity of carbon film and be used for titanium coatings. Carbon is an element with a perspective in tissue engineering due to its biocompatibility and good mechanical properties but as well characterized with bioinetrness. The incorporation of Nb in carbon is meant to alter bioactivity but also topography of carbon film. We hypothesized that Nb-C has improved bioactivity in comparison to bare carbon films and this effect will be investigated by evaluation of two samples with pre osteoblast cell line. Bare titania surface will be used as a control due to its well known bioactivity.

- To resume, the aim of this study is to overcome inert nature of carbon by doping it with bioactive niobium. Final goal is to explore potential of carbon coatings as additional enhancing component of titanium implants.

Goal 2

- To develop a stable biomimetic coating using natural biopolymers. Collagen and alginate will be assembled using layer by layer approach in a compact and covalently crosslinked biopolymer film. Osteoblasts cell activity will be evaluated on two kinds of films, one that is terminated with alginate and other with collagen in order to choose the superior version of this biopolymer coating.

- The collagen/alginate multilayer will be assembled on the titania surface with the aim of forming a fibrilar structure to mimic the natural bone ECM. This structure should provide mechanical properties, topography and the appropriate bio- morphology for cells adherence, leading to improved tissue osseointegration.

Goal 3

- To functionalize titania surface with strontium to enhance bone tissue mineralization. Polymer brushes of polyacrylic acid will be grown on titania, generating a polymer monolayer on the surface of titania with multiple carboxylic groups that have the capability to entrap divalent strontium ions. Following this approach the presence of strontium will be limited to the implant site and its concentration can be controlled.

- The aim is to entrap strontium in titania surfaces and enable its release into the biological media to be uptaken by the osteoblast cells under controlled concentration. This approach should introduce an interface between cells and

titanium that improves differentiation and functionality of osteoblasts in the mineralization stage of the bone remodelling cycle.

Goal 4

- To modify the surface of titanium alloys by applying chemical etching with NaOH. The optimization of the etching parameters: pH, temperature and NaOH concentration will determine the nano and micro topographical features that are closely related to those of natural ECM. Post modification with a strontium solution influence the removal of toxic residuals after the etching and leads to the fabrication of safe and biocompatible implant surface besides doping the alloy with strontium.
- The aim of this work is to confer the capacity of the nano and micro roughened titanium to promote osteoblast activity in comparison to smooth titanium implant surfaces. These altered substrates having larger specific surface will offer high ability for exchange with strontium resulting in perspective implant surfaces with antiresorptive activity.

This thesis is organized into five chapters:

- **Chapter 1: In this chapter** Materials and methods used for conducting this thesis will be detailed.

- **Chapter 2: This chapter deals with the incorporation of Niobium in carbon films.** Niobium (Nb) is incorporated into pure carbon film by non-reactive magnetron sputtering to enhance the bioactivity to the carbon film and improve its mechanical properties and corrosion resistance. It will be shown that the introduction of Nb can also refine the nanotopography of the carbon films inducing topographic alterations. It will also be shown that Nb-C films show better mechanical properties in terms of nanohardness, Young's modulus and superelasticity. At the end of this chapter it will be discussed how a maximised enhancement of the osseointegration is obtained through the synergistic effects of surface topography and surface chemistry, demonstrated by in vitro trial using osteoblasts cell line.

- **Chapter 3: The so called biological approach to the osseointegration enhancement will be presented in this chapter**, based on the assembly of the collagen/alginate films on the titania surface. It will be presented the strategy to obtain the physiologically stable bio- inorganic interface that mimics the ECM in three dimensions; topography, mechanics and bio-morphology. This architecture is achieved on the aminosilanised titania using thelayer by layer technique for assembly combined with carbodiimide chemistry. Stability and morphology characterization of the biopolymer coated titania surfaces revealed highly stable coatings with mechanical properties comparable to the naturally occurring collagen in the bone matrix. *in vitro* experiments will be discussed where it will be shown how this approach results in a superior bioactivity compared to the bioactivity of bare titania surfaces. Furthermore, it will be

discussed how alginate terminated biofilms additionally enhance cellular adhesion due to its polysaccharide nature.

- **Chapter 4: Strontium release from titania in biological fluids and influence on osteoblast activity will be presented in this chapter**. Polymer brushes of polyacrilic acid (PAA) bearing carboxylic acid groups are grown from the titania surface. Strontium is retained in the brushes by complexation with carboxylate groups. Two different densities of polyacrylic acid (PAA) are prepared by means of radical polymerization on the aminosilanised titania. Polymerization chemistry and strontium incorporation is followed by XPS and correlated to amount (%) of Sr on the titania surface. Osteoblast cells are investigated in means of viability, adhesion and mineralization on these surfaces. It will be shown that a high activity of extracellular matrix maturation trough enhanced mineralization markers, osteocalcin and alkaline phosphatase is achieved compared to bare titanium. Denser brushes with higher Sr retention show superior bioactivity.

- **Chapter 5: This chapter will focus on surface etching to tune the surface topography of titanium alloys.** It will be presented how surface etching with sodium hydroxide by varying pH, temperature and time of process can be used to alter titanium topography and design shape and extent of topographical cues. Morphology will be characterized in detail by means of scanning electron microscope (SEM). Surface chemistry will be further changed by incorporation of strontium and the total amount of incorporated strontium will be determined by using energy-dispersive X-ray spectroscopy (EDX) and X-ray photoelectron

spectroscopy (XPS) to evaluate the potential of the nanostuctured surface for divalent ion incorporation. The impact of NaOH concentrations, treatment time, temperature and post treatment on surface features and roughness of the surface will be discussed. Additionally it will be shown how surface morphology influences the final amount of strontium incorporated. Finally, preliminary data of bioactivity will be presented regarding viability of pre osteoblast cells.

List of references

1. Nasab MB, Hassan MR, & Sahari BBS (2010) Metallic Biomaterials of Knee and Hip - A Review. *Trends in Biomaterials and Artificial Organs* 24(2):69-82.

2. Kurtz S, Ong K, Lau E, Mowat F, & Halpern M (2007) Projections of Primary and Revision Hip and Knee Arthroplasty in the United States from 2005 to 2030. *The Journal of Bone & Joint Surgery* 89(4):780-785.

3. OECD (2015) *Health at a Glance 2015* (OECD Publishing, Paris).

4. Mavrogenis AF, Dimitriou R, Parvizi J, & Babis GC (2009) Biology of implant osseointegration. *Journal of Musculoskeletal and Neuronal Interactions* 9(2):61-67.

5. Labek G, Thaler M, Janda W, Agreiter M, & Stockl B (2011) Revision rates after total joint replacement: cumulative results from worldwide joint register datasets. *The Journal of Bone & Joint Surgery* 93-B:293-297.

6. Kurtz SM, *et al.* (2011) International survey of primary and revision total knee replacement. *International Orthopaedics* 35(12):1783-1789.

7. Branemark PI, *et al.* (1969) Intra-osseous anchorage of dental prostheses. I. Experimental studies. *Scandinavian Journal of Plastic and Reconstructive Surgery* 3(2):81-100.

8. American National Institute of Health. *http://www.nih.gov/*.

9. Albrektsson T, Hansson HA, & Ivarsson B (1985) Interface analysis of titanium and zirconium bone implants. *Biomaterials* 6(2):97-101.

10. Albrektsson T, Jansson T, & Lekholm U (1969) Osseointegrated dental implants. *Dental Clinics of North America* 30(1):151.

11. Geetha M, Singh AK, Asokamani R, & Gogia AK (2009) Ti based biomaterials, the ultimate choice for orthopaedic implants - A review. *Progress in Materials Science* 54(3):397-425.

12. Long M & Rack HJ (1998) Titanium alloys in total joint replacement - a materials science perspective. *Biomaterials* 19(18):1621-1639.

13. Kasemo B (1983) Biocompatibility of titanium implants: Surface science aspects. *Journal of Prosthetic Dentistry* 49(6):832-837.

14. Katz JL (1980) Anisotropy of Young's modulus of bone. *Nature* 283(5742):106-107.

15. Elias CN, Lima JHC, Valiev R, & Meyers MA (2008) Biomedical applications of titanium and its alloys. *JOM* 60(3):46-49.

16. Vijayaraghavan V, Sabane AV, & Tejas K (2012) Hypersensitivity to Titanium: A Less Explored Area of Research. *The Journal of the Indian Prosthodontic Society* 12(4):201-207.

17. Ratner BD, Hoffman AS, Schoen FJ, & Lemons JE (2004) *Biomaterials Science* (Elsevier, San Diego, CA, USA) pp 237-345.

18. Bettinger CJ, Langer R, & Borenstein JT (2009) Engineering substrate topography at the micro- and nanoscale to control cell function. *Angewandte Chemie (International ed. in English)* 48(30):5406-5415.

19. McNamara LE, *et al.* (2010) Nanotopographical Control of Stem Cell Differentiation. *Journal of Tissue Engineering* 2010:120623.

20. Martinac B (2004) Mechanosensitive ion channels: molecules of mechanotransduction. *Journal of Cell Science* 117(12):2449-2460.

21. Berbari NF, O'Connor AK, Haycraft CJ, & Yoder BK (2009) The Primary Cilium as a Complex Signaling Center. *Current Biology* 19(13):R526-R535.

22. Galbraith CG, Yamada KM, & Sheetz MP (2002) The relationship between force and focal complex development. *The Journal of Cell Biology* 159(4):695-705.

23. Riveline D, *et al.* (2001) Focal contacts as mechanosensors: externally applied local mechanical force induces growth of focal contacts by an mDia1-dependent and ROCK-independent mechanism. *The Journal of Cell Biology* 153(6):1175-1186.

24. Wang G, Moya S, Lu Z, Gregurec D, & Zreiqat H (2015) Enhancing orthopedic implant bioactivity: refining the nanotopography. *Nanomedicine* 10(8):1327-1341.

25. Palmer LC, Newcomb CJ, Kaltz SR, Spoerke ED, & Stupp SI (2008) Biomimetic Systems for Hydroxyapatite Mineralization Inspired By Bone and Enamel. *Chemical Reviews* 108(11):4754-4783.

26. DeSimone DW, Mecham RP, Choi Y, Holle A, & Engler A (2013) Engineered ECM Microenvironments and Their Regulation of Stem Cells. *Extracellular Matrix in Development,* Biology of Extracellular Matrix, (Springer Berlin Heidelberg), pp 133-160.

27. Bhatia SK, Mason B, Califano J, & Reinhart-King C (2011) Matrix Stiffness: A Regulator of Cellular Behavior and Tissue Formation. *Engineering Biomaterials for Regenerative Medicine*, (Springer New York), pp 19-37.

28. Zhu Y, Dong Z, Wejinya UC, Jin S, & Ye K (2011) Determination of mechanical properties of soft tissue scaffolds by atomic force microscopy nanoindentation. *Journal of Biomechanics* 44(13):2356-2361.

29. Lv H, *et al.* (2015) Mechanism of regulation of stem cell differentiation by matrix stiffness. *Stem Cell Research & Therapy* 6(1):103.

30. Li D, *et al.* (2012) Role of mechanical factors in fate decisions of stem cells. *Regenerative medicine* 6(2):229-240.

31. Watt FM & Huck WTS (2013) Role of the extracellular matrix in regulating stem cell fate. *Nat Rev Mol Cell Biol* 14(8):467-473.

32. Yate L, *et al.* (2015) Nb-C nanocomposite films with enhanced biocompatibility and mechanical properties for hard-tissue implant applications. *ACS Applied Materials & Interfaces*.

33. Gintaras J, Marija S, Ann W, & Tomas B (2007) Titanium Dental Implant Surface Micromorphology Optimization. *Journal of Oral Implantology* 33(4):177-185.

34. Kim HM, Kokubo T, Fujibayashi S, Nishiguchi S, & Nakamura T (2000) Bioactive macroporous titanium surface layer on titanium substrate. *Journal of Biomedical Materials Research* 52(3):553-557.

35. Vercaigne S, Wolke JG, Naert I, & Jansen JA (1998) Bone healing capacity of titanium plasma-sprayed and hydroxylapatite-coated oral implants. *Clinical Oral Implants Research* 9(4):261-271.

36. Harris LG, Meredith DO, Eschbach L, & Richards RG (2007) Staphylococcus aureus adhesion to standard micro-rough and electropolished implant materials. *Journal of Materials Science: Materials in Medicine* 18(6):1151-1156.

37. Mendonca G, Mendonca DB, Aragao FJ, & Cooper LF (2010) The combination of micron and nanotopography by H(2)SO(4)/H(2)O(2) treatment and its effects on osteoblast-specific gene expression of hMSCs. *Journal of Biomedical Materials Research* 94(1):169-179.

38. Ueno T, Tsukimura N, Yamada M, & Ogawa T (2011) Enhanced bone-integration capability of alkali- and heat-treated nanopolymorphic titanium in micro-to-nanoscale hierarchy. *Biomaterials* 32(30):7297-7308.

39. Oliveira DP, Palmieri A, Carinci F, & Bolfarini C (2014) Osteoblasts behavior on chemically treated commercially pure titanium surfaces. *Journal of biomedical Materials Research A* 102(6):1816-1822.

40. Minagar S, Berndt CC, Wang J, Ivanova E, & Wen C (2012) A review of the application of anodization for the fabrication of nanotubes on metal implant surfaces. *Acta Biomaterialia* 8(8):2875-2888.

41. Dalton JE & Cook SD (1995) In vivo mechanical and histological characteristics of HA-coated implants vary with coating vendor. *Journal of Biomedical Materials Research* 29(2):239-245.

42. Liu Y, Groot KD, & Hunziker EB (2004) Osteoinductive Implants: The *Mise-en-scène* for Drug-Bearing Biomimetic Coatings. *Annals of Biomedical Engineering* 32(3):398-406.

43. Liu X, *et al.* (2005) Plasma-treated nanostructured TiO2 surface supporting biomimetic growth of apatite. *Biomaterials* 26(31):6143-6150.

44. Zhao X, *et al.* (2013) Delicate Refinement of Surface Nanotopography by Adjusting TiO2 Coating Chemical Composition for Enhanced Interfacial Biocompatibility. *ACS Applied Materials & Interfaces* 5(16):8203-8209.

45. Sabataitytė J, Oja I, Lenzmann F, Volobujeva O, & Krunks M (2006) Characterization of nanoporous TiO2 films prepared by solâ€“gel method. *Comptes Rendus Chimie* 9(5-6):708-712.

46. Gregurec D, *et al.* (2016) Bio inspired titanium coatings: Self-assembly of collagen- alginate films for enhanced osseointegration *Journal of Materials Chemistry B*, DOI: 10.1039/C6TB00204H.

47. Kariolis MS, Kapur S, & Cochran JR (2013) Beyond antibodies: using biological principles to guide the development of next-generation protein therapeutics. *Current Opinion in Biotechnology* 24(6):1072-1077.

48. Yuasa K, *et al.* (2013) An artificial fusion protein between bone morphogenetic protein 2 and titanium-binding peptide is functional in vivo. *Journal of Biomedical Materials Research Part A* 102(4):1180-1186.

49. Agarwal R & J. GA (2015) Biomaterial strategies for engineering implants for enhanced osseointegration and bone repair. *Advanced Drug Delivery Reviews* doi:10.1016/j.addr.2015.03.013.

50. Dalstra M, Denes G, & Melsen B (2000) Titanium-niobium, a new finishing wire alloy. *Clinical Orthodontics and Research* 3(1):6-14.

51. Lu Z, Roohani-Esfahani S-I, Wang G, & Zreiqat H (2012) Bone biomimetic microenvironment induces osteogenic differentiation of adipose tissue-derived mesenchymal stem cells. *Nanomedicine: Nanotechnology, Biology and Medicine* 8(4):507-515.

52. Chrcanovic BR & Martins MD (2014) Study of the influence of acid etching treatments on the superficial characteristics of Ti. *Materials Research* 17:373-380.

53. Berts I, Ossipov D, Fragneto G, Frisk A, & Rennie AR (2014) Polymeric Smart Coating Strategy for Titanium Implants. *Advanced Engineering Materials* 16(11):1340-1350.

54. Lin H-Y & Chen J-H (2013) Osteoblast differentiation and phenotype expressions on chitosan-coated Ti-6Al-4V. *Carbohydrate Polymers* 97(2):618-626.

55. Cavallaro JF, Kemp PD, & Kraus KH (1994) Collagen fabrics as biomaterials. *Biotechnology and Bioengineering* 43(8):781-791.

56. Rowley JA, Madlambayan G, & Mooney DJ (1999) Alginate hydrogels as synthetic extracellular matrix materials. *Biomaterials* 20(1):45-53.

57. Muiznieks LD & Keeley FW (2013) Molecular assembly and mechanical properties of the extracellular matrix: A fibrous protein perspective. *Biochimica et Biophysica Acta (BBA) - Molecular Basis of Disease* 1832(7):866-875.

58. Park H, *et al.* (2008) 19 - Alginate hydrogels as matrices for tissue engineering. *Natural-Based Polymers for Biomedical Applications*, (Woodhead Publishing), pp 515-532.

59. Jinchen S & Huaping T (2013) Alginate-Based Biomaterials for Regenerative Medicine Applications. *Materials* 6:1285-1309.

60. Kong HJ, Kaigler D, Kim K, & Mooney DJ (2004) Controlling Rigidity and Degradation of Alginate Hydrogels via Molecular Weight Distribution. *Biomacromolecules* 5(5):1720-1727.

61. Chaubaroux C, *et al.* (Collagen-Based Fibrillar Multilayer Films Cross-Linked by a Natural Agent. *Biomacromolecules* 13(7):2128-2135.

62. Marie PJ, Ammann P, Boivin G, & Rey C (2001) Mechanisms of Action and Therapeutic Potential of Strontium in Bone. *Calcified Tissue International* 69(3):121-129.

63. Liu AL-J, Shen P-W, & Chen P-J (2013) Strontium ranelate in fracture healing and joint pain improvement in a rheumatoid arthritis patient. *Clinical Cases in Mineral and Bone Metabolism* 10(3):206-209.

64. Maimoun L, *et al.* (2010) Strontium ranelate improves implant osseointegration. *Bone* 46(5):1436-1441.

65. Wu C, Ramaswamy Y, Kwik D, & Zreiqat H (2007) The effect of strontium incorporation into CaSiO3 ceramics on their physical and biological properties. *Biomaterials* 28(21):3171-3181.

Chapter 1

Materials and methods

1.1. Materials

Titanium alloys discs, diameter 25 mm are purchased from Baoji Junhang Metal Material Co., Ltd, (Baoji-Titanium City, China).

Collagen from bovine Achilles tendon Type I, Alginic acid sodium salt, (3-Aminopropyl) triethoxysilane (APTES), N-3-Dimethylaminopropyl)-N´-ethylcarbodiimide hydrochloride (EDC), N-Hydroxysuccinimide (NHS), toluene, phosphate buffered saline in tablets (PBS), Sodium dodecadocyl sulphate (SDS), Triton-X100 and Strontium chloride hexahydrate ($SrCl_2x6H_2O$) were all purchased from Sigma Aldrich (Madrid, Spain).

Hydrochloric acid and hydrogen peroxide were obtained from Acros organic (Madrid, Spain).

FITC labelled collagen and Rhodamine B labeled alginate were purchased from Creative PEGWorks, (Chapel Hill, USA).

The Actin Cytosceleton and Focal adhesion staining kit, FAK100 containing TRITC-conjugated phalloidin, anti-Vinculin and 4',6-diamidino-2-phenylindole (DAPI) was purchased from Merck Milipore (Madrid, Spain)

Acrylic acid anhydrous (99%) with M_w=72.06, The charge transfer agent (CTA) for the RAFT polymerization was the Bis(carboxymethyl)trithiocarbonate,

M_w=226.29 (98%), initiator used 4,4-Azobis(4-cyanovaleric acid) (CVA), M_w=280.28 (≥98%) and *N*,*N*-Dimethylformamide (DMF), (anhydrous, 99.8%) were all purchased from Sigma Aldrich (Madrid, Spain).

All the buffers and solutions were filtered through the 0.2 µm filters (Fisher, Madrid, Spain) and degassed in bath sonicator prior to use. If stored, polymer solutions were kept at 4 °C in argon atmosphere. The Falcon polystyrene tissue culture plates were purchased from Fisher Scientific (Madrid, Spain).

Nanopure water used in preparation of all the dilutions and buffers was produced with a Diamond UV water purification system (Branstead International, IA, Iowa, USA).

1.2. Methods

The main techniques and methods used to construct this thesis are presented below while more specific methods are presented in the experimental approach of each chapter.

1.2.1. Magnetron Sputtering

Magnetron sputtering belongs to category of plasma coating processes. Scheme of magnetron sputtering is shown in **Figure 1.1** Sputtering is conducted in the ultra high vacuum chamber under inert gas, such as argon. In this process, sputtering material is emitted from the target due to bombardment of argon ions to the target of desired material. During the process, a high voltage is applied creating a glow discharge that accelerates the ions from the target to the surface that is plasma coated. Magnetic fields in this process are keeping plasma in front of the target that additionally intensifies bombardment of ions and creates highly dense plasma.

Metallic target materials are sputtered from the target applying direct current (d.c.),(1) while non conductive materials are sputtered using radio frequency (r.f) power. (2)

Reactive magnetron sputtering is a method when an additional gas is used for coatings. Example is titanium dioxide (TiO_2) that is sputtered from pure titanium (Ti) target under mixture of argon (Ar) and oxygen (O_2) gasses.

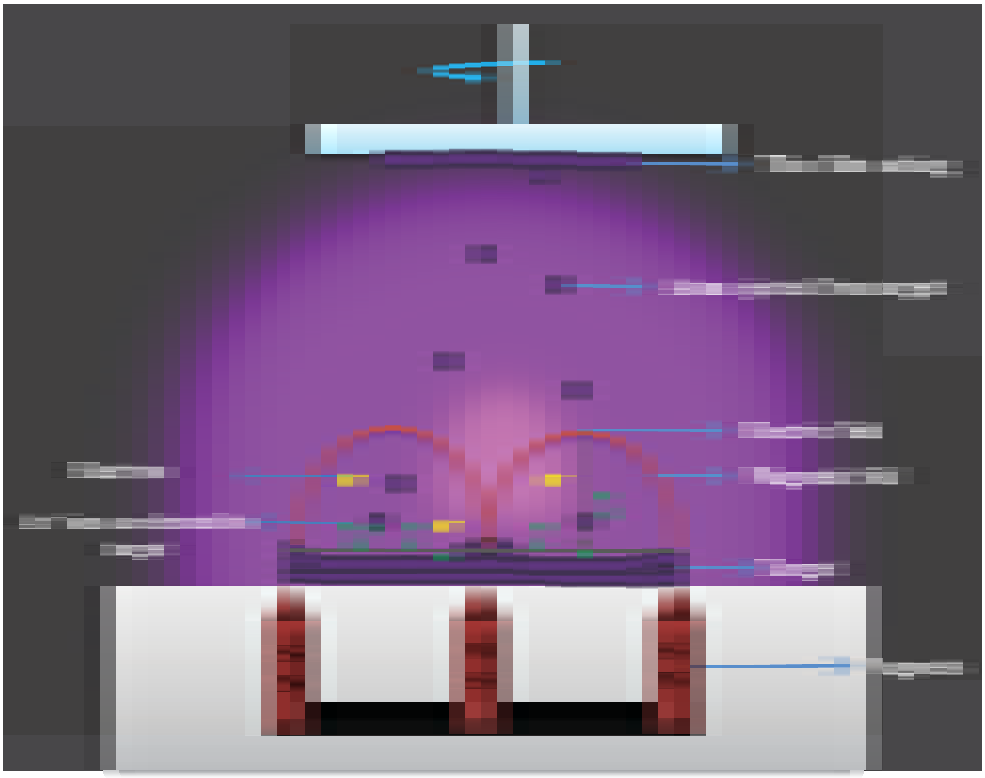

Figure 1.1. Schematic representation of magnetron sputtering in UHV chamber under argon atmosphere. Target material is bombarded with argon ions, atoms from target are ejected and due to applied voltage are accelerated to the surface that is coated with film.

Solid substrates used to construct this thesis are prepared by magnetron reactive sputtering in an ATC 1800 UHV sputtering system (AJA International Inc, MA). This sputtering system is equipped with DC and RF tilting magnetron sources for sputtering conducting and insulating materials. The substrate holder can be heated up to 800ºC and the ion energy in plasma can be controlled by means of a RF bias source to obtain high quality thin films, with high uniformity, dense and homogeneous structures for custom manufacturing and advanced applications. The system has three magnetron sputtering sources which combined with reactive sputtering allows the deposition of multiple thin

film layers (multilayers) and nanocomposite structures. Films can be sputtered over substrates up to 90 mm in diameter and from 1 nm to several microns thick.

Figure 1.2. Plasma from UHV chamber of ATC 1800 UHV sputtering system (AJA International Inc, MA) induced in three magnetrons ejecting ions from titanium (blue plasma), gold (orange plasma) and silicon (pink plasma) targets under 24 sccm of argon flow.

All the metal and oxide coatings used as substrates to construct this thesis are prepared by magnetron sputtering. Specific sputtering parameters for each of surfaces are presented in the experimental part of the each chapter. Thin films consisted of titania (TiO_2), titanium/titania (Ti/TiO_2), amorphous carbon (α-C) and niobium-carbon (Nb-C) are coated on underlying substrates of glass, silica, or gold (Au) quartz crystals.

Before the insertion of substrates in the magnetron, glass and silica substrates were cleaned 10 min in a mixture of H_2O:NH_4OH:H_2O_2 (1,5:1:1) volume ratio, followed by a rinse with nanopure water, and another 10 min in a mixture of H_2O:HCl:H_2O_2 (1,5:1:1 volume ratio) at ~50 °C. Au QCM crystals were cleaned in a mixture of H_2O:NH_4OH:H_2O_2 (1,5:1:1 volume ratio). Clean substrates were rinsed in nanopure water and dried under nitrogen. After the insertion into the load-lock transfer chamber with a

pressure of ~1 × 10^{-8} Pa, the substrates were sputter-cleaned with a negative bias of 180 V (25 W) under certain argon pressure and time as noted in the experimental part of each chapter. Film thicknesses were calculated based on the sputtering rate measured with a built-in Quartz Crystal Microbalance (QCM) sensor in the magnetron and verified by optical ellipsometry.

1.2.2. X-ray photoelectron spectroscopy (XPS)

X-ray photoelectron spectroscopy (XPS), called also ESCA, is a surface analysis technique. It is used to measure the elemental composition, empirical formula, chemical state and electronic state of the elements within a material. (3) XPS is preformed in ultra high vaccum and spectra are obtained by irradiating a solid surface with a beam of X-rays. The basic principle of XPS lays in photoelectric effect described by Einstein.(4) In XPS experiment, kinetic energy is measured from electrons that are emitted from the surface as schematically shown in the **Figure 1.3.** A soft X-ray irradiation is used to excite the core electrons. A bound electron adsorbs the photon, converting some of its energy into kinetic energy (KE). The electron leaves the atom and some of its energy is used to overcome the Coulomb attraction of the nucleus, reducing its KE by its initial state binding energy (BE). At the same time the outer orbitals readjust, lowering the energy of the final state that is being created and giving this additional energy to the outgoing electron. XPS is very surface sensitive technique as atoms emit photons from few top atomic layers. A photoelectron spectrum is recorded by counting ejected electrons over a range of electron kinetic energies. Peaks appear in the spectrum from atoms emitting electrons of a particular characteristic energy.

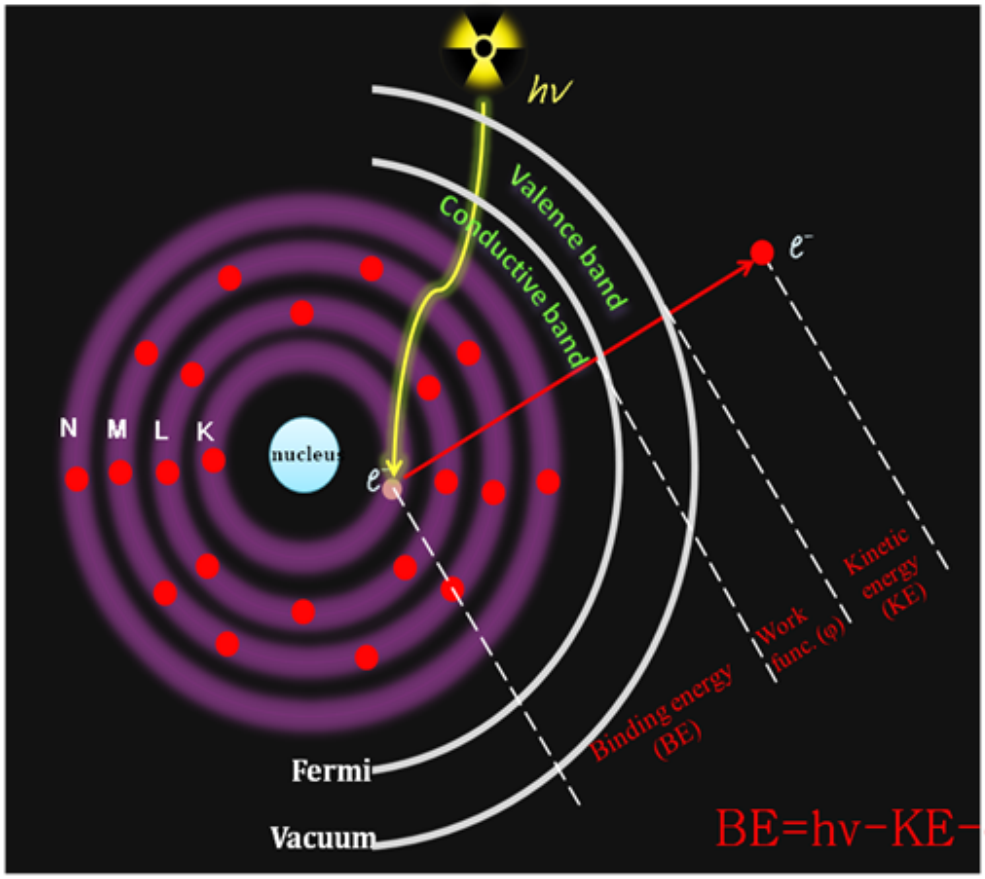

Figure 1.3. Schematic representation of XPS; a core electron is excited with X-ray source, photoelectron is ejected from atom for value of binding energy, kinetic energy and work function of spectrometer.

Surface analysis by XPS was performed in a SPECS SAGE HR 100 system spectrometer in an ultra high vacuum (UHV) chamber. The X-ray sources employed for this analysis were an non monochromatic Mg Kα (1253.6 eV) and 250 W or Al Kα operated at 1.25 kV and 300W, calibrated using the $3d_{5/2}$ line of Ag with a full width at half maximum (FWHM) of 1.1 eV.

The source used for each experiment will be referred to in each chapter where XPS was used to determine surface chemistry. The take- off angle was fixed at 90º and the analysis

was conducted at a pressure of ~10-^{6} Pa. Surfaces were brought into the XPS chamber within 5 min after cleaning/preparation. The selected resolution for the spectra was 30 eV of Pass Energy and 0.5 eV/step for the general survey spectra and 15 eV of Pass Energy and 0.15 eV/step for the detailed spectra of the different elements.

Spectra were analyzed with the CasaXPS 2.3.15dev87 software. The analysis consisted of satellite removal, Shirley background subtraction, calibration of the binding energies related to the C 1s C-C peak at 285 eV, and asymmetric peak fitting with Gaussian-Lorentizan line shapes where the FWHM of all the peaks were constrained while the peak positions and areas were set free.

1.2.3. Atomic force microscopy (AFM)

Atomic force microscope (AFM) is a high resolution scanning probe microscope (SPM) used to measure local properties using a probe. The AFM setup for the imaging consists of a cantilever with a sharp tip (probe) at its end used to scan the specimen surface. The cantilever is typically silicon or silicon nitride with a tip radius of curvature on the order of nanometers. When the tip is brought into proximity of a sample surface, forces between the tip and the sample lead to a deflection of the cantilever according to Hooke's law.(5) In most cases a feedback mechanism is employed to adjust the tip-to-sample distance to maintain a constant force between the tip and the sample. In the AFM setup that is schematically shown in **Figure 1.4,** the tip or sample is mounted on a three piezo crystals, with each responsible for scanning in the x, y and z directions.(5)

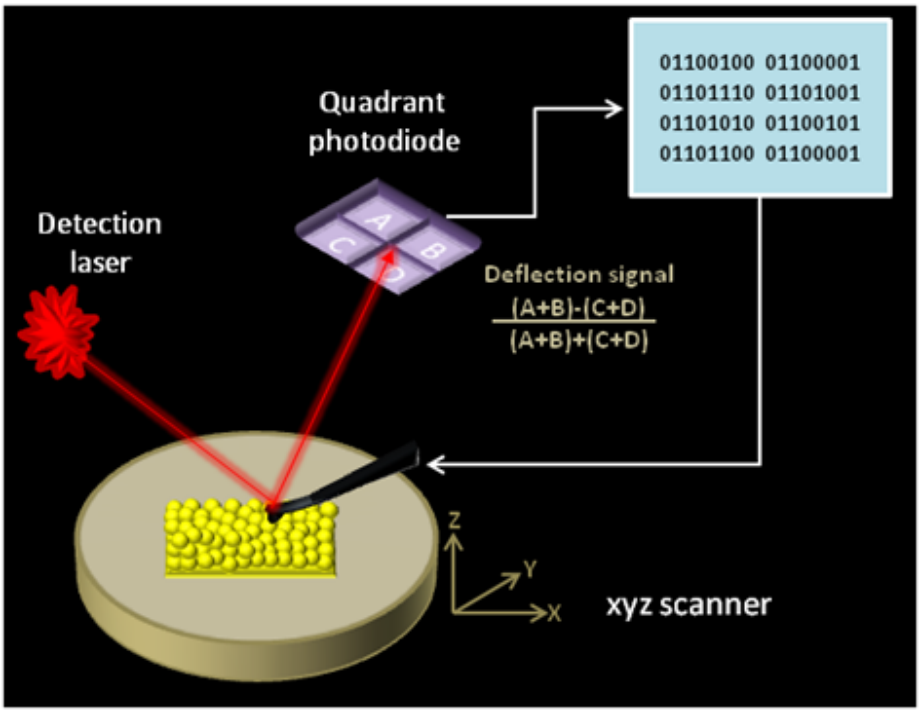

Figure 1.4. Principle of the AFM. The vertical deflection of the cantilever due to forces acting on the tip is detected by a laser. The laser is reflected by the cantilever onto a photodetector. The movement of the laser spot on the photodetector gives a measurement of the movement of the probe.

The imaging modes are divided into static or contact modes and a variety of dynamic (non-contact or "tapping") modes where the cantilever is vibrated or oscillated at a given frequency.

In contact mode, the tip is "dragged" across the surface of the sample. While the tip scans along the surface, the sample topography induces a vertical deflection of the cantilever. A feedback loop maintains this deflection at a preset load force and uses the feedback response to generate a topographic image. Close to the surface of the sample, attractive forces can be quite strong, causing the tip to "snap-in" to the surface. Thus, contact mode

AFM is almost always done at a depth where the overall force is repulsive, that is, in firm "contact" with the solid surface below any adsorbed layers.

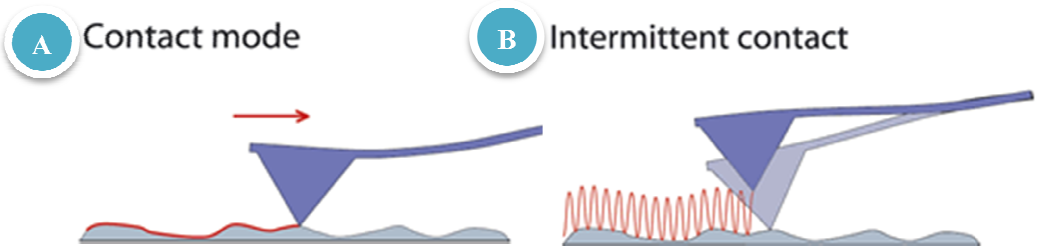

Figure 1.5. Imaging modes of AFM. **A** contact mode where the tip is "dragged" over the surface and **B** Intermittent contact or "tapping" mode where cantilever oscillates and the tip makes repulsive contact with the surface. Image source: JPK instruments, USA.

In tapping mode, AFM maps topography by lightly tapping the surface with an oscillating probe tip. The cantilever is driven to oscillate up and down at or near its resonance frequency by a small piezoelectric element mounted in the AFM tip holder similar to non-contact mode. The interaction of forces acting on the cantilever when the tip comes close to the surface, Van der Waals forces, dipole-dipole interactions, electrostatic forces, etc. cause the amplitude of this oscillation to decrease as the tip gets closer to the sample. An electronic servo uses the piezoelectric actuator to control the height of the cantilever above the sample. The servo adjusts the height to maintain a set cantilever oscillation amplitude as the cantilever is scanned over the sample. A tapping AFM image is therefore produced by imaging the force of the intermittent contacts of the tip with the sample surface.(6)

Structural details of all the solid surfaces in this thesis and collagen- alginate films in chapter 4 were investigated using a Nanowizard II AFM (JPK, Berlin, Germany) and a Nanoscope V Multimode AFM (Santa Barbara, CA). Topography of the solid substrates was determined by contact mode in air using TESP-V2 or oxide-sharpened silicon nitride tips DNP S10 cantilevers (Bruker, Berlin, Germany) as it will be detailed in experimental section of chapters where AFM was used to characterize topography. Topography of softer samples, such as biopolymer films was obtained in intermittent contact preformed in liquid environment, using buffers, with a DNP-S10 cantilevers (Bruker, Berlin, Germany) with a nominal spring constant 0.350 N/m and resonant frequency at ~13 kHz for DNP-S10A cantilevers.

In order to measure the height of the films, nanolithography was performed on a Nanowizard II AFM with TESP-V2 cantilever (Bruker, Berlin, Germany) with a nominal spring constant of 40 N/m and the resonant frequency was ~130 kHz. Lithography was achieved by defining an area of 8 μm × 2 μm that was rasterized in contact mode at a 160 μm/s and subsequently imaged. This was repeated several times, until a smooth surface of the substrate could be observed and no increment in the height of the film edges could be seen. After performing nanolithography, tip direction was rotated for 90° to acquire images and measure height profiles.

1.2.4. Atomic force spectroscopy (AFS)

In force spectroscopy experiment preformed on AFM, the tip is moved directly towards the sample until the contact and then retracted again. Once the cantilever is in contact with the surface, it can be pushed into it with some force. This nanoindentation of

sample with an AFM probe is used to extract mechanical information in the means of Young's modulus.

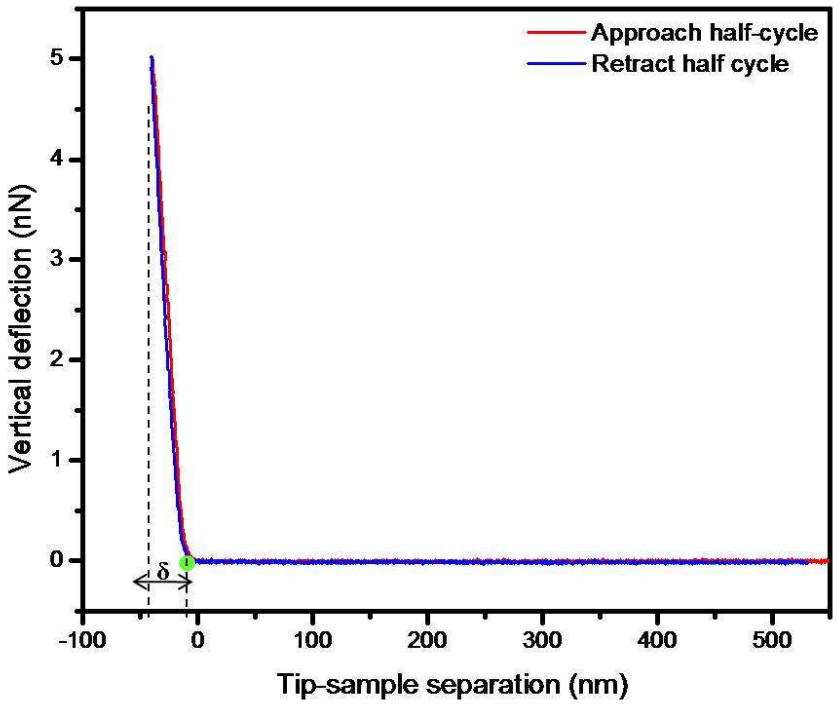

Figure 1.6. Typical force-distance curve. Colloidal probe approaches to surface (red curve) until the contact point (a green dot) where the cantilever starts to deflect. Approach half-cycle is followed by indentation of the sample for δ value. After indentation, probe is retracted to its starting position (blue curve), with minimal hysteresis in particular case.

Soft material elasticity is commonly investigated using a colloidal probe since they avoid the sample puncturing and probe contamination, Moreover, they increase the resolution detecting Young´s modulus as low as few Pa.(7)

The data from an experiment are displayed as a force- distance curves that are a plot of tip-sample interaction forces vs. tip-sample distance.(8) In order to obtain such a plot, the tip is ramped along the vertical axis (Z axis) and the cantilever deflection is acquired. The

Young´s modulus is than extracted from force- distance curves by fitting them to the appropriate model. A typical force-distance curve is shown in **Figure 1.6**.

Collagen- alginate film elasticity presented in the chapter 3 was determined from the nanoindentation experiments preformed on a NanoWizard II AFM (JPK, Berlin, Germany) acquiring force-distance (f-d) curves in liquid medium. Measurements were performed with a 2 μm borosilicate colloidal probe attached to the cantilever (Novascan Technologies, USA). Cantilever spring constant was calibrated through the thermal noise method in the medium where measurements were preformed (Na acetate and PBS buffers). The cantilever spring constant was determined to be 0.065 N/m. 200 f-d curves were acquired with setpoint forces of 0.5, 0.1 and 0.05 nN over a sample area of 10 μm × 10 μm. For each film, a total of five different sample areas were probed and the resulting data screened and processed using the JPKSPM Data Processing software. The Young's elastic modulus (E) of each film was obtained by fitting the force data in the entire compressive part (curve) of the indentation cycle to the Hertz model assuming a Poisson ration of 0.40. Further statistical analysis of resulting E values was performed with OriginPro 2015 software.

1.2.5. Quartz crystal microbalance with dissipation monitoring (QCM-D)

Quartz Crystal Microbalance with Dissipation monitoring (QCM-D) is a real-time, nanoscale technique for thin film formation, interactions and reactions. A QCM sensor consists of a thin quartz disc between a pair of electrodes. The sensor can be excited to oscillate at its resonance frequency by the application of an alternating voltage. The resonance frequency depends on the total oscillating mass of the sensor and sensor

surface adhering layers, including coupled water. The frequency decreases when a thin film is attached to the sensor. If the film is thin and rigid the decrease in frequency is proportional to the mass of the film.(9)

QCM-D is used in chapter 4 of this thesis for *In situ* monitoring of film assembly. The assembly of collagen-alginate films was monitored with an E4 QCM-D from Q-Sense, Goteborg, Sweden. QSX 301 Au quartz crystals (Q-sense) were coated with Ti/TiO2 (50 nm), and then functionalised with APTES prior to assembly in the QCM-D chamber. The LbL assembly was performed by passing 0.5 mg/mL polyelectrolyte solution in 0.1 M Na acetate buffer (pH 4) with a peristaltic pump through the chamber. LbL deposition was monitored by the decrease in the resonance frequency of the quartz crystal. Once the frequency values stabilized, the polymer solution was replaced by Na acetate buffer until a plateau in the frequency response was recorded. This procedure was repeated for the deposition of a desired number of polyelectrolyte layers, alternating collagen and alginate. After deposition, the film was shortly rinsed with PBS buffer to exchange pH and further crosslinked by passing EDC/NHS (6.5/1 mg/mL) in PBS trough the chamber.

1.2.7. Scanning electron microscopy (SEM) and Energy dispersive X-ray spectroscopy (EDX)

A scanning electron microscope (SEM) is an electron microscope used for surface imaging with a focused beam of electrons. In the SEM imaging, a beam of incident electrons is generated by a thermal emission. The electrons interact with atoms in the sample, producing signals that can be detected and contain information about the surface topography and composition. The electron beam is scanned in a raster

scan pattern, and the beam's position is combined with the detected signal to produce an image. Samples in SEM are commonly observed in high. The most common SEM mode is detection of secondary electrons emitted by atoms excited by the electron beam.(10)

Energy Dispersive X-Ray Spectroscopy (EDX) is a surface chemical analysis technique used in combination with SEM. The EDX technique detects X-rays emitted from the sample during bombardment by an electron beam to characterize the elemental composition of the sample. Similar as in XPS, the energy is characteristic of the element from which it was emitted. The EDX detector measures the relative abundance of emitted X-rays versus their energy.

Scanning electron microscopy (SEM) images presented in this thesis were collected with SEM JEOL JSM-6490LV microscope. Images were obtained in second electron imaging (SEI) detection mode in a point by point scanning mode and with a penetration depth less than 10 nm. Chemical composition was determined using OXFORD INCA EDX system coupled to the SEM microscope.

1.2.7. Confocal laser scanning microscopy (CSLM)

Confocal laser scanning microscopy (CLSM) is an optical imaging technique with increased resolution and depth selectivity. The key feature of confocal microscope is in ability to acquire in-focus images from selected depths. Images are acquired point-by-point and reconstructed with a computer, allowing three-dimensional reconstructions of topologically complex objects. The quality of the image is greatly enhanced over simple microscopy because image information from a confocal microscope is constructed as one depth level at a time. In effect, the CLSM achieves a controlled and highly

limited depth of focus(11). Schematic represeantation of Confocal microscope and image construction is shown in **Figure 1.7.**

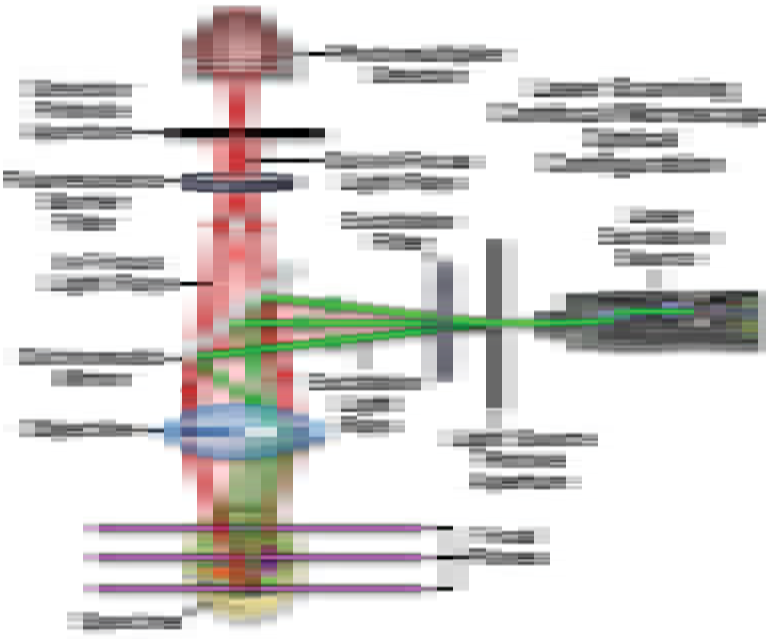

Figure 1.7. Principle of confocal microscopy. A laser beam passes through a light source aperture and then is focused by an objective lens into a small focal volume within the specimen. Laser light and fluorescent light from the illuminated spot passes back through the objective lens. A beam splitter separates some of the light into the detection apparatus and selectively passes the fluorescent wavelengths while blocking the original excitation wavelength. After passing a pinhole, the light intensity is detected by a photodetection transforming the light signal into an image. Image source: Zeiss, Germany.

Fluoresecence images of stained pre-osteoblast cells and polyelectrolte multilayers presented in this thesis were acquired on a Zeiss LSM 510 confocal microscope (Carl Zeiss, Göttingen, Gremany).

1.2.9. Cell culturing

A preosteoblast MC3T3-E1 subclone 4 was purchased by ATCC (Manassas, Virginia, USA). This cell line is a good model for studying in vitro osteoblast differentiation, particularly ECM signaling. They have behavior similar to primary calvarial osteoblasts and exhibit high levels of osteoblast differentiation after growth in ascorbic acid and inorganic phosphate. They form a well mineralized extracellular matrix (ECM) after 10 days of osteogenic culturing (12). The culturing medium was α-MEM (Life technologies, Madrid, Spain) supplemented with 10% fetal bovine serum and 1% penicillin/streptomycin (both from Sigma Aldrich, Madrid, Spain), referred as a full culturing medium. Vials with the cells in the full culturing medium medium containing DMSO were stored in liquid nitrogen and thawed when needed. All the operations were carried under strict aseptic conditions. Vials were quickly thawed in 37 ºC water bath, transferred to the centrifuge tube containing full culturing medium and centrifuged at 150 x g for 5 minutes. The cell pellet was resuspended in the full medium and dispensed in a culturing flask. Cells were cultured at 37 °C in an atmosphere of 5% CO_2 and the medium was refreshed every three days. Upon the cells reached 80% confluence, they were trypsinized and resuspended in fresh full medium to arrive at a cell suspension with a desired cell density for seeding on the samples and further biological evaluation. Cells were differentiated in osteogenic medium that is full medium additionally supplemented with 50 µg/mL of ascorbic acid and 2 mM β- betaglycerophosphate.

1.2.10. Actin cytoskeleton and focal adhesion staining

The actin cytoskeleton is composed of actin polymers and various associated proteins. It mediates a diversity of essential biological functions in eukaryotic cells. The organization of the actin cytoskeleton is tightly regulated both temporally and spatially. Actin polymers are superorganized into a filamentous network that is mediated by actin side-binding or cross-linking proteins. A disruption of normal regulation may lead to cell transformations that have been shown to contain less F-actin and exhibit atypical coordination of F-actin levels to the cell cycle (13).

Focal adhesion and adherens junctions are membrane-associated complexes that serve as nucleation sites for actin filaments and as cross-linkers between the cell exterior, plasma membrane and actin cytoskeleton. The function of focal adhesions is structural, linking the ECM on the outside to the actin cytoskeleton on the inside. Focal adhesions consist of integrin-type receptors that are attached to the extracellular matrix and are intracellularly associated with protein complexes containing vinculin (universal focal adhesion marker), talin, a-actinin, paxillin, tensin, zyxin and focal adhesion kinase (FAK).

After the cells reached 80% confluence, they were trypsinized and resuspended in fresh medium to arrive at a cell suspension with a final cell density of 2.5-3 $\times 10^4$. 1 mL of cell suspension was added into each well of 12 well cell culture plate. Cell adhesion was evaluated after 2 to 24 hours after cells were seeded onto samples. Cells were then fixed in a 4% paraformaldehyde solution. F-actin, nuclei and focal adhesion of the cells were stained with actin cytoskeleton and focal adhesion staining kit FAK100 (Merck Millipore, Madrid, Spain). Cells cultured on the surfaces were first permeabilized with Triton-X100

(Sigma) for 4 min at room temperature. Then, the cells were incubated in diluted primary antibody (anti-vinculin) solution for 1 hour at room temperature, followed by three times washings with PBS for 5-10 min each, and then by 1 hour further incubation with a secondary antibody (FITC-conjugated) solution and TRITC-conjugated Phalloidin at room temperature. After three washing steps with PBS, cells were incubated with DAPI for 3 min at room temperature, followed again by three washing steps with PBS.

1.2.11. Alkaline phosphatase acivity

Alkaline phosphatase is an important component in hard tissue formation, highly expressed in mineralized tissue cells. The ALP in hard tissue formation serves as a marker for osteogenic activity has and it occurs at an early step in the mineralization process. Proliferating Osteoblasts show alkaline phosphatase (ALP) activity in the stage of extracellular matrix maturation, being greatly enhanced during in vitro bone formation. ALP activity is therefore a feasible marker for differentiating and mineralizing oseoblastic formation (14).

For alkaline phosphatase (ALP) staining, the cells were seeded with a density of 2×10^4 cells/mL on samples in osteogenic medium. After culturing for 12, cells were fixed 4% paraformaldehyde solution, and then stained with an ALP staining kit (1-Step TM NBT/BCIP, Thermo) for 1 h. ALP stained samples are imaged on Leica bright field microscope and ALP area is determined in MacBiophotonics ImageJ and further statistical analysis concerning ANOVA analysis is done in OriginPro 2016 software.

1.2.12. Cell proliferation

After reaching the 80% confluence, cells were trypsinized and resuspended in fresh medium to a final cell density of 2.5-3×10^4. 1 mL of cell suspension was added into each well of 24 well cell culture plate. A cell proliferation colorimetric assay was conducted with the Cell Counting Kit-8 (CCK-8) (Sigma Aldrich, Madrid, Spain) containing WST-8[2-(2-methoxy-4-nitrophenyl)-3-(4-nitrophenyl)-5-(2,4-disulfophenyl)-*2H*-tetrazolium, monosodium salt], an nontoxic dye used for continuous cell culturing. Colorimetric analysis was performed at a certain time periods of cell culturing, in days scale, as noted in each of chapter. For this assay, the cells cultured on the samples were refreshed with 12.5 % v/v of CCK-8 containing medium. After 2 hours of incubation at 37 °C, aliquot of 50 μL was placed into 96 well cell plate. Optical density of reaction solution was acquired using a plate reader (GENios Pro, Tecan) equipped with a 450 nm filter.

List of references

1. Safi I (2000) Recent aspects concerning DC reactive magnetron sputtering of thin films: a review. *Surface and Coatings Technology* 127(2-3):203-218.

2. Maurya D, Sardarinejad A, & Alameh K (2014) Recent Developments in R.F. Magnetron Sputtered Thin Films for pH Sensing Applications: An Overview. *Coatings* 4(4):756-771.

3. Hüfner S (2003) *Photoelectron Spectroscopy- Principles and Applications* (Springer-Verlag, Berlin Heidelberg) 3 Ed.

4. Einstein A (1905) Über einen die Erzeugung und Verwandlung des Lichtes betreffenden heuristischen Gesichtspunkt. *Annalen der Physik* 322(6):132-148.

5. Binnig G, Quate CF, & Gerber C (1986) Atomic Force Microscope. *Physical Review Letters* 56(9):930-933.

6. Geisse NA (2009) AFM and combined optical techniques. *Materials Today* 12(7-8):40-45.

7. McConney ME, Anderson KD, Brott LL, Naik RR, & Tsukruk VV (2009) Bioinspired Material Approaches to Sensing. *Advanced Functional Materials* 19(16):2527-2544.

8. Cappella B & Dietler G (1999) Force-distance curves by atomic force microscopy. *Surface Science Reports* 34(1-3):1-104.

9. Reviakine I, Johannsmann D, & Richter RP (2011) Hearing What You Cannot See and Visualizing What You Hear: Interpreting Quartz Crystal Microbalance Data from Solvated Interfaces. *Analytical Chemistry* 83(23):8838-8848.

10. Goldstein J, *et al.* (2003) *Scanning Electron Microscopy and X-ray Microanalysis-Third Edition* (Springer US, New York) 3 Ed.

11. Pawley J (2006) *Handbook of Biological Confocal Microscopy* (Springer US, New York) 3 Ed.

12. Wang D, *et al.* (1999) Isolation and Characterization of MC3T3-E1 Preosteoblast Subclones with Distinct In Vitro and In Vivo Differentiation/Mineralization Potential. *Journal of Bone and Mineral Research* 14(6):893-903.

13. Defilippi P, *et al.* (1999) Actin cytoskeleton organization in response to integrin-mediated adhesion. *Microscopy Research and Technique* 47(1):67-78.

14. Weinreb M, Shinar D, & Rodan GA (1990) Different pattern of alkaline phosphatase, osteopontin, and osteocalcin expression in developing rat bone visualized by in situ hybridization. *Journal of Bone and Mineral Research* 5(8):831-842.

Chapter 2

Nb-C nanocomposite coatings for enhanced hard tissue implants

2.1. Motivation

One of the well accepted methodology to improve the surface properties of implants and enhance their overall performance is to change their surface chemistry and modulate their surface topography at the micro and nanoscale. The impact of surface characteristics on implant performance highlights the significance of surface chemistry and topography on cell behavior and tissue formation.(1) Beside titanium materials, other metals and metall-like coatings are exhibiting interesting properties for use in tissue engineering. Carbon films especially, amorphous carbon (α-C) or diamond-like carbon (DLC) are chemically inert in the body, and have been widely used for improving the hemocompatibility and biocompatibility of implant materials in the biomedical field.(2) As well, DLC films show high hardness and low coefficient of friction that is desirable characteristic in tailoring new implant biomaterials.(2, 3) Although their biocompatibility has been well established, these films are not bioactive, in regards to their ability to induce new bone tissue formation. This drawback limits use of carbon materials in the design of orthopaedic and dental implant materials.

On the other hand, Niobium (Nb) has received great attention in development of the new implant alloys. Addition of Nb in the alloys changes the chemistry of materials and such alloys, for example Ti-Nb and Zr-Nb, have enhanced corrosion resistance and biocompatibility.(4-6) Additionally there is evidence that changes in titanium surface chemistry caused by the incorporation of Nb enhanced the osteoblast differentiation of titanium materials. (7-9) Titanium alloys doped with Nb display an enhanced alkaline phosphatase **(**ALP) activity and promoted more rapid maturation of the osteoblasts, suggesting the potential of Nb in inducing osteogenic functions of osteoblast.(9) In addition, it has been found that introduction of Nb_2O_5 into plasma sprayed TiO_2 coatings induced a significant change in the nanotopography of the TiO_2 coating besides changes in surface chemistry.(10) Therefore, it is also expected that the addition of Nb in the a-C film can also induce topographic alteration.

In the work presented in this chapter we have incorporated Nb into a-C films with the goal of enhancing the bioactivity of the a-C film coated orthopedic implants. This work has an aim to explore the bioactivity of these Nb-C coatings in order to conclude on its perspective in design of improved orthopaedic and dental implants.

2.2. Experimental approach

2.2.1. Sample preparation: Magnetron sputtering of the Nb-C and TiO_2 films

Thin films used in this study, amorphous carbon (a-C), Nb-C and TiO_2 were deposited with non-reactive and reactive magnetron sputtering on silicon (100) and glass substrates using an AJA-ATC 1800 system. The deposition of the films was done with three separate 2 inch elemental targets, with a purity of 99.999% for carbon (Demaco-Holland), 99.95% for Nb (AJA International-USA) and 99.995% for Ti (Kurt J. Lesker-USA), at a pressure of 0.25 Pa of pure Ar.

The a-C film was deposited by applying a d.c. power of 380 W to the carbon target. The Nb-C film was deposited by applying simultaneously a d.c. power of 380 W and r.f. power of 100 W to the C and Nb targets, respectively. In order to improve the adhesion of the a-C and Nb-C films to the substrates, a pure Nb layer of ~30 nm was deposited onto the substrates at Nb target r.f. power of 230 W.

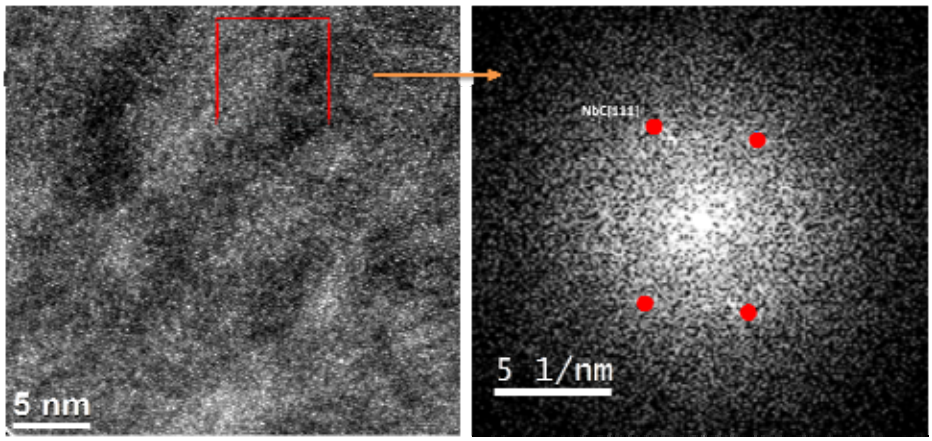

Figure 2.1. HRTEM Image of Nb-C film, revealing nanocomposite structure consisting of NbC nanocrystals.

The Nb-C films coated by using these sputtering parameters exhibit a nanocomposite structure where the Nb-C nanosized crystals are embedded in an amorphous carbon matrix.(11) Such a nanocomposite is shown in **Figure 2.1.**

2.2.2. Material characterization and cell activity

Surface chemistry of coatings is investigated by X-ray photoelectron spectroscopy (XPS). Topography of thin films is revealed using a Nanoscope V Multimode Atomic force microscopy (AFM).

Nanohardness, Young´s modulus and elastic recovery of the films were measured by nanoindentation (Hysitron TI 950 TriboIndenter) using a Berkovich diamond indenter at different loads. The elastic recovery of the samples was determined as the percentage of the residual imprint compared to the total displacement of the load-displacement curves.

For evaluation of material biocompatibility and bioactivity an osteoblast precursor cell line, MC3T3-E1 was used. Visualization of cell morphology is assessed after culturing up to 24 hours by AFM and scenning electron microscope (SEM).

Fluorescence images of focal adhesion staining after 3 and 24 hour are collected on confocal scanning laser microscope (CSLM).

Cell viability on thin films is evaluated by CCK-8 proliferation test up to 7 days. The osteogenic differentiation is studied by alkaline phosphatase (ALP) activity of the preosteoblast cells by staining with an ALP staining kit (1-Step TM NBT/BCIP, Thermo).

2.3. Results and discussion

2.3.1. Chemical and structural characterization of coatings

The chemical composition of the samples was studied by XPS and relative percentage of elemental contribution was calculated based on the relative areas of the different photoelectron peaks. The XPS survey spectra of the three films are shown in **Figure 2.2.** and the chemical compositions expressed as atomic percentages (at.%) are listed in **Table 2.1**. The a-C film (in black) is composed of almost 100 % carbon, while the film incorporated with Nb film, Nb-C (in blue) is composed of around 39 % carbon and 52 % niobium beside the oxygen found in surface chemical composition.

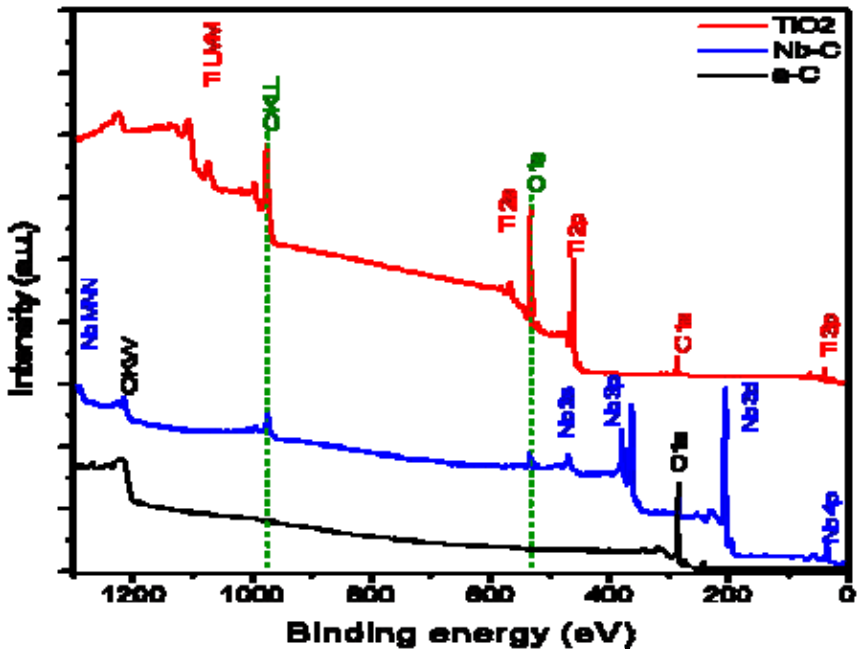

Figure 2.2. XPS survey spectra of Nb-C, a-C and TiO_2 films, main photoelectron signals are noted for each film as well O 1s and O KLL photoelectron lines of oxygen that is found in Nb-C and TiO_2 films.

The TiO_2 film shows a composition of around 29 % titanium and 63 % oxygen. Ti 2p photoelectron line can be fitted to two or three oxidation states, with around 95 % assigned to Ti IV. A Ti/O ratio is around 2, close to the stoichiometric ratio of TiO_2.

Table 2.1. Chemical compositions obtained from XPS analysis, RMS roughness obtained from AFM measurement and mechanical properties measured by nanoindentation.

Sample	Nb (at. %)	Ti (at.%)	C (at. %)	O (at. %)	RMS roughness (nm)	Hardness (GPa)	Young's modulus (GPa)
Nb-C	52.1	-	39.0	9.0	1.20	22.5	191.7
a-C	-	-	99.3	0.7	0.79	12	96.6
TiO_2	-	28.9	7.7	63.4	1.55	7-11*	80-120*

* Values obtained from the work of Jung et al.(13)

2.3.2. Surface topography and mechanics of thin films

Figure 2.2 shows three dimensional AFM images **(Figures 2.3. A, B** and **C**) presenting the surface topography of the film samples. All samples exhibit nanoscale topographic features with RMS roughness below 1.55 nm, as shown in **Table 2.1**. Among these samples, the a-C film has smoothest surface resulting in lowest RMS **(Figure 2.3.** and **Table 1.1.**), the TiO_2 film display the highest roughness, while the Nb-C film shows an intermediate RMS roughness profile. In the **Figures 2.3. D-F** are shown typical AFM top views of the films. Compared to other samples, the a-C film has the largest grains

with a size of around 50 nm in average. The Nb-C film shows smaller grains with a size of around 17 nm, close to the grains of TiO_2 films.

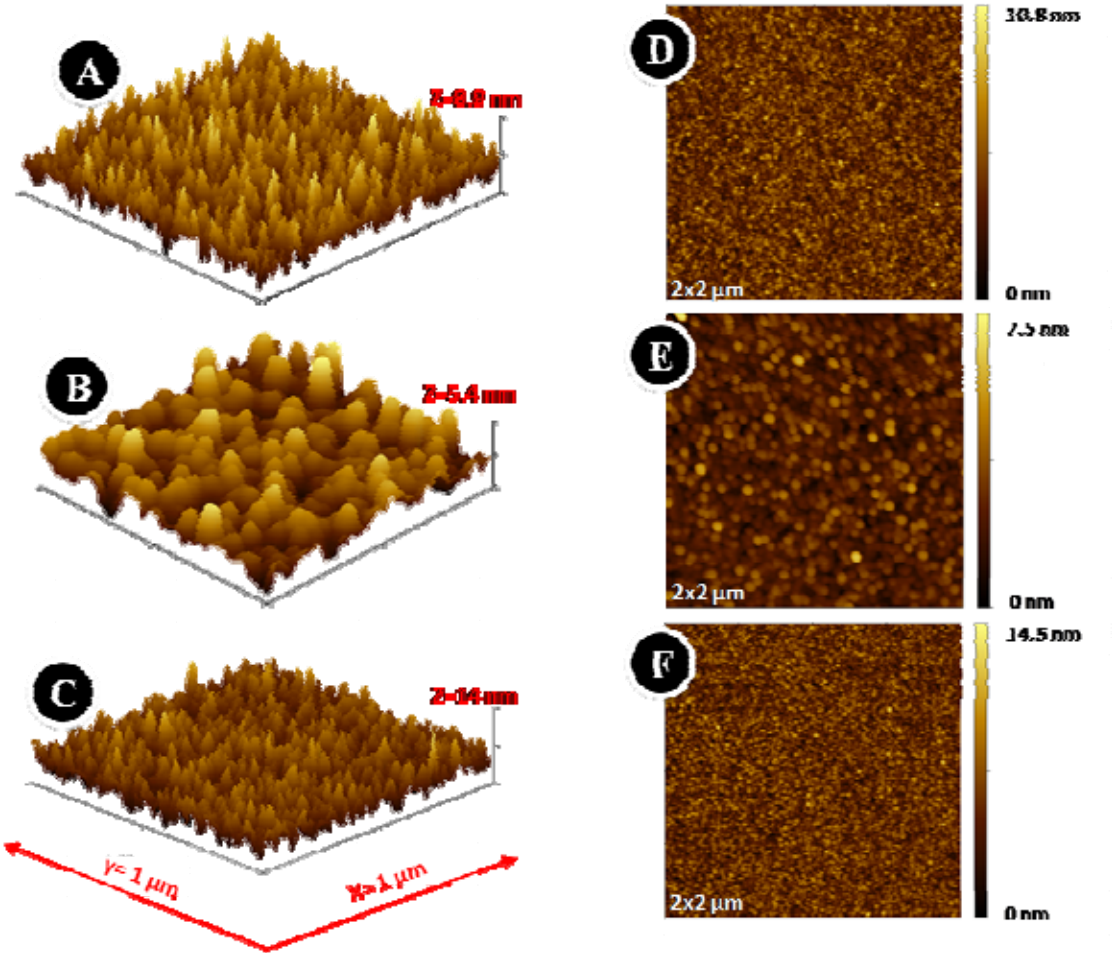

Figure 2.3. AFM images of (A, D) Nb−C, (B, E) a-C and (C, F) TiO_2 samples. The images in on the left (A, B and C) are three-dimensional AFM images and on the right (D, E and F) are the representative AFM top view images.

In summary, the introduction of Nb into the a-C films not only changes the surface chemistry, but also significantly alters the surface topography at nanoscale by tailoring the grain size and surface roughness as can be seen in **Figure 2.3.**

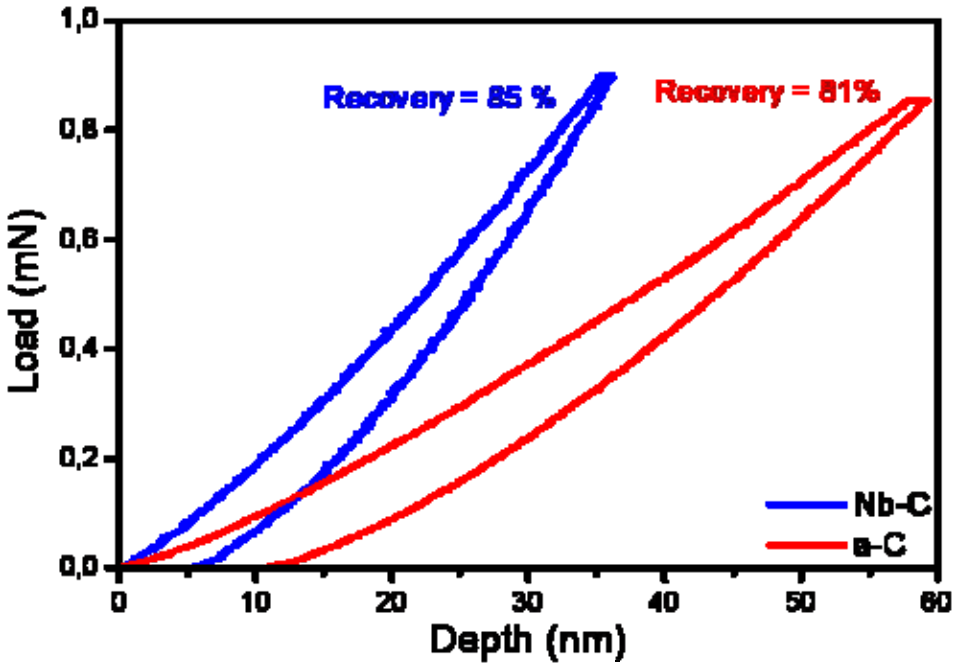

Figure 2.4. Load-displacement nanoindentation curves of the Nb-C and a-C films. The curves are used to calculate hardensess and Young's modulus.

Figure 2.4. shows the load-displacement nanoindentation curves for the a-C and the Nb-C films. The hardness and Young´s modulus was calculated based on these curves using the method proposed by Oliver and Pharr (12) are listed in **Table 2.1.** The hardness values for the a-C films are around 12 GPa. It is noted that the Nb-C films have a hardness as high as 22.5 GPa, significantly higher than the nanohardness of the reported values for TiO_2 films, between 7 and 11 GPa,(13) and Ti-6Al-4V alloys, around 4-5 GPa. (14)

From **Table 2.1.**, we can see that Nb-C film also has the highest elastic modulus (191.7 GPa), much higher than those reported values of TiO_2 thin films (13) and somewhat higher than Ti alloys. (14, 15) From the load-displacement curves, it can be seen that the elastic recovery of Nb-C film and a-C film after deformation is 85% and 81%,

respectively, suggesting that the Nb-C film exhibits a slightly better super-elastic recovery behavior than the a-C film. Super elastic properties are of special interest in medical applications due to the large strains and deformations at which implants, stents or bone staples are subjected.(16)

These results indicate that introduction of Nb into the a-C films can maintain and even slightly improve the super-elastic property of the a-C film, and meanwhile improve the nano-hardness and the Young's modulus.

2.3.3. Biocompatibility and bioactivity of thin films

The initial adhesion of cells on biomaterials is a key regulator of cell proliferation, migration and differentiation, which determines the fate of the biomaterial. We used MC3T3-E1 cells, an osteoblast precursor cell line, to evaluate the cell adhesion on the film samples.

Figure 2.5. shows the AFM images of the cells after culturing for 3 and 24h on the Nb-C, a-C and TiO_2 films. From the images, we can clearly see the cell membrane and also the cell nuclei showing a bright color due to their higher height. After culturing of 3h, the cells cultured on all the films already partially flatten, showing a satellite-shaped morphology with cellular protrusions (lamellipodia and filopodia) extending from cell bodies to explore the underneath substrates.

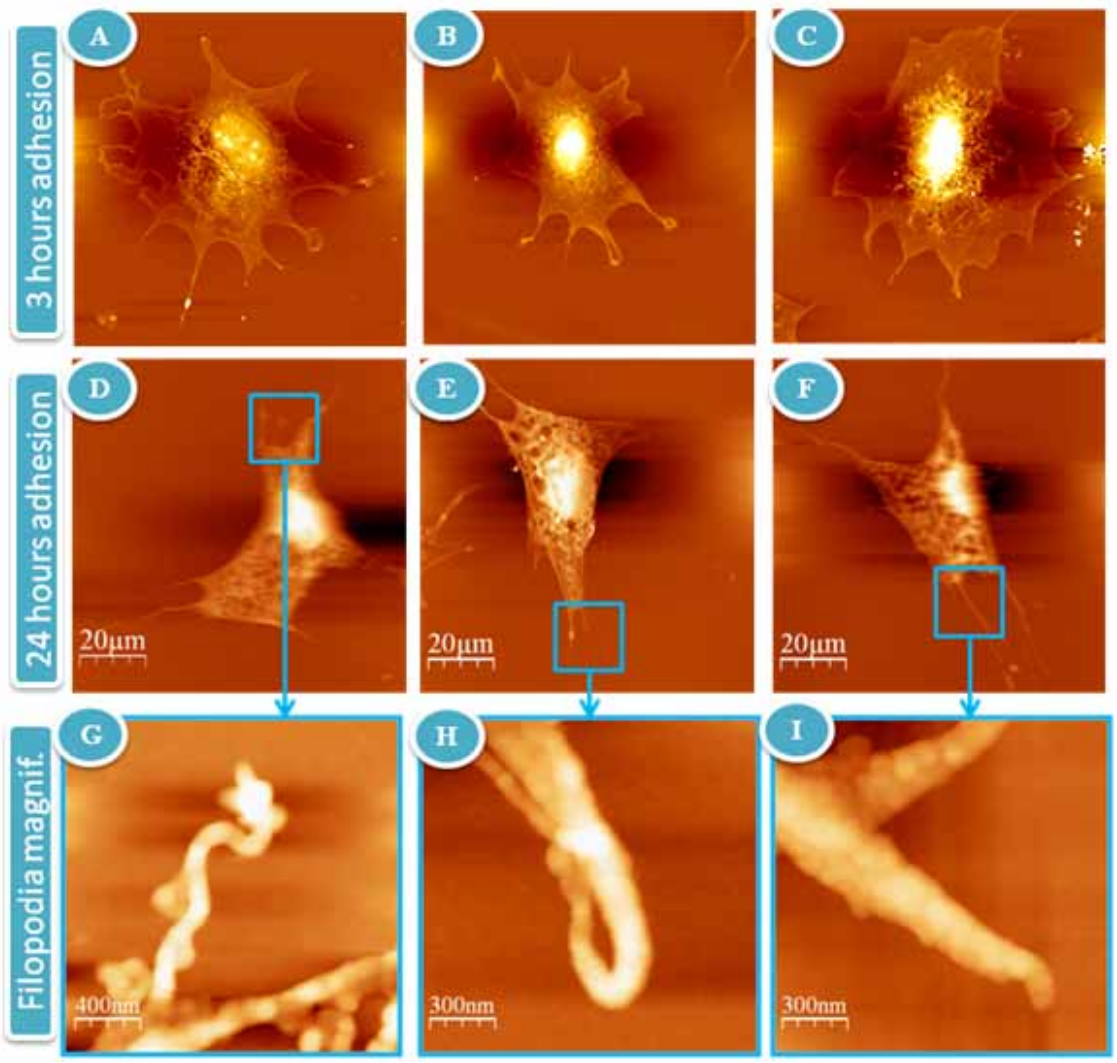

Figure 2.5. AFM Images of the cells cultured on the Nb-C (A,D.G) , a-C (B,E,H) and TiO_2 (C,F,I) films for 3hours (A-C) and 24hours (B- H). Images G-I are the higher magnification views of D,E and F, respectively.

At 24h, cells on all the films become fully flattened and their morphologies change from satellite-shapes to polygonal shapes with different degree of elongation, which are a characteristic morphology of osteoblasts. From the higher magnification images, we can clearly see the filopodia of the osteoblasts **in Figure 2.5. G-I.**

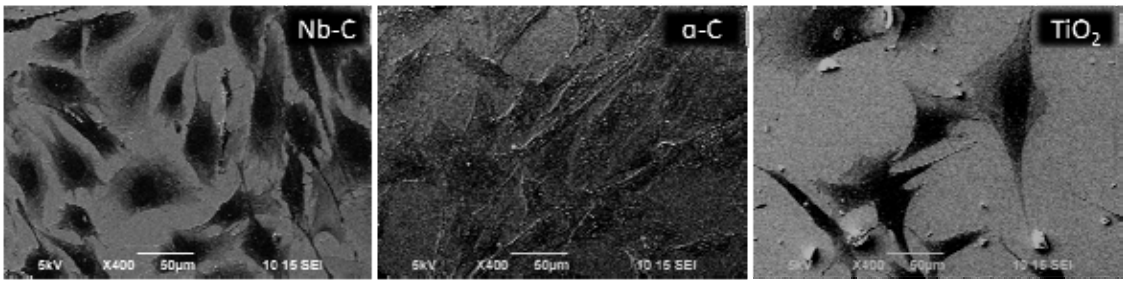

Figure 2.6. SEM images of preosteoblast cell line seeded on Nb-C, α-C and TiO_2 films after 24 hours of cell adhesion. 400 x magnification

In addition, after 24 hours of cell culturing we observe more cells on the Nb-C and α-C films when compared to TiO_2 as seen from SEM images shown in **Figure 2.6.** Same as observed in previously shown AFM images, cells are fully flattened after 24 hours of culturing, but on Nb-C and α-C films they are exhibiting more of elongated filopodia.

Figure 2.7. shows the confocal laser scanning microscope images of the cells cultured on the Nb-C, a-C, and TiO_2 films for 24h. The nucleus (blue), F-actin (red) and vinculin (green) were stained and are shown in the second, third and fourth column in **Figure 2.7.**, while the merged images are shown in the first column. From the images of F-actin, it can be seen that cells cultured on the Nb-C and a-C films share a similar size and exhibit obvious rearranged cytoskeleton with distinctive stress fibers inside the cytoplasm, especially at the border of the cells. By contrast, the size of the cells cultured on the TiO_2 film varied significantly: some of them are large in size with distinctive actin networks, whereas some of them have a smaller size showing a diffuse cytoskeleton with less obvious stress fibers in their cytoplasm.

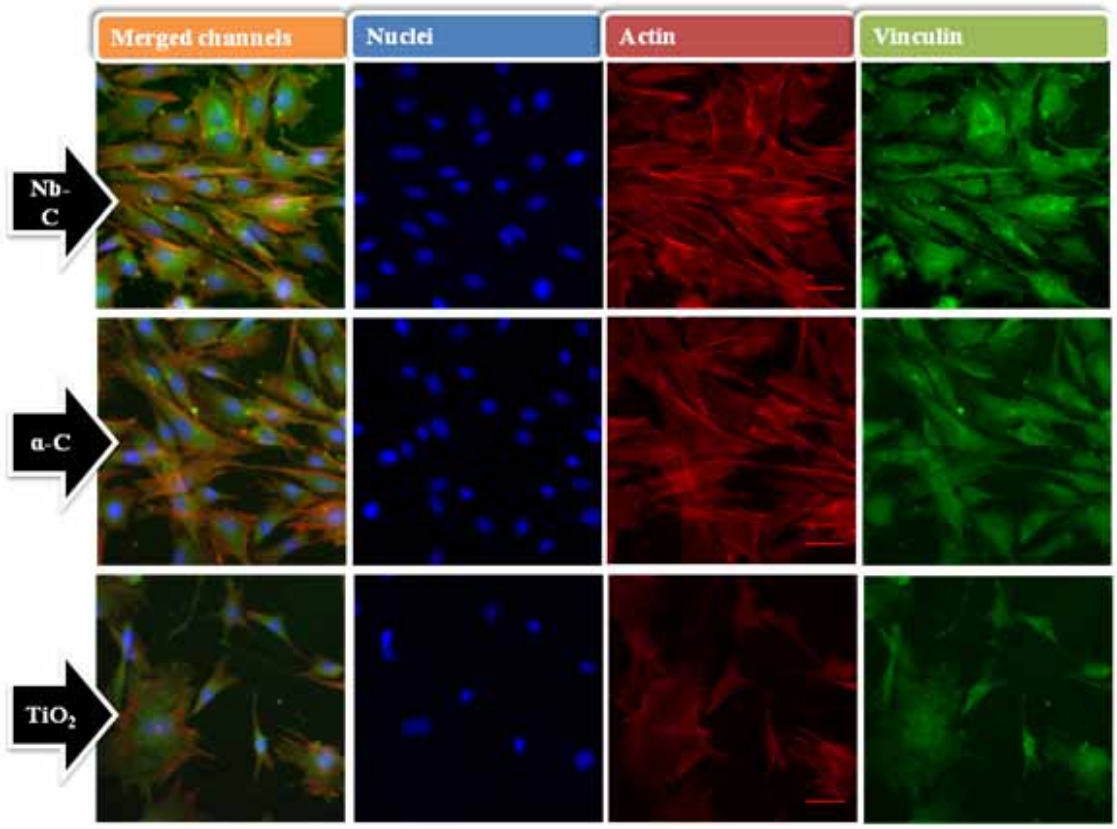

Figure 2.7. Confocal laser scanning microscope images of the cells cultured on the Nb-C, a-C, and TiO_2 films for 24h: the nucleus (blue), F-actin (red), and vinculin (green).

In the image of vinculin staining, more green spots can be found at the border of the cells cultured on the Nb-C film, compared to the cells cultured on the other films. In addition, we can also see some peri-nucleus regions showing a bright green color in the cells cultured on the Nb-C films. These results indicate enhanced focal adhesion of cells on the Nb-C film sample. For the cells cultured on the a-C films, we can also see some green spots, however, much less can be found in the cells cultured on the TiO_2 films. From images of the cell nuclei, we can see that some of the nuclei show a round shape and some of them exhibit an elongated shape. It can be found that a significantly larger percentage of cell nuclei have an elongated shape in the cells cultured on the Nb-C and

percentage of cell nuclei have an elongated shape in the cells cultured on the Nb-C and a-C films, compared to those cultured on the TiO_2 films, indicating that the Nb-C film exerts more profound influence on the behavior of the osteoblasts. In summary, AFM and confocal microscope images revealed that osteoblasts can adhere well on all the film samples. However, it is noted that the Nb-C films are superior to the a-C and TiO_2 films in terms of the enhancement of cell adhesion embodied in the reorganized cytoskeleton, formation of stress actin fibers and elongation of the nuclei. Similar effects of Nb on the morphology of bone-related cells were also found in other studies. Olivares Navarrete et al. (17) investigated the biocompatibility of Nb films prepared by magnetron sputtering on the stainless steel substrates and they found that human alveolar bone-derived cells cultured on the Nb films assumed elongated fibroblastic appearance, while those cultured on the stainless steel exhibited round shapes, indicating the influence of Nb on the behavior of bone-related cells.

Cells sense chemical and topographical cues in their surrounding microenvironment. These cues can be converted into intracellular signals and transduced to the nucleus in order to respond and adapt its functions. (18) (19) Therefore, the cytoskeleton and nuclei morphology can be modulated by simply changing the surface chemistry and topography of the underlying substrates. In this study, the addition of Nb to the a-C film not only changed the surface chemistry but also altered the nanotopography of the film, which can be the reasons for the better interaction of the nanocomposite Nb-C films with osteoblasts.

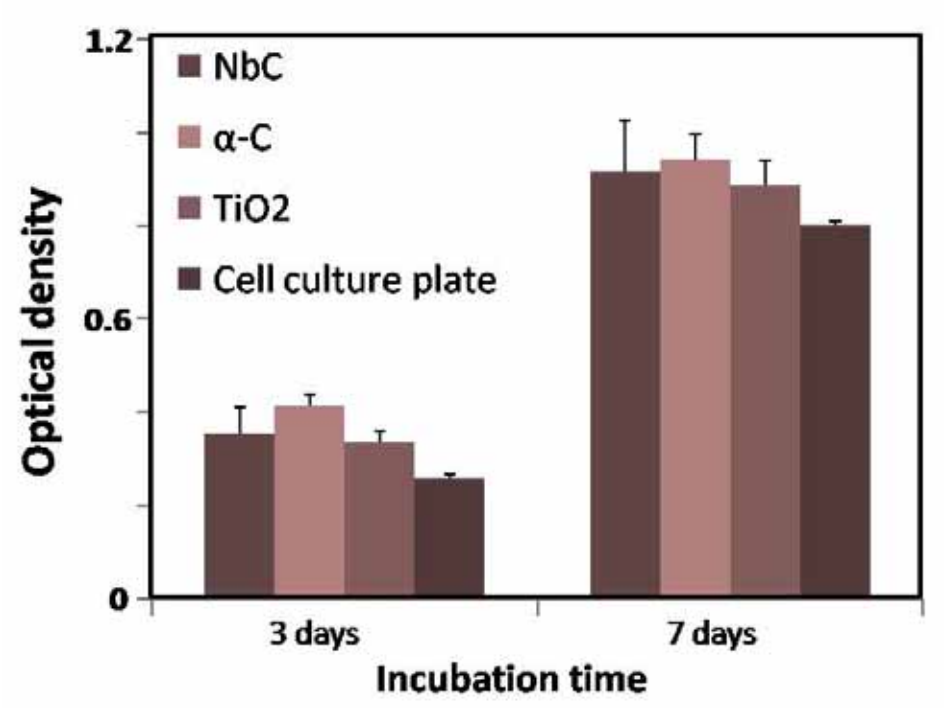

Figure 2.8. Proliferation of pre-osteoblast cells cultured on the Nb-C, a-C and TiO_2 films for 3 and 7 days.

The proliferation of the cells cultured on the Nb-C, a-C and TiO_2 films was also evaluated and the result is displayed in **Figure 2.8.** The cell culture plates were also used as a control in this assay. It can be seen that at both time points (3 days and 7 days) cells cultured on the films have a higher proliferation rate than those cultured on the cell culture plates ($P<0.05$). The average proliferation rates of the cells cultured on the Nb-C and a-C films are higher without significant difference, compared to the cells cultured on the TiO_2 films. This result indicates that all the film samples can promote the cell proliferation. The proliferation rates of cells cultured on the a-C and Nb-C films are at least comparable to that of cells cultured on the TiO_2 films.

In this study, we also evaluate ALP activity of the osteoblasts cultured on the film samples. ALP activity is one of the gene markers in the early stage of the osteogenic differentiation. **Figure 2.9.** shows the ALP activity of the cells cultured on the Nb-C, a-C and TiO_2 films. More cells cultured on the Nb-C films after staining exhibit a darker blue color, compared to those cultured on the other two films, especially on the TiO_2 film. These results indicate that the cells cultured on the Nb-C film have enhanced ALP activity compared to those on the a-C film and the TiO_2 film, implying the positive effects of Nb on the osteoblast differentiation ability. The enhancement on the ALP activity by the Nb has been reported by others. Shapira et al. reported that osteoblasts cultured on Ti-6Al-7Nb showed enhanced ALP activity, higher expression levels of osteocalcin and transforming growth factor, compared to those cultured on the currently used Ti-6Al-4V. (9)

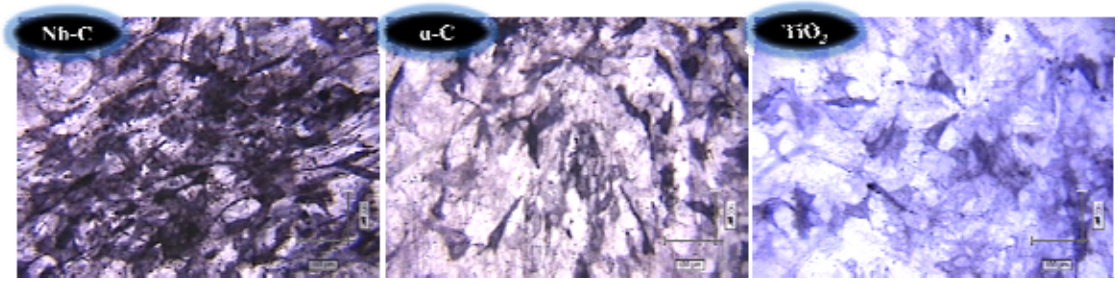

Figure 2.9. ALP staining of cells cultured on the Nb-C (A), a-C (B) and TiO_2 (C) films for 14 days.

The surface properties of orthopedic implants are of critical importance for their success after implantation. Among them, surface chemistry and nanotopograpy have been proved to be especially significant in enhancing the functions of osteoblasts and promoting bone tissue regeneration. (20-22) Therefore, chemical and topographical

modification of the implant surface becomes a dominant approach for improving the biological performance of the implants.(23) In summary, we, in this study, successfully "bioactivate" the bioinert carbon films by the incorporation of Nb. As indicated by the results, the addition of Nb not only changes the surface chemistry of the a-C films, but also leads to the refinement of the nanotopography of the film (**Figure 2.3**.), which are supposed to jointly contribute to the enhancement on the cell adhesion and the increase in the ALP activity. It is known that there is a thin TiO_2 layer caused by the natural oxidation on the outmost layer of the Ti based alloy implants, which can enhance the corrosion resistance and biocompatibility of the implants. (24) Therefore, we choose TiO_2 films as a control group in this study for comparison. Besides the better biological performance, our developed Nb-C films also possess better nano-mechanical properties and comparable corrosion resistance compared to the TiO_2 films. This indicates the potential of the Nb-C nanocomposite films for orthopedic applications.

2.3.4. Conclusions and perspectives

In this study, we incorporated Nb into the a-C films using non-reactive magnetron sputtering to endow inert surface coatings with the ability to activate the functions of bone-related cells. The a-C films show a lower nanoroughness and larger grains, which are increased and decreased, respectively, after addition of Nb. The newly formed Nb-C films show better mechanical properties in terms of nanohardness, Young´s modulus and especially super-elasticity (with around 85% elastic recovery). In vitro cell experiments using preosteoblasts (MC3T3-E1) revealed that the Nb-C films enhance the cellular adhesion and increase the expression of ALP activity of the cells cultured on their surfaces. This study provides a strategy to bioactivate bioinert/biocompatible films that can be used for titanium coatings in orthopedic applications and points out the potential significance of Nb in the enhancement on the bioactivity of the orthopedic implants.

Further work in this area might consider Nb bioactive doping of bioinert ceramics. Beside carbon, there are other inorganic materials exhibiting high strength and biocompatibility, such as alumina or zirconia ceramic. These materials showed a perspective as an implant surfaces, however too high Young's modulus and biointertness limits their use for implant purposes. Coating of titanium with these ceramics may result in optimal elastic modulus while Nb doping can bioactivate the ceramics and additionally influence the surface roughness.

List of references

1. Roach P, Eglin D, Rohde K, & Perry CC (2007) Modern biomaterials: a review-bulk properties and implications of surface modifications. *Journal of Materials Science: Materials in Medicine* 18(7):1263-1277.

2. Dearnaley G & Arps JH (2005) Biomedical applications of diamond-like carbon (DLC) coatings: A review. *Surface and Coatings Technology* 200(7):2518-2524.

3. Tiainen V-M, Soininen A, Alakoski E, & Konttinen Y (2008) In situ surface oxide reduction with pulsed arc discharge for maximum adhesion of diamond-like carbon coatings. *Diamond & Related Materials* 17(12):2071-2074.

4. Yate L, *et al.* (2015) Nb-C nanocomposite films with enhanced biocompatibility and mechanical properties for hard-tissue implant applications. *ACS Applied Materials & Interfaces*.

5. Dalstra M, Denes G, & Melsen B (2000) Titanium-niobium, a new finishing wire alloy. *Clinical Orthodontics and Research* 3(1):6-14.

6. Xu J, *et al.* (2013) Potential Use of Porous Titanium-Niobium Alloy in Orthopedic Implants: Preparation and Experimental Study of Its Biocompatibility In Vitro. *PLoS ONE* 8(11):e79289.

7. Challa VSA, Mali S, & Misra RDK (2013) Reduced toxicity and superior cellular response of preosteoblasts to Ti-6Al-7Nb alloy and comparison with Ti-6Al-4V. *Journal of Biomedical Materials Research Part A* 101A(7):2083-2089.

8. Osathanon T, Bespinyowong K, Arksornnukit M, Takahashi H, & Pavasant P (2006) Ti-6Al-7Nb promotes cell spreading and fibronectin and osteopontin synthesis in osteoblast-like cells. *Journal of Materials Science: Materials in Medicine* 17(7):619-625.

9. Shapira L, Klinger A, Tadir A, Wilensky A, & Halabi A (2009) Effect of a niobium-containing titanium alloy on osteoblast behavior in culture. *Clinical Oral Implants Research* 20(6):578-582.

10. Zhao X, *et al.* (2014) Refining nanotopographical features on bone implant surfaces by altering surface chemical compositions. *RSC Advances* 4(97):54226-54234.

11. Yate L, *et al.* (2014) Tailoring mechanical properties and electrical conductivity of flexible niobium carbide nanocomposite thin films. *RSC Advances* 4(106):61355-61362.

12. Oliver WC & Pharr GM (1992) An improved technique for determining hardness and elastic modulus using load and displacement sensing indentation experiments. *Journal of Materials Research* 7(06):1564-1583.

13. Jung H, Park C, Lee J, & Park YS (2014) Tribological and electrical properties of TiO2 thin films for polymer insulator as the dielectric coating of electric railroad. *Materials Research Bulletin* 58:44-48.

14. Murr LE, *et al.* (2009) Microstructure and mechanical behavior of Ti–6Al–4V produced by rapid-layer manufacturing, for biomedical applications. *Journal of the Mechanical Behavior of Biomedical Materials* 2(1):20-32.

15. Elias CN, Lima JHC, Valiev R, & Meyers MA (2008) Biomedical applications of titanium and its alloys. *JOM* 60(3):46-49.

16. Zheng YF, *et al.* (2011) Introduction of antibacterial function into biomedical TiNi shape memory alloy by the addition of element Ag. *Acta Biomaterialia* 7(6):2758-2767.

17. Olivares-Navarrete R, Olaya JJ, Ramírez C, & Rodil SE (2011) Biocompatibility of Niobium Coatings. *Coatings* 1(1):72-87.

18. Burdick JA & Vunjak-Novakovic G (2009) Engineered microenvironments for controlled stem cell differentiation. *Tissue Engineering Part A* 15(2):205-219.

19. Gittens RA, *et al.* (2013) The roles of titanium surface micro/nanotopography and wettability on the differential response of human osteoblast lineage cells. *Acta Biomaterialia* 9(4):6268-6277.

20. Dohan Ehrenfest DM, Coelho PG, Kang B-S, Sul Y-T, & Albrektsson T (2010) Classification of osseointegrated implant surfaces: materials, chemistry and topography. *Trends in Biotechnology* 28(4):198-206.

21. Wang G, Meng F, Ding C, Chu PK, & Liu X (2010) Microstructure, bioactivity and osteoblast behavior of monoclinic zirconia coating with nanostructured surface. *Acta Biomaterialia* 6(3):990-1000.

22. Yim EK, Darling EM, Kulangara K, Guilak F, & Leong KW (2010) Nanotopography-induced changes in focal adhesions, cytoskeletal organization, and mechanical properties of human mesenchymal stem cells. *Biomaterials* 31(6):1299-1306.

23. Zhao X, *et al.* (2013) Delicate Refinement of Surface Nanotopography by Adjusting TiO2 Coating Chemical Composition for Enhanced Interfacial Biocompatibility. *ACS Applied Materials & Interfaces* 5(16):8203-8209.

24. Velten D, *et al.* (2002) Preparation of TiO(2) layers on cp-Ti and Ti6Al4V by thermal and anodic oxidation and by sol-gel coating techniques and their characterization. *Journal of Biomedical Materials Research* 59(1):18-28.

Chapter 3

Biopolymer coatings for improved titanium implant surfaces

3.1. Motivation

In the natural bone environment, functionality and differentiation of osteoblast cells is a response of the mechanical and bio- morphological properties of the extracellular matrix, a substrate they are adhering onto. Therefore, the efforts to achieve advantageous bioactive implant surfaces are directed to the architectures that closely mimic the environment of the natural bone.

The relatively hard hydroxyapatite bone core is covered by an extracellular matrix (ECM). This matrix has a hybrid hierarchical mesh structure built of protein fibers, e.g. collagen and elastin, providing a scaffold support abundant with topographical information for the cells. The bone's ECM consists of a large number of micro and nanotopographical features, where the collagen molecules forming collagen fibrils with diameters between 260 nm and 410 nm extending for tens of microns in length.(1) The size of the apatite crystals embedded in the collagen fibrils is at the nanoscale level, measuring around 30- 50 nm in length and 20- 25 nm in width.(2) In addition, a large number of nano and submicron pores are featured in the bone ECM structures providing topographical cues to the cells. Beside the chemical and topographical cues, mechanical response of the matrix in means of its stiffness and elasticity has a significant influence for cell activity and function.(3) As cells adhere to substrate, they closely interact with

the ECM by mechanotransduction converting mechanical stimuli to biochemical signals. (4) The local stiffness of ECM that guides the cells is significantly lower than of underlying hard bone, in the range of few kPa. (5, 6) Therefore, higher Young's modulus of biomaterials will determine its long range implementation and while low E values at its surface will influence activity of the cells adhering to the material previous to osseointegration.

Therefore, the surface of the implanted material with its morphological and chemical features will provide the support for cell adhesion and subsequent tissue formation leading to the fixation of the implant in the bone or it will result in immunogenic response causing the rejection of the implant and infections of surrounding tissue.(7-9) Cell adhesion, migration and differentiation can be influenced by modulating the nanoscale substrate topography, i.e. introducing nano and micro features into the metallic or alloy substrate.(10)

Alternatively, the so- called biological approaches can be applied, such as substrate coating with natural polymers. A biological coating introduces a biochemical environment closer to the natural one. Some examples of biological coatings are found in literature and it has been shown, for example, that a modified hyaluronan coating provides titania surfaces with enhanced release of growth factors for activation of bone regeneration.(11) Also, chitosan covalently bound to titanium alloy promotes cell proliferation and collagen fibre deposition. (12)

Collagen and alginate are natural polymers and are approved by the U.S. Food and Drug Administration (FDA) for human use in many types of medical applications. In the last

three decades, they are applied for wound dressings, artificial skin and tissue matrices due to their low inflammatory response and good biocompatibility. (13)

The two biopolymers are exceptional building blocks for the design of biological inspired artificial ECM. Collagen, a main structural protein of the connective tissue, in the form of elongated fibers found in a bone ECM, provides structural and mechanical support to the bone.(14) Alginate is a natural polysaccharide known for its excellent biocompability and for having a degradation rate which depends on its molecular weight, and when incorporated in tissue scaffolds additionally can be tuned by the selection of fabrication methodology.(15-17) The combination of these two polymers in a polyelectrolyte multilayer has already shown high stability and biocompatibility to endothelial cells after crosslinking with genipin, which also lead to the improved cell proliferation.(18)

Titania is a relatively passive surface in regards to polymer adsorption if it is not functionalized with OH- groups by plasma or exposure to UV. This activation enables electrostatic driven deposition of positively charged polymer. Alternatively, silane bonding to titania, which provide charged functional groups, can be used for electrostatic or covalent bonding of polymers. A polymer coating with collagen-hyaluronan was achieved via the so called “covalently modified” layer by layer (LbL) technique.(19) The LbL technique is a simple and straightforward technique for surface functionalisation based on the alternating assembly of polyelectrolytes of opposite charge. The driven force for polyelectrolyte assembly is the electrostatic interaction between polycations and polyanions favoured by entropic considerations. The LbL

assembly results in a polyelectrolyte multilayer with controlled nanoscale thickness and composition on the vertical direction.

In this study we present an approach to assembly collagen-alginate multilayer films on titanium substrates forming a physiologically stable bio- inorganic hybrid interface. This interface matches topographical, mechanical and biological properties of the ECM. For this, we apply LbL assembly combined with biopolymer cross-linking using carbodiimide chemistry onto amino- functionalised titania. The multilayer coatings display high stability in biological fluids and a bioactivity superior to the bare titania surfaces, making them highly attractive for bone tissue engineering.

3.2. Experimental approach

3.2.1. Sample preparation

A semi-transparent, 25 nm thick TiO_2 layer was coated by direct current (d.c.) magnetron reactive sputtering onto glass coverslips (thickness 0.13-0.16 mmand a 50 nm Ti/TiO_2 layer was deposited onto QSX 301 Au quartz crystals. A 2 in. diameter Ti target at a distance from substrate of 30 mm with applied a d.c. power of 228 W at 0.4 Pa was used. The sputtering was performed at a room temperature at a substrate rotation of 80 rpm. TiO_2 was deposited in the argon/oxygen atmosphere generated by combining 10 sccm of argon flow with 20 sccm of oxygen flow for 120 min and Au quartz crystals were sputtered for 150 sec in Ar atmosphere of 24 sccm flow. Surface chemical composition of the films was analyzed by X-ray photoelectron spectroscopy (XPS) after UV-ozone cleaning.

Prior polymer deposition, surfaces were aminosilanised to enable covalent bond between TiO_2 and first layer deposited, alginate. After titania was cleaned for 30 min in 2% SDS, and UV-ozone for 30 min, surfaces were immediately inserted into a 1% solution of (3-Aminopropyl) triethoxysilane (APTES) in toluene. Aminosilanisation was carried out overnight at 115°C, the temperature of boiling toluene. In order to remove excess of APTES, surfaces were cleaned three times in fresh toluene followed by washing three times in nanopure water with sonication and each cleaning cycle lasting 30 min.

Further, polymer films were assembled onto aminosilanised titania surfaces by alternating dipping into polymer solutions with 0.5 mg/mL polymer concentration

starting with alginate dissolved in PBS followed with collagen and alginate in Na acetic buffer at pH 4 up to desired number of layers. For the crosslinking, samples were shortly rinsed in PBS buffer at a pH 7.4 and immersed into EDC/NHS dissolved in PBS buffer at a 6.5:1 mass ratio. After the crosslinking reaction, the samples were rinsed with PBS to remove excess of crosslinker.

Aminoilanisation and polymer deposition were preformed as shown in scheme in **Figure 3.1.**

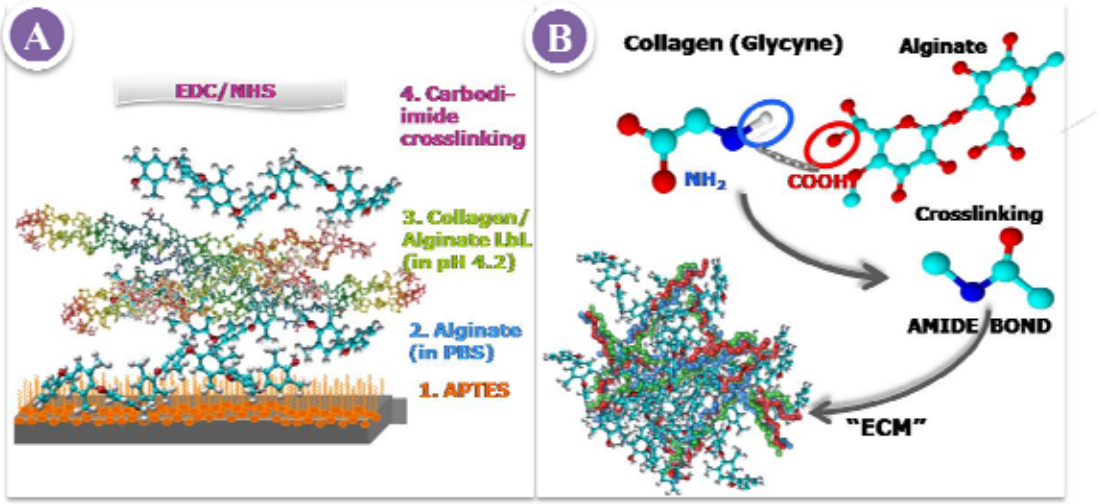

Figure 3.1. Schematic representation of the alginate collagen film assembly in **A** and film crosslinking in **B** to produce an "ECM-like" structure. In a) TiO_2 is first functionalized with APTES and alginate is deposited as first layer in PBS. Assembly of collage/alginate following layers is performed in acidic medium up to desired layer number and film is finally crosslinked according to scheme in B: amino groups of glycine are covalently linked to carboxyl groups of alginate forming amide bonds.

3.2.2. Material characterization

Aminoslianisation of titaia surfaces was confirmed with X-Ray photoelectron spectroscopy (XPS) using Mg kα source. Survey spectra were obtained with pass energy of 30 eV and detailed spectra were acquired for C 1s, O 1s, Ti 2p and N 1s regions with pass energy of 15 eV. Calibration of the binding energies was related to the C 1s CC peak at 285 eV. The in situ assembly of collagen-alginate biofilms was monitored with an E4 QCM on Au quartz crystals were coated with Ti/TiO_2 (50 nm) functionalised with APTES. LbL deposition was monitored by the decrease in the resonance frequency of the quartz crystal. The film assembly and crosslinking in QCM-D chamber was as described for titania coated glass.

Topographical images of bare titania, TiO_2 coated with collagen-alginate before and after crosslinking were obtained by atomic force microscope (AFM) using a Nanowizard II AFM and a Nanoscope V Multimode AFM. Tapping mode imaging in liquid (PBS or Na acetate buffers) was using a DNP-S10A cantilevers (Bruker, Berlin, Germany) with a nominal spring constant 0.350 N/m and resonant frequency at ~13 kHz. In order to measure the height of the films, nanolithography was performed on a Nanowizard II AFM with TESP-V2 cantilever with a nominal spring constant of 40 N/m and the resonant frequency ~130 kHz. Lithography was achieved by defining an area of 8 μm × 2 μm that was rasterized in contact mode at160 μm/s and subsequently imaged. This was repeated several times, until a smooth surface of the substrate could be observed and no increment in the height of the film edges could be seen. After performing nanolithography, tip direction was rotated for 90° to acquire images and measure height profiles.

Film elasticity was determined from the nanoindentation experiments preformed on a NanoWizard II AFM (JPK, Berlin, Germany) acquiring force-distance (f-d) curves in liquid medium. Measurements were performed with a 2 μm borosilicate colloidal probe attached to the cantilever (Novascan Technologies, USA). Cantilever spring constant was calibrated through the thermal noise method in the medium where measurements were preformed (Na acetate and PBS buffers). The cantilever spring constant was determined to be 0.065 N/m. 200 f-d curves were acquired with setpoint forces of 0.5, 0.1 and 0.05 nN over a sample area of 10 μm × 10 μm. For each film, a total of five different sample areas were probed and the resulting data screened and processed using the JPKSPM Data Processing software. The Young's elastic modulus (E) of each film was obtained by fitting the force data in the entire compressive part (curve) of the indentation cycle to the Hertz model (Equation 1), assuming a Poisson ration of 0.40. Further statistical analysis of resulting E values was performed with OriginPro 2015 software.

3.2.3. Cell biocompatibility and bioactivity

Fluoresecence imaging of labelled polymers and cells was performed on confocal microscope. Osteoblast precursor, MC3T3-E1 cells were used to evaluate the biocompatibility and bioactivity of the produced films. Cells were seeded on the samples at a density of 3×104 for proliferation and adhesion experiments. 1 mL cell suspension was added into each well of 12 well cell culture plates. The samples had been placed in the plate wells and sterilized by UV irradiation for 60 minutes prior to cell addition. After culturing for 24 hours, cells were fixed in a 4% paraformaldehyde solution. F-actin, nuclei and focal adhesion of the cells were stained with actin

cytoskeleton and focal adhesion staining kit FAK100.Cell proliferation colorimetric assay was conducted with the Cell Counting Kit-8 (CCK-8), a nontoxic dye used for continuous cell culturing. Colorimetric analysis was performed after 3, 7 and 11 days of cell culturing using a plate reader (GENios Pro, Tecan) equipped with a 450 nm filter.

For alkaline phosphatase (ALP) staining, cells were seeded with a density of 2 × 104 cells/mL. Cells were differentiated in osteogenic medium that is additionally supplemented with a 50 µg/mL of ascorbic acid and 2 mM β- betaglycerophosphate.

After culturing for 12 days in osteogenic medium, cells were fixed with a 4% paraformaldehyde solution, and then, stained with an ALP staining kit (1-Step TM NBT/BCIP, Thermo) for 1 h. ALP area is determined with the MacBiophotonics ImageJ program and further statistical analysis concerning ANOVA analysis is done in OriginPro 2016 software.

3.3. Results and discussion

3.3.1. Biopolymer film fabrication

Multilayer biopolymer films of alginate and collagen were prepared on titania substrates by means of layer by layer (LbL) – electrostatic deposition in acid medium where collagen has a positive charge and alginate maintains negative charge. After multilayer assembly, the film was quickly rinsed with PBS to exchange the acidic medium for physiological conditions and films were finally crosslinked via carbodiimide chemistry. A schematic representation of the procedure followed for film fabrication is shown in **Figure 3.1. A.** In order to enable stable bonding between the TiO_2 surface and the biopolymer film, surfaces were aminosilanized prior to film deposition with APTES providing the surface with NH_2 groups, which are easily bound to the COOH groups of alginate using carbodiimide chemistry. Successful silanization of titania was confirmed by X-ray photoelectron spectroscopy (XPS) as revealed in **Figure 3.2.** In this figure we show a survey surface chemistry spectra of bare TiO_2 (in black) and TiO_2 functionalised with APTES (in red). The inset in the **Figure 3.2.** shows the appearance of a peak at 401 eV, assigned to NH_2 group in nitrogen 1s region for the APTES functionalized TiO_2. (20)

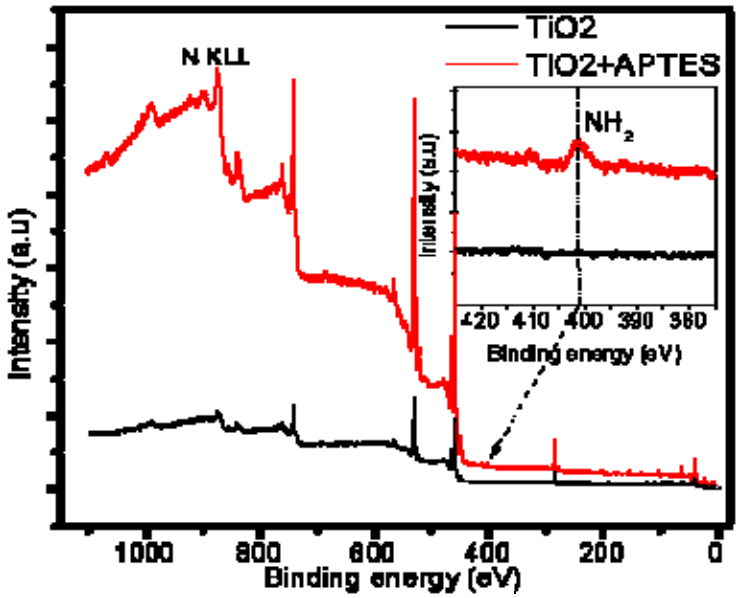

Figure 3.2. XPS survey of APTES on TiO_2 Appearance of the NH2 peak in the N 1s region after APTES functionalization (in red).

The assembly of the biofilm performed without silanization of TiO_2 surface was not stabile in cell culture medium and detached from the substrate (data not shown). This is understandable considering the relatively smooth titania surface used here, which results in a low surface charge density and therefore, does not provide enough OH^- groups for strong electrostatic bonding of the polymers. (21, 22)

The average zeta potential (zP) of alginate is more negative in PBS (-30.0 +/-1.5 mV) than in acetic buffer at a pH 4 (-7.8+/-4.4 mV). This trend for the zP of alginate with increasing in pH is in agreement with a study of Carneiro-da-Cunha et al. where authors investigated influence of pH on zP of polysaccharide solutions.(23) Therefore, the first alginate layer was deposited in PBS buffer followed by the alternating deposition of collagen and alginate in Na acetic buffer at a pH 4 where collagen is dissolved and has a

positive charge. A limitation for the deposition in physiological conditions arises partially from collagen structure; at the isoelectric point, around physiological 7.4, amino acids across collagen molecule have a net charge close to zero. This results in the aggregation of collagen molecules leading to impossibility to be dissolved under these conditions. In acidic pH, on the other hand, the collagen molecules are positively charged and collagen can dissolve in the medium. Therefore, the whole assembly was first performed in acid conditions. To achieve a compact structure and physiologically stable films on titania, we performed the crosslinking of the carboxylic groups of alginate and the amino groups of proline, accessible amino acid of the collagen molecules via cabodiimide chemistry using EDC/NHS as shown in scheme in scheme in **Figure 3.1. B**. Crosslinking resulted in the formation of an amide bond between the two polymers. Prior to crosslinking, films were shortly rinsed with PBS to raise the pH as the NHS ester- activated cross- linker reacts with primary amines in physiological to slightly alkaline conditions. The crosslinking and the changes to physiological pH will result in a fibrillar network structure arising from collagen fibers. Changing the pH from acid to physiological causes the precipitation of the collagen proteins that will then form fibres as the collagen molecule nucleation is pH induced and growth into fibers occurs around pH 7 at concentration of a 0.5 mg/mL used for assembly of these films. (24)

The in situ assembly of the film on an aminosilanized titania surface was followed by means of the quartz crystal microbalance with dissipation monitoring (QCM-D) technique as shown in **Figure 3.3**. The film assembly was followed at 3rd overtone, referred in Figure as “n=3”. In QCM-D experiments the frequency (ΔF) of the crystal

decreases proportionally to the mass deposition.(25) In the experiment shown in the figure, we used a titania covered quartz crystal sensor.

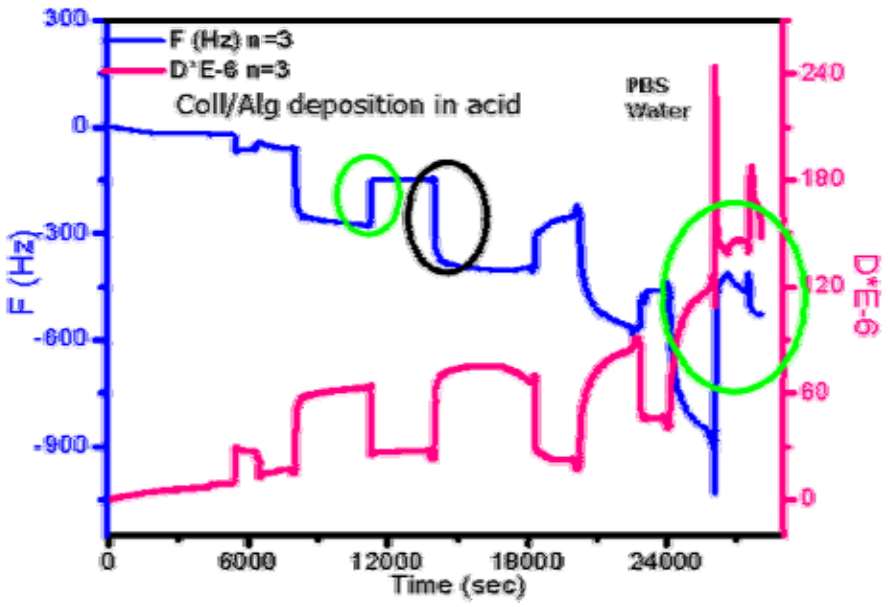

Figure 3.3. In situ Biofilm assembly: Alginate-collagen assembly followed by QCM-D, green circles represent frequency increase after alginate deposition and upon change to PBS and crosslinking at the end, black circle represents change in frequency upon deposition of collagen.

Prior to the QCM-D measurements, crystals were silanized outside of the device. Silanization was not performed in the QCM-D chamber because the toluene solvent used in the process is not compatible with the QCM-D device. In the QCM-D chamber we deposited a film of up to 9 layers observing a decrease in frequency after each collagen deposition ranging between 220 to 310 Hz as noted in black circle in **Figure 3.3.**, but also a relatively high frequency increase of ~ 120 Hz after every deposition of alginate, as indicated in the figure by a green circle on the left. Frequency also largely increases, for ~400 Hz upon pH change to 7.4 followed by crosslinking with EDC/NHS

in PBS as shown in green circle on the right in the graph. Similarly, increase in frequency upon alginate deposition was also observed in the study of Chaubaroux et al. where they followed collagen-alginate assembly on SiO_2 crystals. (18) The frequency increase observed by QCM-D can be indicative of polymer removal but it can also be related to the removal of water in the film and changes in viscoelastic properties of the film associated with the water liberation. A decrease in the water content in the film, which would result in a decrease in frequency, implies a densification of the layers and a more rigid and stable structure. Despite the increase in frequency for alginate, the film assembles as the total frequency continues to decrease with increasing number of layers.

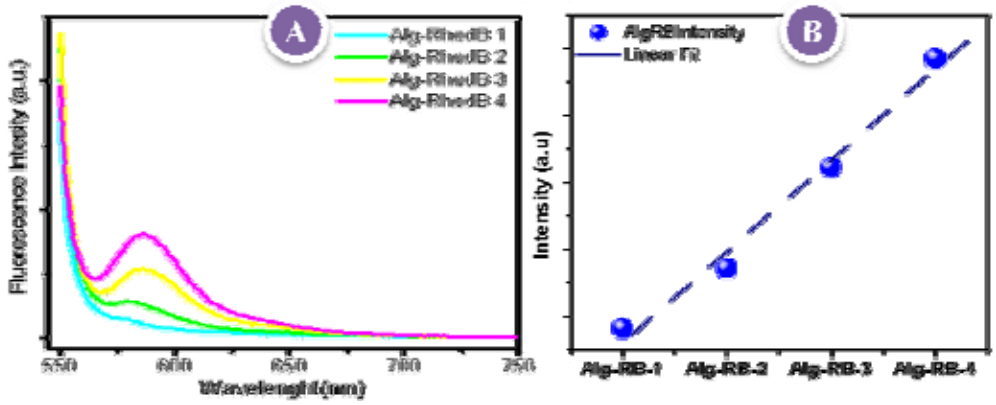

Figure 3.4. Fluorescence emission spectra for films including Rhodamine B-labeled alginate in A. Fluorescence emission is recorded at every step of alginate layer deposition. In B linear increase in Increase in Rhodamine B when plotted maxima from spectra in A, at ~585 nm.

In order to gain more information on the alginate assembly, we assembled Rhodamine B labeled alginate and measured the fluorescent emission spectra after each alginate deposition. In **Figure 3.4. A** we show the fluorescence spectra of the collagen-alginate

film assembled on TiO_2 surface for four depositions of alginate. Fluorescence intensity clearly increases with increasing number of labeled layers. Moreover, the increase of the Rhodamine B fluorescence is linear as shown in **Figure 3.4. B** The fluorescence data here serve as evidence that alginate deposits at each deposition step.

3.3.2. Morphological and mechanical characterization of the biofilms

Further, AFM imaging reveals a fibrillar structure arising from collagen fibers after the crosslinking as seen from the topography image in **Figure 3.5. A**. Bare titania surface on the other hand is relatively flat in comparison to biopolymer coated film, as shown in **Figure 3.5. B**.

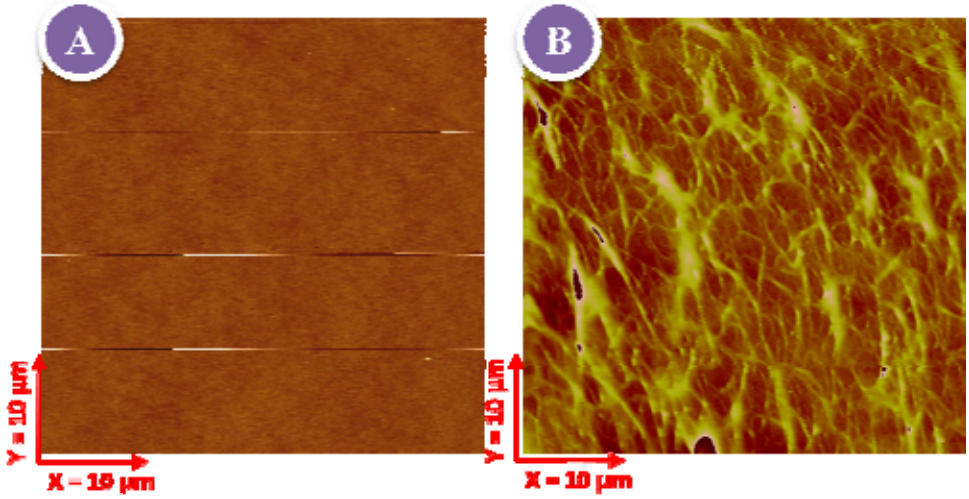

Figure 3.5. AFM images of bare and biopolymer multilayer coated TiO_2. Bare titania is shown in A, presented in B is 9 layer collagen-alginate film deposited on top of a silanized TiO_2 surface.

The height of the film (shown in **Figure 3.6. A**) was 30 nm for 9 layer film assembly. To measure the height, we removed an area of the film revealing the substrate, as

explained in the methods section and determined a z profile of the film from the step separating substrate and film deposited on substrate.

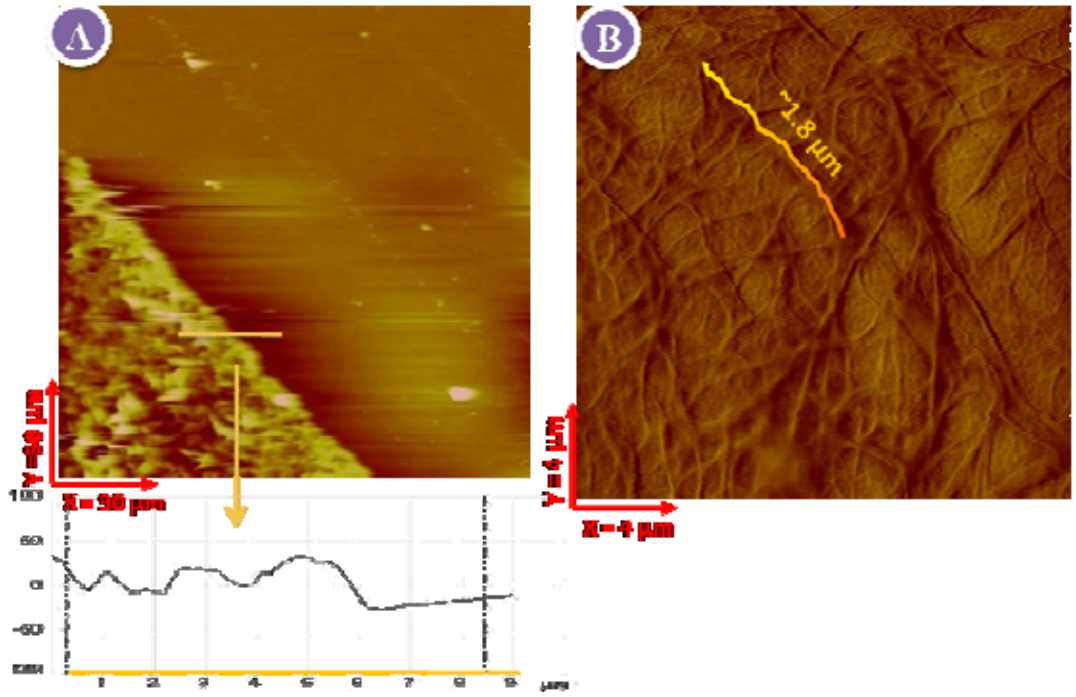

Figure 3.6. Dimensions of film and fibrilar structure by AFM imaging. A height of the 9 layer film is calculated to be on average 30 nm and B phase image of the same film at a higher magnification, showing an example of fiber (in orange) extending to ~ 1.8 µm in length connecting to other fibres.

The diameters of fibers ranged from ~20 to ~120 nm with most of them having diameter of ~50 nm (49.0 +/-27 nm) as calculated for average value. The length of long fibers is in micrometer range, from couple of hundred nanometers to ~3 µm and the distance between two parallel fibers vary from ~100 nm to ~600 nm. The length can be seen clearly on a phase AFM image as shown in **Figure 3.6. B.** The fibrillar network presented in this work reassembles the topology of the natural ECM, which is reported to be formed by fibers with roughly 50 nm in diameter and with lengths of several

micrometers.(26) The coating based on our strategy gives more compatibility to the implant material as we will show later in the manuscript.

Prior to access the biocompatibility and bioactivity tests, structural changes upon pH switch and crosslinking were investigated with AFM. In **Figure 3.7.** we show a 4 layer film assembled in acid before pH changes and crosslinking.

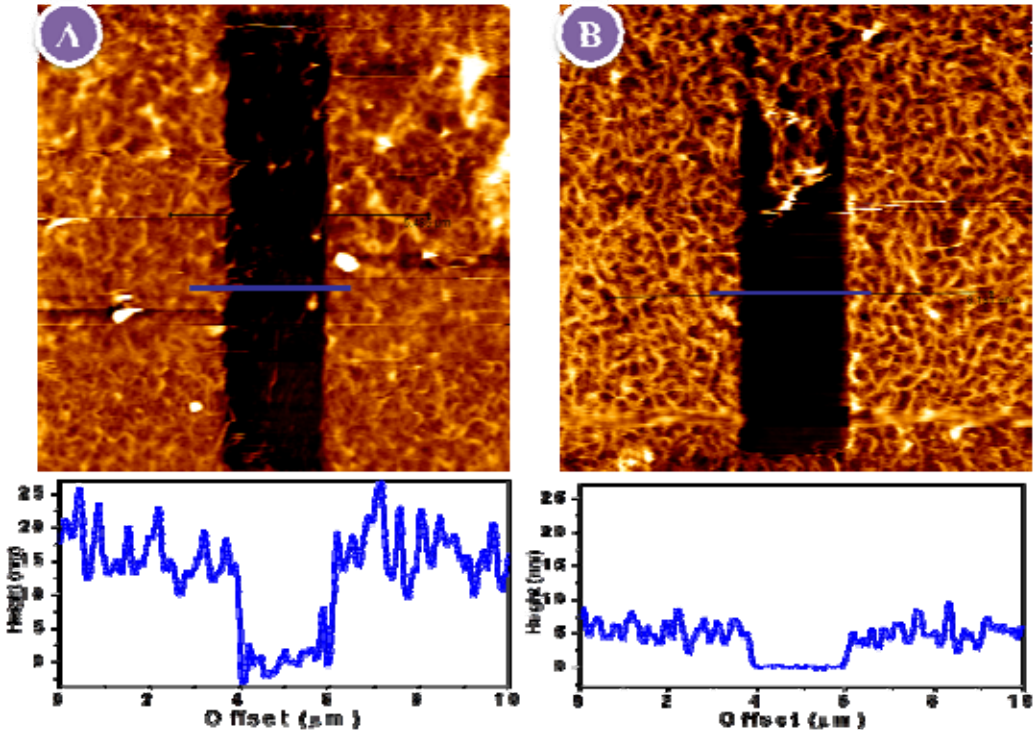

Figure 3.7. AFM topography and height profile. 10 x 10 µm performed by JPK. Topography of 4 layer films prepared as A LbL, in acid medium and B after crosslinking imaged in PBS. Bottom panels are height profiles measured at a cross section indicated in a figures A and B.

This assembly has some network like structure but during imaging we could notice a "wobbly" structure where the features of the film are drifting with tip during scanning even by use of very soft tip, implying film of limited stability. However, the height of

this film before crosslinking is three times larger than after the crosslinking. A thickness of approx. 15 nm was measured for the LbL assembled film and of ~ 5 nm for the crosslinked one, as shown in **Figure 3.7.** After crosslinking, we observed a more pronounced fibrillar structure (**Figure 3.7. B**) and no drifts of film features during imaging. We can conclude that crosslinking induces a more stable and compact film, developing the fibrillar structure.

Film mechanics was further investigated by nanoindentation and by measuring the Young's elastic modulus that can allow us to correlate elastic properties to changes in the structural and morphological properties of the films. The Young's modulus (modulus of elasticity, E) was determined using atomic force spectroscopy (AFS) measuring the force applied by the tip of a cantilever as a function of its indentation into the sample resulting in force distance (F-d) curves. Experiments were conducted with a colloidal probe and the resulting F-d curves were fitted with the Hertz model (**Equation 3.1.**) that best describes our system, considering non-adhesive elastic contact between a stiff sphere and an elastic surface.

$$F = \frac{4}{3}\frac{E}{(1-\nu^2)}\sqrt{R}\,(\delta_0 - \delta)^{\frac{3}{2}} \qquad \textbf{Equation (3.1.)}$$

Equation 3.1. Hertz model describing the indentation of a relatively flat surface with a rigid sphere where E= Elastic modulus (Young's modulus, E), R= radius of the sphere, v= Poisson's ratio and δ= indentation depth.

We consider that our evaluation of the elastic modulus is a rational approximation concerning numerous assumptions and variables introduced in the experimental setup

and analysis. These variables are for example the size and shape of the probe, loading force and further analytical variables such as fixing contact point and baseline or Poisson ratio used to fit the curves to the model. However, under the same experimental parameters and equal approach to curve fitting for two samples, we can compare their E values and estimate their relative elastic properties. In order to decrease the variability coming from uneven topography and to improve quality of the results, force curves were collected on rather large statistical population of at least 500 curves across different sample areas. Representative f-d curve for experiments conducted on these films are shown in **Figure 3.8.**

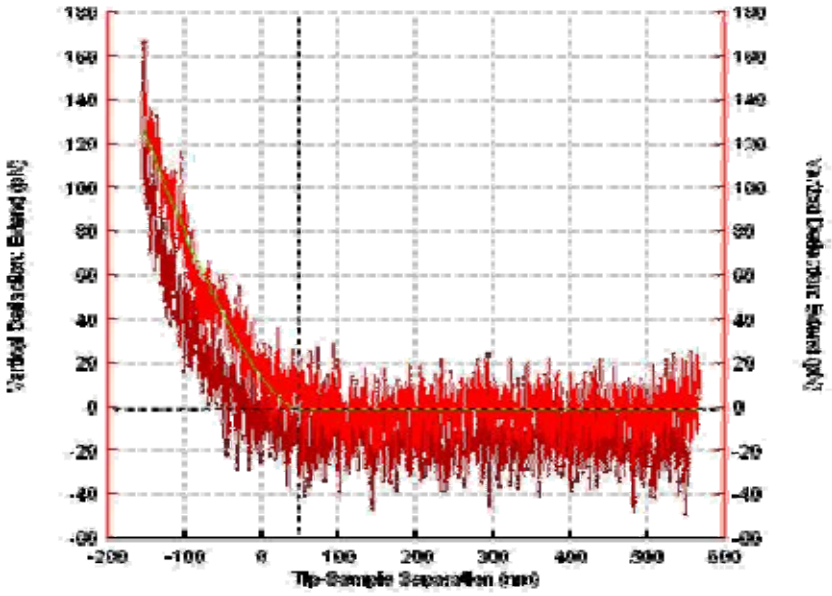

Figure 3.8. AFS typical f-d curve, raw data fit. Bright red is the approach curve and dark red is the retract curve in the cycle.

Figure 3.9. shows E values for two sets of films; 5 layer films where alginate is deposited as a last layer (**Figure 3.9 A**) and 6 layers with collagen as a last layer in **Figure 3.9 B**. Mean E values between these 2 sets are quite similar resulting in an E

value of ~ 35 kPa for LbL deposited films and ~ 10 kPa for crosslinked with a higher error for non-crosslinked (LbL) films.

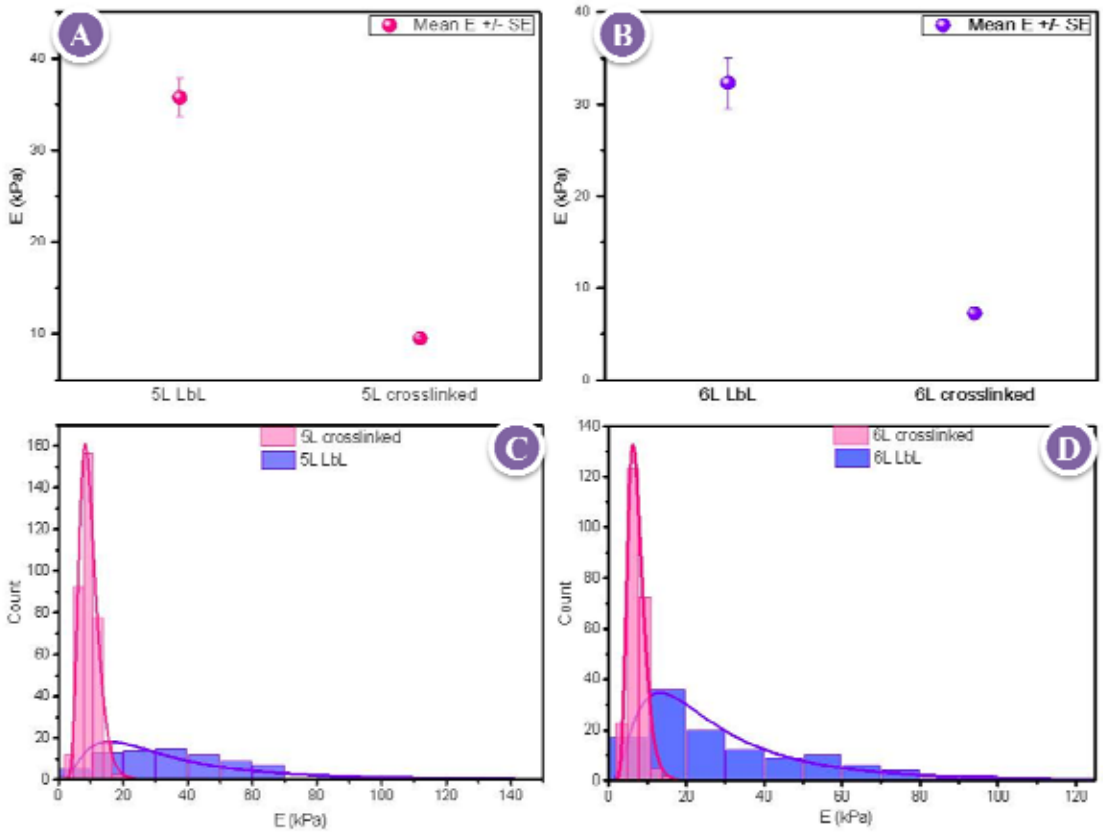

Figure 3.9. Young´s modulus (E) of biofilms before and after crosslinking. Mean E for A films consisted of 5 layers and for B 6 layer films, measured with a loading force 0.5 nN. Error bars are representing standard error of the mean value. In A the E values correspond to 5 layer films with alginate as a last layer and in B to 6 layer films where collagen is deposited as a last layer. Distribution of Young's modulus for C films with alginate deposited as a last layer and D collagen deposited as a last layer. Distribution curves are Lognormal fit to the histograms of apparent Young's modulus.

E values themselves are in a nice agreement with the literature for collagen fibers.(5) but as well our data are agreeing with elasticity of soft bone tissue of 25-40 kPa.(6) From the results shown here, we can drive two conclusions. Crosslinked films, though

visualized as a more compact structure, have lower apparent Young's modulus than the ones assembled by LbL in acid. Since the calculation of the elastic modulus of thin films based on AFS is typically affected by the characteristics of the substrate on top of which the film is assembled, the so called "substrate effect" our results are unexpected. As titania has a Young's modulus of 200-300 GPa, one would expect that given the decrease in height of the crosslinked film the apparent E would be much more significantly affected by the substrate underneath. Nevertheless, even though the thinner, crosslinked films showed lower apparent elastic modulus. This can be considered as an indication that crosslinking significantly altered the mechanical properties of the multilayers. Furthermore, we observe this behavior in both 5- and 6-layer films. Since crosslinking will lead to increased coupling between polymer fibers, we can expect that upon indentation a significant fraction of the energy dissipation will be converted into tensile load across the fibers (and associated elastic response) rather than in dislodging them from their resting position. We can expect the inverse tendency in the case of LBL films, which can make them more susceptible to the "substrate effect", leading to an increase in the apparent elastic modulus. The decrease in the apparent E for the crosslinked film can be explained by a tighter mechanical coupling between individual fibers.

Another conclusion that we can draw is that the film is highly homogeneous. This is manifested in the standard deviation of the mean E value (distribution curves in **Figure 3.9 C and D**). Wider distribution of E values in the case of the LbL films indicates less homogeneous coating due to variability in the indentation curves across the sample

while crosslinked films seems to be more homogeneous regarding their elastic properties.

3.3.3. Biocompatibility and bioactivity of the biopolymer films

Once the stable films on titania were prepared and characterized, their biocompatibility was evaluated by investigating the influence of the films on cell adhesion and proliferation in the experimental section. Additionally, we have studied the impact of the coatings on cells measuring the cellular ability to deposit mineralized tissue. Biological evaluation reveals important information on how the osteoblast cells interact with the biopolymers. First, we used CLSM to visualize the structure of the films assembled by Rhodamine B labelled alginate and FITC labelled collagen films. As seen in **Figure 3.10. A**, collagen shows a pronounced fibrillar structure, while alginate is homogeneously distributed over the film.

In the **Figure 3.10. C** we merged the Rhodamine B channel with the transmission light channel used to visualize pre-osteoblast cells, we noticed that the areas of high intensity of rhodamine labelled alginate overlays in space with the cell nuclei. This is, however, not the case with collagen for which we did not observe the cells following the path of the collagen fibers.

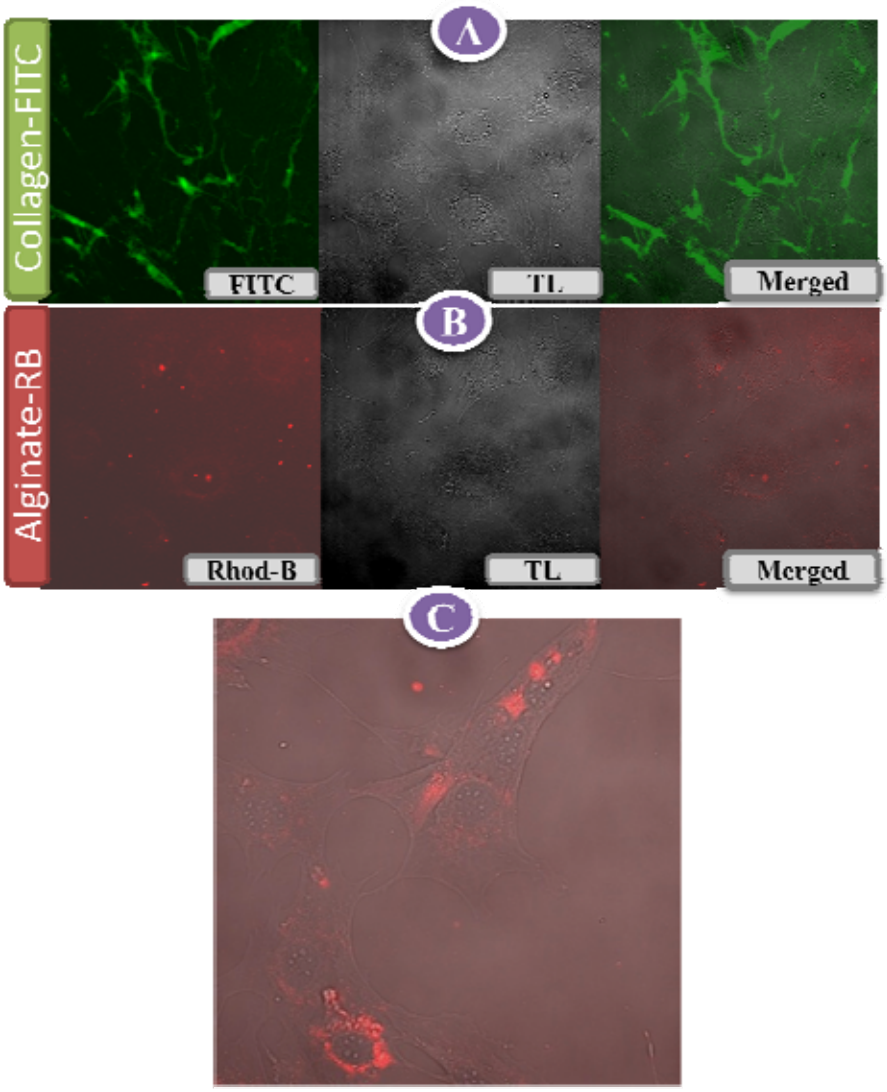

Figure 3.10. 3D structure of films by CLSM. **A** 4 layer film prepared with collagen-FITC and non-labeled alginate, collagen is deposited as last layer and **B** 5 layer film prepared from non-labeled collagen and alginate-labeled with Rhodamine B, with alginate being the last deposited layer. Pre-osteoblast cells are incubated for 24 hours on top of the films and shown in transmission light (TL) channel, while merged TL with fluorescent channel is shown in last panel. 40 x magnification images have a size of 225 x 225 micrometers. In **C** is shown Confocal image of Pre-osteoblast cells exposed to Alginate- RhodamineB. Fluorescence is clearly concentrated around cell nuclei. For this experiment, solution of Alg-Rhodamine B in PBS was mixed with cells and left to incubate 24 hours in tissue culturing well.

Results of the proliferation tests are shown in **Figure 3.11.** Cells proliferate over the whole incubation period on all the samples. There is no significant difference in the proliferation rate of the cells cultured on bare titania, with the film with collagen as the last layer and films with alginate as the last layer, indicating that the biocompatibility of the assembled films is comparable to the bare titania film. From this result, we can conclude that the coated films promote proliferation of osteoblast cells as well as titania do, which is known for its biocompatibility.

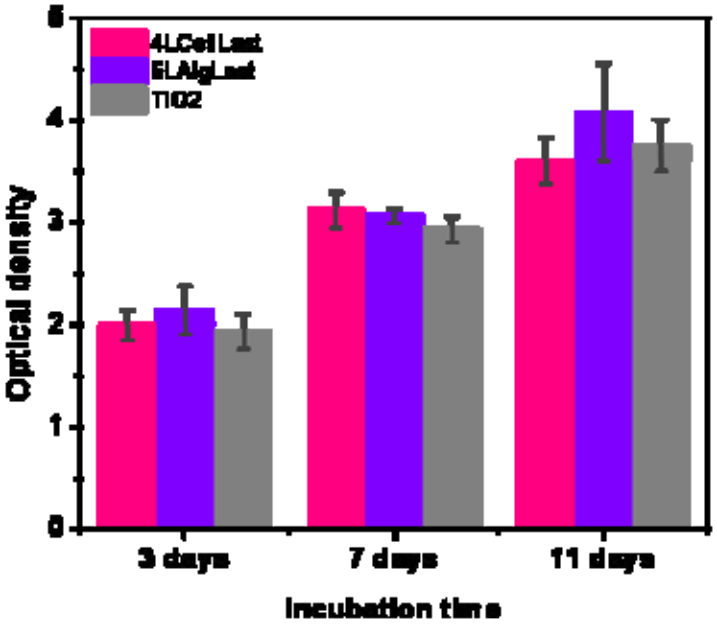

Figure 3.11. Proliferation of pre-osteblast cells cultured on a 4 layer collagen-alginate film with collagen deposited as a last layer (pink), 5 layer film with alginate deposited as a last layer (purple) and bare TiO_2 serving as a control (gray).

The biopolymer coating is expected to have however an impact on cell functions, especially on cellular adhesion. The initial adhesion of cells on biomaterials is a key

regulator of cell proliferation, migration and differentiation, which lately determines the fate of the biomaterial.

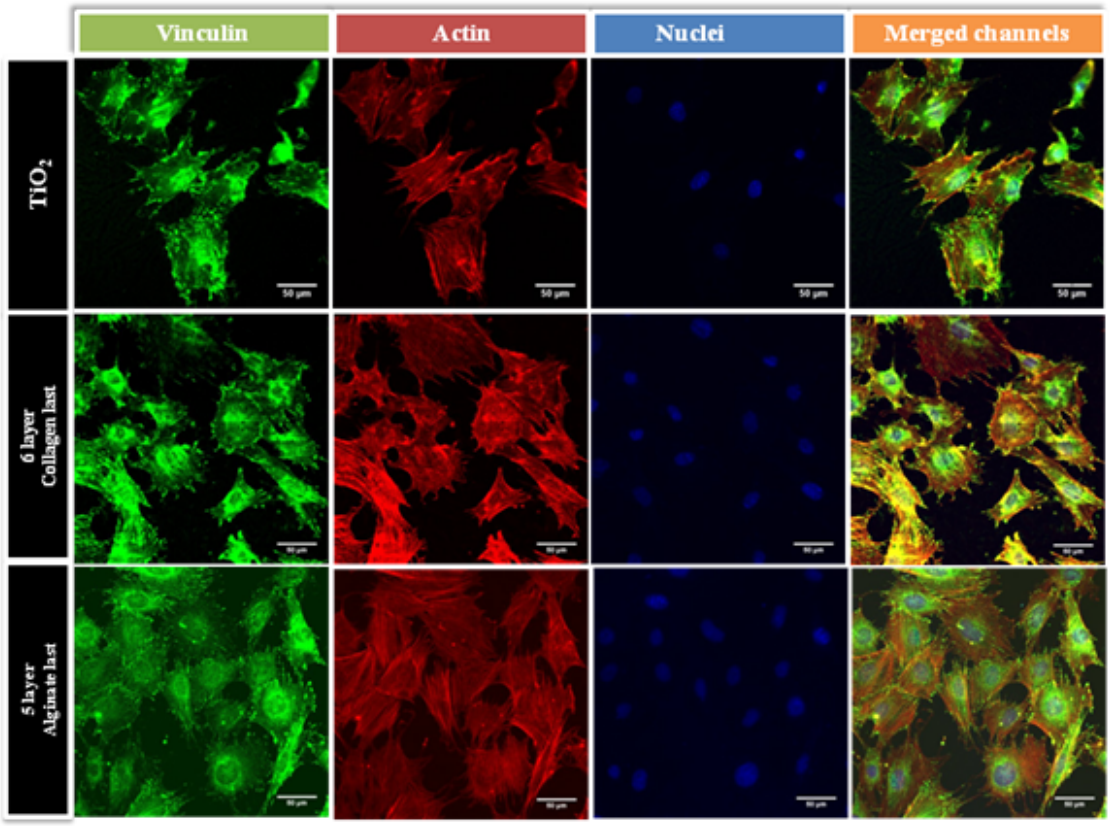

Figure 3.12. CLSM images of focal adhesion and nucleus staining after 24 hours. In first row is shown titanium control sample, second row represents 6 layer film with collagen last layer and shown in last row is staining of 5 layer film with alginate last layer. Green channel is vinculin staining, red actin, blue nucleus and last panel are all channels merged into one. 40x magnification.

Presented in **Figure 3.12** osteoblast cells were cultured on titania coated with collagen-alginate 6 layers film with collagen as the top layer, and collagen- alginate 5 layer film with alginate as the top layer to evaluate the individual effects of collagen and alginate on the adhesion of osteoblasts. Cells were cultured on bare titania as a control sample

shown in first row of **Figure 3.12.** Cells staining of Vinculin (green), F-actin (red) and nucleus (blue) are shown in the first, second and third panels, respectively, and merged channels are shown in the last panel.

On average, cells cultured on bare titania are smaller and less numerous than those cultured on alginate- terminated films. They also show a diffuse cytoskeleton with less stress fibres in their cytoplasm as observed in the images of F-actin staining. In the images showing vinculin staining, more green spots can be seen at the border of the cells cultured on the film with alginate as a last layer compared to the cells cultured on film with collagen as a last layer. We can also distinguish more peri-nucleus regions displaying a bright green color in the cells cultured on the film finishing with alginate. From the images of F-actin, in red channel, we appreciate that cells cultured on the films with last layer alginate are somewhat larger in size and show a rearranged cytoskeleton with distinctive stress fibres inside the cytoplasm. On average, cell number on biofilm coated films is higher than on bare titania, as shown in **Figure 3.13**, where there is 50% cells more on multilayer terminated with alginate in comparison to cell number on titania.

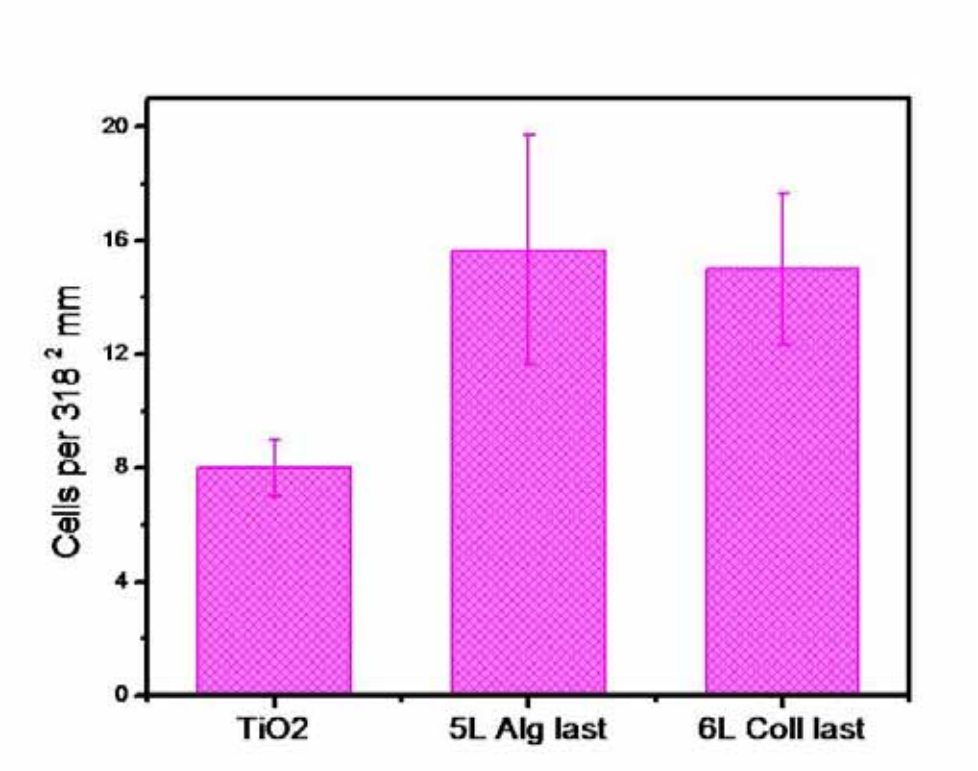

Figure 3.13. Average osteoblast cell number after 24 hours of incubation in osteogenic medium. Average number is calculated from three samples and cell counts are expressed as cell per area of 318x318 μm

One would expect that alginate decreases cell adherence as it is known to have antifouling properties and limited interaction with cells. However, it is necessary to bear in mind that the properties of layer by layer films are a combination of those of both the cationic and anionic polymers. In the particular case of using fibers like collagen and a lineal polymer like alginate the assembly of the alginate at each layer deposition is restricted to the collagen fibers, which do not form an homogeneous structure. Because of geometrical consideration each deposition of collagen will result in a different arrangement of fibers and each layer of alginate will deposit on the surface of the fibers. In these conditions there will only be one layer of alginate on top of each collagen layer

and consequently the alginate will not form a dense coating on the collagen fibers. If the alginate is not covering the fibers homogeneously we can expect that the antifouling action be limited. Most likely cells will sense the collagen as well, which will probably contribute to cell adherence. The improved cell adherence with alginate as top layer over the adherence with collagen as top layer must be related to the alginate uptake by the cells.

Finally, we have evaluated the alkaline phosphatase (ALP) activity of the differentiating osteoblast cells on the crosslinked films and titania.

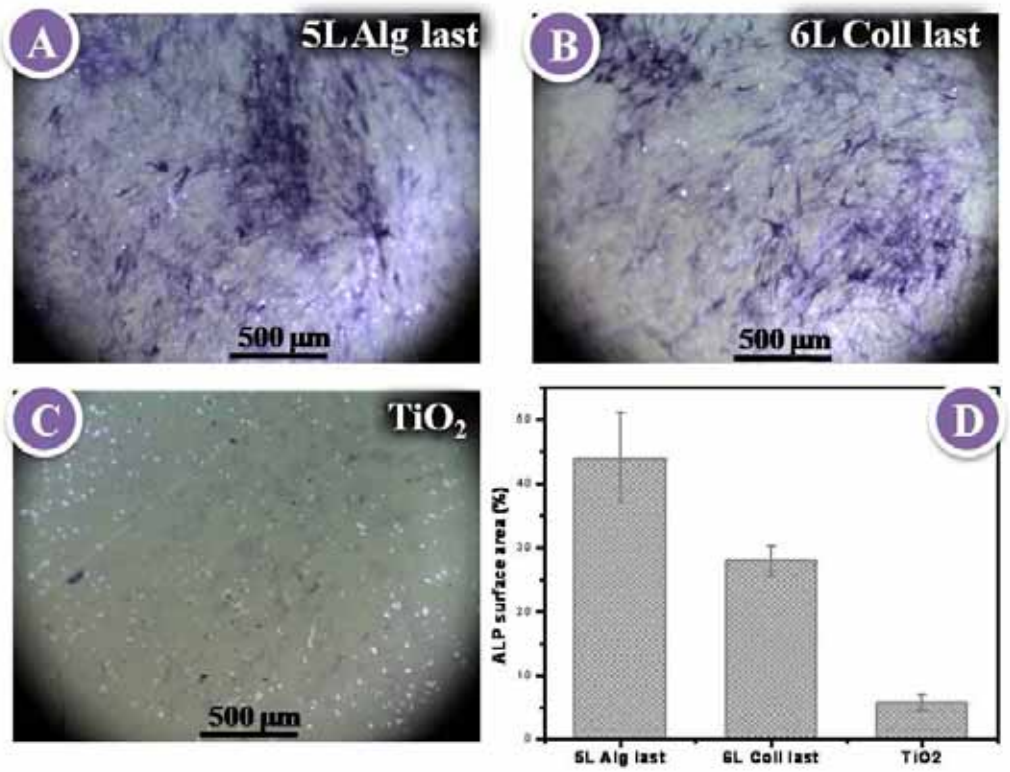

Figure 3.14. ALP activity of osteoblast cells after 12 days of mineralization. Images of ALP staining for osteoblast 12 days cultured on **A** 5 layer alginate terminated coating, **B** 6 layers coated titania terminated with collagen and in **C** TiO_2 control sample. In **D** is shown ALP staining of osteoblasts, expressed as ALP stained surface area.

ALP activity is used as a gene marker in the early stage of the osteogenic differentiation and their ability to deposit mineralized tissue. Optical images of ALP stained osteoblast after culturing in osteogenic medium for 12 days are shown in **Figure 3.14 A, B** and **C** for alginate terminated film, collagen terminated film and bare titania as a control sample. Cells cultured on the coated titania after staining exhibit more of darker blue-purple color, compared to cells cultured on the TiO_2. These results indicate that the cells cultured on the multilayer coated titania have enhanced ALP activity implying the positive effects of biopolymers on the osteoblast differentiation and mineralization ability. The staining was quantified by measuring the ALP positive area (**Figure 3.14 D**). Area quantification shows that ALP on samples with alginate as top layer is 9 times larger than on bare titania while on collagen terminated films this increase is 6 times larger than titania. Our results show a positive effect of the films on mineralization and in agreement with the adhesion experiments show a better performance when alginate is the top layer.

The observation that alginate results in a better cell functionality correlates with the uptake of alginate, which is not observed when collagen is the top layer. Alginate, an anionic polysaccharide, could serve as energy source for the cells when degraded to monosaccharides.(27) Alginate degradation is slow in physiological conditions but since we have assembled alginate at pH 4 the molecule maybe partially hydrolyzed when is uptaken by the cells. (28) It may also be that there is a specific effect of alginate in the functionality of osteoblasts, which has not been reported before. Further biological studies should be conducted to understand the relation between an improved functionality in osteoblasts and alginate uptake.

These results indicate that the cells cultured on the crosslinked biofilm coated titania have enhanced ALP activity implying the positive effects of biopolymers on the osteoblast differentiation and mineralization ability.

3.4. Conclusions and perspectives

In this work we reported on the development of highly biocompatible coatings on aminosilanised titania substrates via layer by layer assembly of natural polyelectrolytes, collagen and alginate. LbL assembly was conducted at low pH followed by a reversal of pH to more basic media and crosslinking by carbodidimide chemistry. This result in a compact fibrillar structure that morphologically and chemically mimics bone's extracellular matrix that can be used to enhance biocompatibility of currently used titania implant material. Stability and morphology characterisation of the coatings revealed highly stable coatings with mechanical properties comparable to the naturally occurring collagen in the bone matrix. We found that these coatings enhanced the adhesion and mineralization of osteoblast cells compared with the bare titania surfaces with a superior adhesion and activity onto the alginate- terminated films. Ultimately, we have presented a strategy for the assembly of biocompatible and stable coatings based on two natural molecules on top of the clinically relevant titania substrate mimicking ECM structure with bioactive properties greater than on bare titania and showed the potential of the coating to overcome the bodily implant rejections.

The application of these natural coatings shown in this chapter can be further directed in implementation of essential strontium and its release trough these films with aim of therapeutic effect on the bone remodeling. In next chapter it will be discussed on the enhanced bioactivity of titanium substrates with strontium entrapped into the surface. Additionally, our preliminary data obtained from electrochemical studies showed that release of small ions trough these biopolymer films can be tuned with number of

polyelectrolyte layers and addition of lipid structures. As it will be shown in next two chapters, the amount of strontium can be tuned on titania surface with different approaches. One is complexation of strontium in the polymer brushes bound to titania with promising therapeutic effect on the bone tissue deposition. Thus, further work that combines titania functionalized with polymer brushes- strontium complex and collagen alginate coatings may result in superior implant interfaces with dual activity; enhanced osseointegration of implant substrates and therapeutic effect that accelerates bone healing.

List of references

1. Bettinger CJ, Langer R, & Borenstein JT (2009) Engineering substrate topography at the micro- and nanoscale to control cell function. *Angewandte Chemie (International ed. in English)* 48(30):5406-5415.

2. Palmer LC, Newcomb CJ, Kaltz SR, Spoerke ED, & Stupp SI (2008) Biomimetic Systems for Hydroxyapatite Mineralization Inspired By Bone and Enamel. *Chemical Reviews* 108(11):4754-4783.

3. DeSimone DW, Mecham RP, Choi Y, Holle A, & Engler A (2013) Engineered ECM Microenvironments and Their Regulation of Stem Cells. *Extracellular Matrix in Development,* Biology of Extracellular Matrix, (Springer Berlin Heidelberg), pp 133-160.

4. Bhatia SK, Mason B, Califano J, & Reinhart-King C (2011) Matrix Stiffness: A Regulator of Cellular Behavior and Tissue Formation. *Engineering Biomaterials for Regenerative Medicine*, (Springer New York), pp 19-37.

5. Zhu Y, Dong Z, Wejinya UC, Jin S, & Ye K (2011) Determination of mechanical properties of soft tissue scaffolds by atomic force microscopy nanoindentation. *Journal of Biomechanics* 44(13):2356-2361.

6. Lv H, *et al.* (2015) Mechanism of regulation of stem cell differentiation by matrix stiffness. *Stem Cell Research & Therapy* 6(1):103.

7. Wang G, Moya S, Lu Z, Gregurec D, & Zreiqat H (2015) Enhancing orthopedic implant bioactivity: refining the nanotopography. *Nanomedicine (London)* accepted.

8. Li D, *et al.* (2012) Role of mechanical factors in fate decisions of stem cells. *Regenerative medicine* 6(2):229-240.

9. Watt FM & Huck WTS (2013) Role of the extracellular matrix in regulating stem cell fate. *Nat Rev Mol Cell Biol* 14(8):467-473.

10. Yate L, *et al.* (2015) Nb-C nanocomposite films with enhanced biocompatibility and mechanical properties for hard-tissue implant applications. *ACS Applied Materials & Interfaces*.

11. Berts I, Ossipov D, Fragneto G, Frisk A, & Rennie AR (2014) Polymeric Smart Coating Strategy for Titanium Implants. *Advanced Engineering Materials* 16(11):1340-1350.

12. Lin H-Y & Chen J-H (2013) Osteoblast differentiation and phenotype expressions on chitosan-coated Ti-6Al-4V. *Carbohydrate Polymers* 97(2):618-626.

13. Rowley JA, Madlambayan G, & Mooney DJ (1999) Alginate hydrogels as synthetic extracellular matrix materials. *Biomaterials* 20(1):45-53.

14. Muiznieks LD & Keeley FW (2013) Molecular assembly and mechanical properties of the extracellular matrix: A fibrous protein perspective. *Biochimica et Biophysica Acta (BBA) - Molecular Basis of Disease* 1832(7):866-875.

15. Park H, *et al.* (2008) 19 - Alginate hydrogels as matrices for tissue engineering. *Natural-Based Polymers for Biomedical Applications*, (Woodhead Publishing), pp 515-532.

16. Jinchen S & Huaping T (2013) Alginate-Based Biomaterials for Regenerative Medicine Applications. *Materials* 6:1285-1309.

17. Kong HJ, Kaigler D, Kim K, & Mooney DJ (2004) Controlling Rigidity and Degradation of Alginate Hydrogels via Molecular Weight Distribution. *Biomacromolecules* 5(5):1720-1727.

18. Chaubaroux C, *et al.* (Collagen-Based Fibrillar Multilayer Films Cross-Linked by a Natural Agent. *Biomacromolecules* 13(7):2128-2135.

19. Ao H, *et al.* (Fabrication and in vitro evaluation of stable collagen/hyaluronic acid biomimetic multilayer on titanium coatings.

20. Beamson G & Briggs D (1992) *High Resolution XPS of Organic Polymers - The Scienta ESCA300 Database*, (John Wiley and Sons, Chichester).

21. Diebold U (2003) The surface science of titanium dioxide. *Surface Science Reports* 48(5â€“8):53-229.

22. Borghi F, Vyas V, PodestÃ A, & Milani P (2013) Nanoscale Roughness and Morphology Affect the IsoElectric Point of Titania Surfaces. *PLoS ONE* 8(7):e68655.

23. Carneiro-da-Cunha MG, Cerqueira MA, Souza BWS, Teixeira JA, & Vicente AA (2011) Influence of concentration, ionic strength and pH on zeta potential and mean hydrodynamic diameter of edible polysaccharide solutions envisaged for multinanolayered films production. *Carbohydrate Polymers* 85(3):522-528.

24. Wood GC (1960) *The formation of fibrils from collagen solutions. 2. A mechanism for collagen-fibril formation* pp 598-605.

25. Kanazawa K & Cho N-J (2009) Quartz Crystal Microbalance as a Sensor to Characterize Macromolecular Assembly Dynamics. *Journal of Sensors* 2009.

26. Lodish H, *et al.* eds (2000) *Molecular Cell Biology, 4th edition* (W. H. Freeman, New York), Vol 4th edition.

27. Hillis DM, Sadava DE, Heller HC, & Price MV (2011) *Principles of Life* (Macmillan Higher Education, London, England, London).

28. Holtan S, Zhang Q, Strand WI, & Skjak-Braek G (2006) Characterization of the hydrolysis mechanism of polyalternating alginate in weak acid and assignment of the resulting MG-oligosaccharides by NMR spectroscopy and ESI-mass spectrometry. *Biomacromolecules* 7(7):2108-2121.

Chapter 4

Superior osseo- activity on TiO_2 via polymer brush-strontium coatings

4.1. Motivation

Bone is an exceptional tissue possessing unlimited capacity for renewal and repair through the dynamic process of bone remodeling. This process maintains the surface and the bone topographical properties, which in turn establishes bone strength and proficiency. The bone remodeling cycle involves the removal of mineralized bone by osteoclasts followed by the formation of bone matrix through osteoblasts that subsequently becomes mineralized. As shown in scheme in **Figure 4.1**, there are three consecutive phases in the remodeling cycle: resorption, during which osteoclasts digest old bone; reversal, where mononuclear cells appear on the bone surface; and formation, when osteoblasts deposit new bone until the resorbed bone is completely replaced. (1)

The most important consequence of a disruption in the process of bone remodeling is the bone loss and the microtopographical damage resulting in bone thinning and loss of trabecular (spongy) bone tissue. An unbalanced process of bone resorption and bone formation represents the essence of bone material loss pathogenesis.

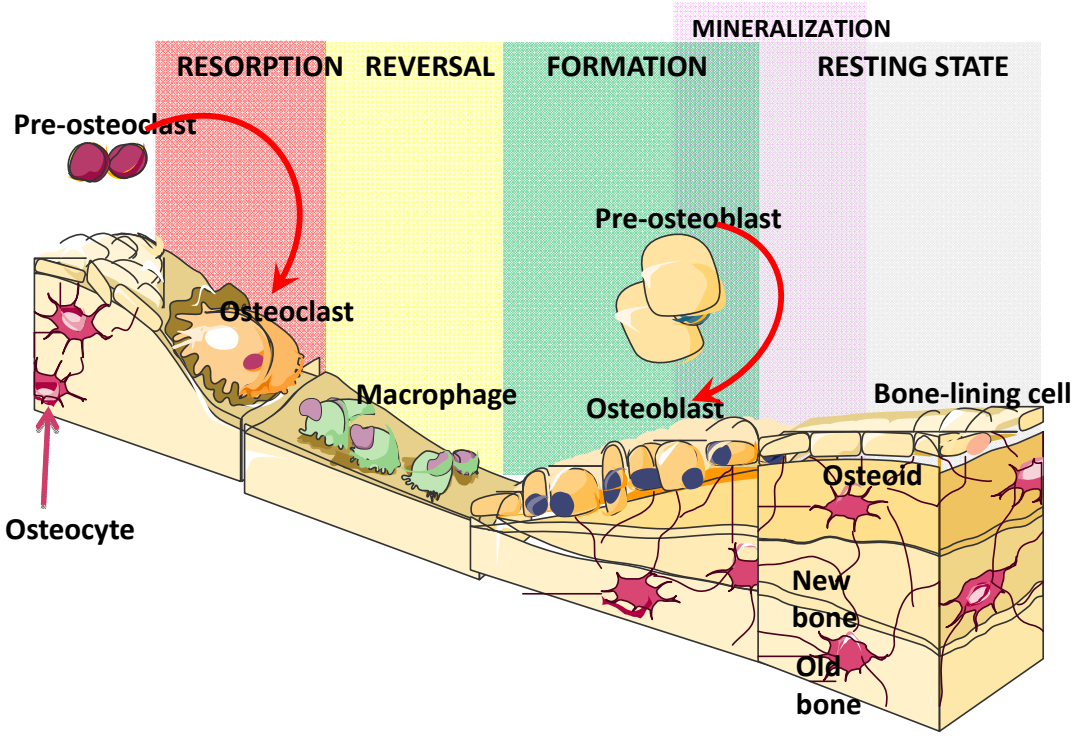

Figure 4.1. Schematic representation of the bone remodeling cycle. Osteoclast, differentiated from pre-osteoclast, resorb the old bone tissue. Next phase is reversal where macrophages appear on the surface. Final phase, formation, is liability of osteoblasts where the new bone formation starts from the production of an organic matrix of collagen followed by calcium and phosphates deposition forming a strong and dense mineralized tissue.

An unbalanced remodeling cycle influences as well the failure of the implant osseointegration at the site of injury or implantation. In an early stage of implantation, the implant may become instable before new bone formation trough the rapid resorption of remnant bone. In the case of revision implant surgeries, bone grafts are often necessary to transplant bone tissue and to achieve instant implant stability. These bone grafts can be fast resorbed by osteoclast and leave instable prosthetic devices and inviting additional treatments and more surgeries (2).

Strontium plays a major role in new bone formation slowing the process of old bone breakdown and thus impacts on bone density. The effect of strontium on the cellular level is to increase the pool of active osteoblasts and decrease the number of less active osteoclasts (3-6). The absorption efficiency of strontium is age-dependent and is in competition with calcium due to their similar chemical nature. Almost all the absorbed strontium (99.1%) is deposited in bone, mainly in newly formed bone (7). Several studies have proved that strontium can stimulate the extracellular calcium- sensing receptor, CaSR, situated in the membrane of osteoblasts and osteoclasts (8-10). In this way, strontium positively influences osteoblasts activity trough calcium receptors. It has been shown that strontium induced osteoblast proliferation, differentiation and mineralization by activating the CaSR, thus hinting that the therapeutic efficacy of strontium may be partly mediated by the CaSR (11). There are also other possible extracellular receptors of strontium, such as the GPRC6A that senses extracellular divalent cations (12).

Therapeutic applications of strontium by means of strontium renalate (SrRan) is for long time in clinical use as an exclusive drug that promotes bone healing in osteoporosis (13). Strontium ranelate increases in vitro osteoblast differentiation, activity and survival (8, 14). On the other hand, it decreases osteoclast differentiation and activity, while increasing their apoptosis (15).

This drug has also contributed to the increase of mechanical fixation of the implants when taken orally (16, 17). In the study of Maimoun et al, titanium was implanted in rodents that received strontium renalate orally. The osseointegration of the implants was significantly higher compared to control animals that received no SrRan (18). However,

since 2013 the use of SrRan is greatly restricted due to a high risk of myocardial infarction and other serious risks such as blood clots and rare skin reactions. (19)

Other drawbacks in the use of SrRan come from the possible high concentration of strontium in the bone through oral administration that causes failure in the remodeling cycle and thus decreases bone mass. Studies in normal rats demonstrated that high doses of strontium, more than 8 mmol/kg/day can induce alterations in the mineralization expressed by a decreased bone mineral density and decreased size of bone apatite.(20, 21).

However, the therapeutic effects of strontium used in bone disease healing, as well its contribution to implant fixation have been clearly proven. Because of this, strontium has been incorporated into surface- engineered biomaterials such as bioactive ceramics, for applications in bone tissue engineering, with encouraging results.(22) The promising studies performed in this subject have motivated us to apply strontium as osseointegration promoter of titanium implants.

In the present work we have followed a novel approach to incorporate strontium in titania implants. We have first functionalized the titania surface with polyacrylic acid (PAA) polymer brushes, which are covalently linked to titania. The carboxylate grous of the PAA brush are then used to complex Sr^{2+}. By using the brush coating of the titania we are then able of limiting the presence of Sr^{2+} to the surface of the implant of clinical importance. This design enabled us to overcome the drawbacks of strontium oral use by fixing its activity at the site of implantation. It allowed as well tuning concentration of

strontium, thus maintaining its positive effects on the bone remodeling cycle and osseointegration of the implant.

Polymers of acrylic acid offer the possibility to entrap strontium by complexation with the carboxylic groups present in the acrylic acid monomers as it is shown in **Figure 4.2. A**. Therefore, PAA modified titania has been incubated with strontium solution with the aim to complex divalent Sr between COO^- groups of PAA. Polymer brushes are defined as assemblies of macromolecules chemically tethered at one end to a substrate or interface, while the other side of the chain remains free (23, 24). Polymer brushes can be grafted either "from" or "to" a surface, meaning that the synthesis of the polymer chains is respectively done from the surface or that the chains are synthesized first and then attached to the surface.

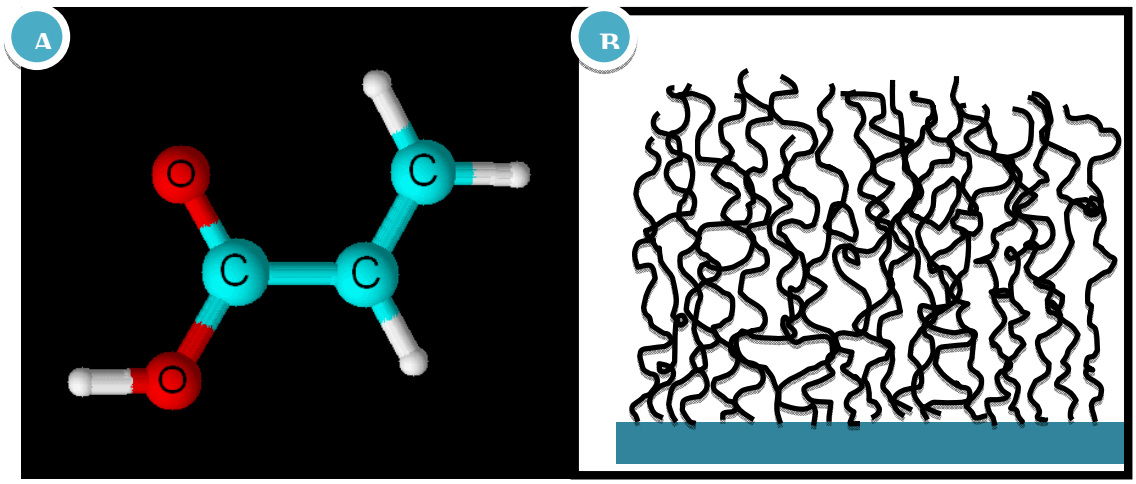

Figure 4.2. Acrylic acid and polymer brush structure. In **A** the structure of acrylic acid is shown, the monomer with terminal carboxylic group used for modification of titania with a brush. The sketch in **B represents the structure of the brush with a dense arrangement of polymer chains attached to a surface on one end while the other end is free**.

In our work polymer brushes are synthesized from aminosilanized titania surfaces. A scheme of the brush is shown in **Figure 4.2. B**.

Beside the application intended here to complex strontium, polymeric coatings are implied in health benefits when used for the modification of implant surfaces. Various studies on the mineralization process of calcium phosphates, oxalates, and carbonates have shown that macromolecules with carboxylate functional groups play a major role inducing nucleation during biomineral formation (25, 26). It has been shown that titanium surfaces functionalized by self-assembled monolayers (SAMs) containing –COOH groups preferentially induce hydroxyapatite crystallization over hydroxyl, phosphate or sulfonic acid. The carboxyl end groups of SAMs results with crystalline characteristics similar to one of a human bone thus providing a biomimetic template for enhancement of biomineralization (27, 28). Therefore, the brush coating can have a positive impact on mineralization besides acting as a source of strontium.

On the other hand, polymeric brushes are known to enrich titanium with antibacterial properties. Although antimicrobial effect is not a subject to the present study, it is worth to note that polymer coatings are shown to have a positive impact in reduction of bacterial infections associated with implanted devices. (29-31).

Titania coatings modified with a PAA brush and with entrapped strontium in the PAA brush have potential to positively influence the bone remodeling cycle in means of enhanced mineralization and bone tissue binding to the surgface. We will show that by varying the grafting density, we are able to vary the amount of strontium in the polymer

brush. Furthermore, we will show that brush complexing with strontium have a positive effect on the bioactivity and functionality of the differentiating osteoblast cells

4.2. Experimental approach

4.2.1. Sample preparation: Growth of PAA brushes and strontium implementation

A semi-transparent, 25 nm thick TiO_2 layer was coated by direct current (d.c.) magnetron reactive sputtering onto glass coverslips. The substrates were sputter-cleaned with a negative bias of 180 V (25 W) in a 4 Pa Ar atmosphere for 3 min. A 2 in. diameter Ti target (99.995% purity, Kurt J. Lesker-USA) at a distance from substrate of 30 mm with applied a d.c. power of 228 W at 0.4 Pa was used. The sputtering was performed at a room temperature at a substrate rotation of 80 rpm. TiO_2 was deposited in the argon/oxygen atmosphere generated by combining 10 sccm of argon flow with 20 sccm of oxygen flow for 120 min.

Aminosilanization. Prior to polyacrylic acid brush growth, titania surfaces were aminosilanized. First, surfaces were cleaned 30 min in 2% SDS, rinsed with nanopure water, dried under nitrogen stream and treated in an UV-ozone chamber for 30 min. Surfaces were immediately inserted into a 1% solution of APTES in toluene. Aminosilanisation was carried out overnight at 115°C, the temperature of boiling toluene. In order to remove excess of APTES, surfaces were cleaned three times in fresh toluene followed by washing three times in nanopure water with sonication and each cleaning cycle lasting 30 min.

Polymerization and strontium incorporation. Polymer brushes were synthesized by Reversible addition fragment chain transfer polymerization (RAFT), which is schematically shown in **Figure 4.3.**

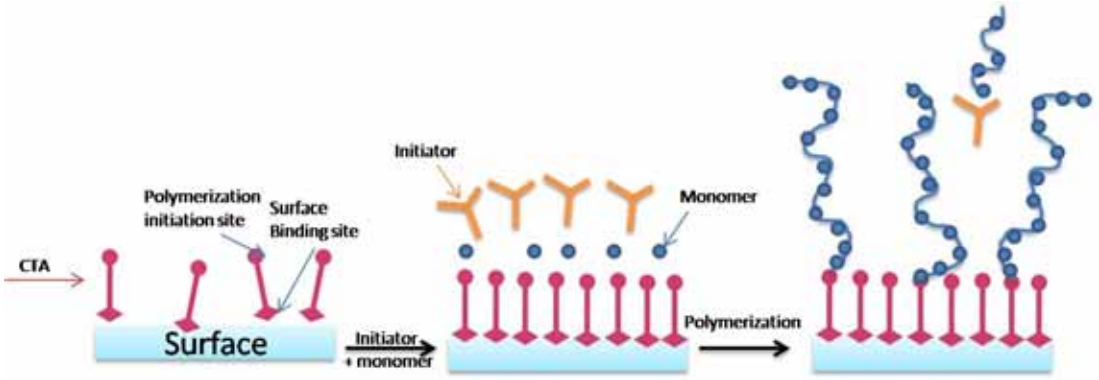

Figure 4.3. Schematic representation of RAFT polymerization on the surface. CTA attaches for the surface from one side while on the other side bears the polymerization initiation site. Upon addition of initiator and monomer a polymer brush grows on the surface. Also, free polymer is present in the solution resulting from the bulk PAA polymerization from the free azo-initiator in solution.

The technique is basically a simple radical polymerization with the addition of a thio-compound, generally named CTA- chain transfer agent, to the solution for controlling the propagation and characteristics of the polymeric chain.

In our experiments bis(carboxylmethyl) trithiocarbonate as CTA is anchored on the aminosilanised titania from which the polymer brushes will be grown (grafted "from" strategy). The CTA is grafted over the surface to the free amino groups on the titanium, by using N,N-dicyclohexylcarbodiimide (DCC) and 4-Dimethylaminopyridine (DMAP). The reagents were used in the molar ratio of 1.00: 1.08: 0.18 (CTA: DCC: DMAP). Two CTA concentrations were employed, 50 mmol and 35 mmol. Each CTA concentration will result in a different grafting density.

The chain density will define the density of carboxylic monomers available and finally impact on the amount of strontium to be complexed. 4,4′-Azobis(4-cyanovaleric acid) (CVA) was used as initiator due to its hydrophilic character. For the polymerization a solution of the monomer (AA), initiator (CVA) and solvent (DMF) was purged under an inert atmosphere for several hours at a total concentration of 5% w/v. A polymerization time of 12 h and temperature of 70^0C were chosen. After polymerization, the substrates were placed into a sonicator bath for a few minutes to remove unreacted species.

The different ratios for the [M]/[CTA] and the [CTA]/[I] are very important in the synthesis of brushes by RAFT polymerization since they control the degree of polymerization and the molecular weight of the polymer.

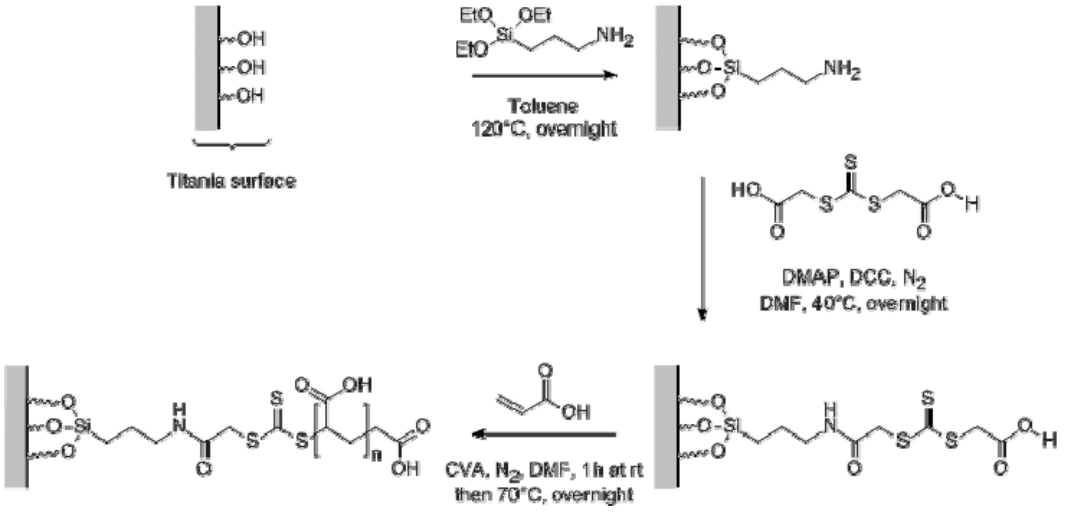

Figure 4.4. Scheme of the polymerization of polyacrylic acid brush on the -NH_2 modified titania surface trough RAFT polymerization.

For preparation of denser brushes we chose [M]/[CTA] ratios of [0.0605]/[0.605] (in mmol) and [CTA]/[I] ratios of [30.25]/[0.605] (mmol). The [M]/[CTA] and [CTA]/[I] ratios for the less dense brushes were [0.220]/[2.201] and [110.05]/[2.20] (mmol),

respectively. The steps for the modification of titania: silanization, CTA attachment and RAFT polymerization are shown in the scheme of **Figure 4.4.**

After the polymerization the surfaces were washed with water to remove free polymer and excess of products. Samples were further incubated in 10 mM Strontium chloride hexahydrate ($SrCl_2x6H_2O$) for 18 hours and rinsed with nanopure water prior to further experimental evaluation.

4.2.2. Surface characterization and cell bioactivity

The reactions steps of aminosilanisation, initiation, and polymerization of acrylic acid (AA) on TiO_2, shown in **Figure 4.4.** and the subsequent strontium incubation, were followed by XPS to confirm the success of each step. XPS experiments were performed with a non-monochromatic X-ray source (Magnesium Kα line of 1253.6 eV energy and 250 W) with the selected resolution for the survey spectra was 30 eV of Pass Energy and 0.5 eV/step and 15 eV of Pass Energy and 0.15 eV/step for the high resolution spectra of the different elements.

The quantitative determination of strontium incorporated into the PAA brushes of two grafting densities was performed using XPS on the titania modified with the PAA brush and entailing Sr (TiO2-PAA-50-Sr and TiO2-PAA-50-Sr).

Osteoblast cells were used to evaluate the biocompatibility and bioactivity of the samples. The adhesion of the cells after 24 hours was evaluated by confocal fluorescent microscopy staining actin, vinculin and the nucleus of the cells. A cell proliferation colorimetric assay was conducted with the Cell Counting Kit-8 (CCK-8) containing WST-8[2-(2-methoxy-4-nitrophenyl)-3-(4-nitrophenyl)-5-(2,4-disulfophenyl)-*2H*-

tetrazolium, monosodium salt], a nontoxic dye used for continuous cell culturing. Cell medium was refreshed with 12.5% v/v CCK-8 containing full medium and after 2 hours of reaction, an aliquot of 50 μm was transferred in 96 well cell culturing plate. Colorimetric analysis of the samples was performed over days of cell culturing in osteogenic medium using a plate reader with a 450 nm filter.

In order to determine the mineralization capacity of the samples, the ALP activity assay was performed after 12 days of osteogenic culturing allowing the cells to deposit components of extracellular matrix. Qualitative data on osteocalcin formed by osteoblast during the process of mineralization were assessed by staining the samples with Alizarin red, a calcium specific dye. Samples were imaged using Leica brightfield microscope.

4.3. Results and discussion

4.3.1. Titania functionalization with poly acrylic acid and strontium

Brush density on Titania is controlled by the density of CTA on the surface which defines number of active sites for growths of polymer. The main components taking place in the RAFT polymerization in present study are monomer acrylic acid (AA), trithiocarbonate, chain transfer agent (CTA) that is responsible for the grafting density and the initiator cyanovaleric acid (CVA). The ratio of AA/CTA will determine molecular weight of polymer where higher ratio will result in higher Mw of the poltymer. The CTA/CVA ratio has been adjusted to favor polymerization from the surface and to avoid abundant initiation in the solution that occurs with too high concentration of CVA in relation to CTA. By varying the density of polymer chains in the brush we can vary strontium amount incorporated into the PAA brushes since two carboxylic groups can complex one divalent strontium atom. Thus, if the density of PAA on the surface is higher there will be more of available carboxylic groups and consequently more of strontium entrapped in the brushes.

In order to evaluate the cell activity for the different concentration of strontium on the surface, we have prepared PAA on titania with two densities, using 35 and 50 milimolar CTA. Fully functionalized titania surfaces are further referred to as TiO_2-PAA-35-Sr and TiO_2-PAA-50-Sr where the first one has a lower density of the PAA chains and consequently a lower concentration of strontium. PAA brushes are prepared on aminosilanised titania surfaces rather than on bare titania because in polymerization on OH^- functionalized surfaces in common use is a CTA that contains relatively toxic cyno

groups, cyanomethyl [3-(trimethoxysilyl)propyl] trithiocarbonate. Preliminary experiments using this initiator showed that the biocompatibility of the modified titania was rather low compared to brushes prepared on aminosilanized titania (data not shown).

4.3.2. Surface characterization

The polymerization reaction was followed step-by-step by XPS. As example we show the XPS spectra for the modification of the TiO2-PAA-35-Sr surface presented in **Figure 4.5.** We can appreciate comparing the TiO_2 (black) and TiO_2+NH_2 (red) spectra the appearance of low intensity nitrogen peak at ~401 eV in the TiO_2+NH_2 sample that confirms the successful aminosilanisation of the titania surface. The silicon peak at 100 eV appears in parallel resulting from the silane groups that bind to hydroxides from TiO_2 trough formation of -SiO_3 on the surface (32).

Amino groups will bind CTA and polymer will be synthesized from CTA. CTA contains thiocarbonylthio group (S(S)CS). The presence of sulfur on the surface after CTA binding is confirmed in blue spectrum in **Figure 4.5** at binding energy of ~162 eV. Atomic percentages of the elements are calculated from high resolution spectra of each region and are shown in **Table 4.1.**

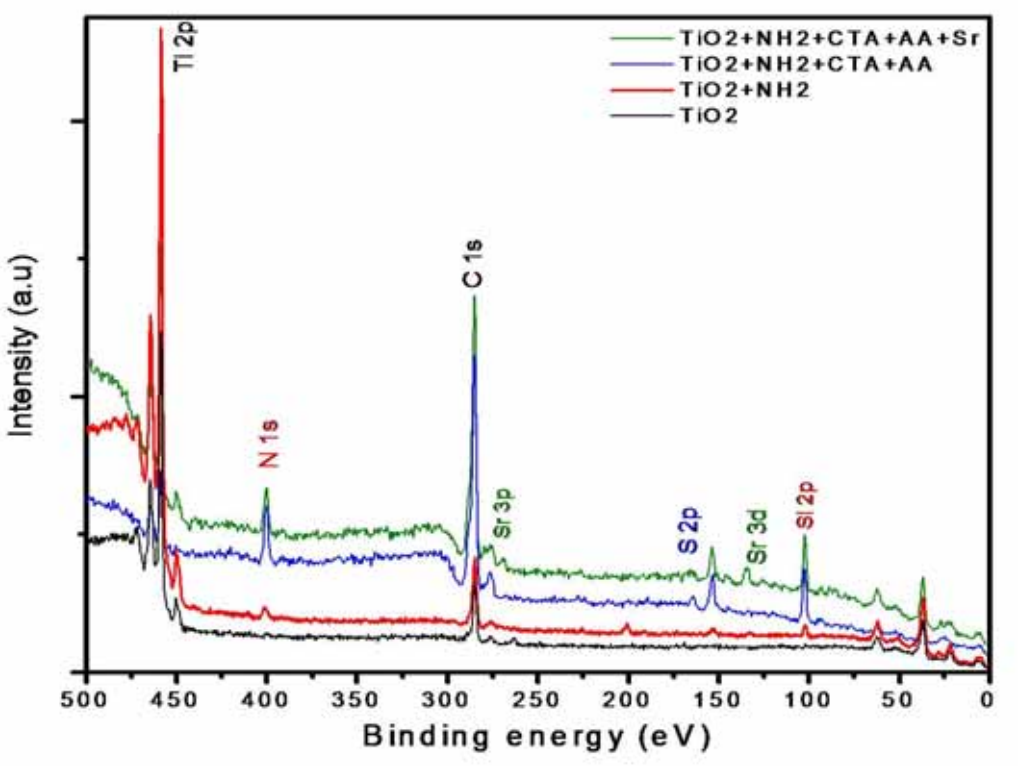

Figure 4.5. XPS Survey scans of PAA polymerization on titania and strontium incorporation in the brush. The steps of functionalization of titania are followed with XPS for the TiO2-PAA-35-Sr sample.

Table 4.1. Elemental composition calculated from XPS. Atomic percentages are calculated from spectra recorded at every step of polymerization reaction and strontium incorporation in TiO2-PAA-35 as shown in Figure 5.5.

Atomic percentage of elements (%) by XPS		Element				
		C	Sr	Ti	O	N
Sample	TiO2	31,3	/	23,6	45,0	/
	TiO2 + NH2	22,6	/	22,4	52,6	2,4
	TiO2-NH2+CTA+AA	58,7	/	2,5	32,1	6,7
	TiO2-NH2+CTA+AA+Sr	51,2	0,7	6,3	37,0	4,9

A more than a double increase, from 2.4% to 6.9 %, observed in the nitrogen intensity at this reaction step coming from imides from DCC (dicyclohexylcarbodiimide) that is used as reaction catalyst.

It is important to notice here that the increase in carbon intensity found at 285 eV results from the PAA polymer chains thus verifying the growth of the polymer. Finally, the green spectra in **Figure 4.5** correspond to our end surface, which has strontium incorporated into polymer brush. Strontium core level signal, Sr 3d 5/2 appears at binding energy of ~134 eV as shown in spectra, but additionally confirmed with appearance of Sr 3p photoelectron peak at ~282 eV. (33-35)

A high resolution XPS scans of Sr 3d region are shown in **Figure 4.6.** for surfaces TiO_2-PAA-35-Sr and TiO_2-PAA-50-Sr. Main Sr 3d spin orbit couple, 5/2 is found at energy of 133.5 eV and is assigned to SrO (33, 34) as expected since strontium is supposed to bind to COO^- groups of PAA. Furthermore, we observe an increase in strontium amount in PAA brushes prepared at a higher grafting density. Strontium in TiO2-PAA-35-Sr sample totals 0.7 % while in TiO2-PAA-50-Sr is increased to 1 % of total surface elemental composition. The increase comes from denser brushes at the surface that can offer more carboxylic groups for strontium incorporation.

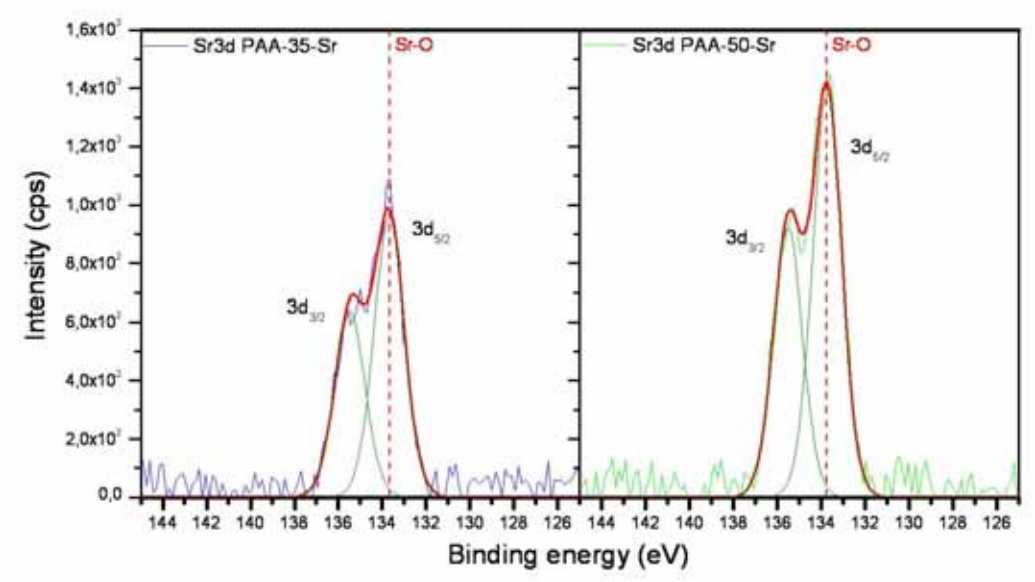

Figure 4.6. XPS detail region of strontium core level, Sr 3d for TiO_2-PAA-35-Sr (on the left) and TiO_2-PAA-50-Sr. the intensity scale is presented in CPS units and increase in intensity in strontium signal is notable for PAA prepared at higher grafting density ($_{TiO2}$-PAA-50-Sr).

In subsequent experiments, we exposed samples to cell culturing medium and afterwards examined them by XPS, which showed no strontium after 1 day of incubation. This implies that all the strontium is released into biological fluid within 24 hours or that amount lowered so that is not possible to detect it by XPS. Rate of strontium release therefore should be quantified with other approach, such as inductively coupled plasma mass spectrometry (ICP-MS) that is able to detect very low concentrations of the elements.

As perspective work denser PAA brushes could be to increase the retention of strontium till the limits of its therapeutic effect on the bone healing and remodeling.

4.3.3. Osteoblast biocompatibility and bioactivity

Once the synthesis of the brush and strontium incorporation was proved the biocompatibility and bioactivity of the coating were assessed with osteoblast cells. Osteoblast cells were seeded on the TiO2-PAA-Sr samples and controls at a density of 2.5 x 10^4 cells/well. Cell proliferation was recorded over 8 days time on TiO_2-PAA-35-Sr and TiO_2-PAA-50-Sr and two controls, TiO_2 and well of cell culturing plate as shown in **Figure 4.7.**

First, we can note increase in cell proliferation over time on all the samples. This implies that all samples, titania with brushes and with brushes and strontium are biocompatible. On the first days, more cells are proliferating on bare TiO_2 but with the time there is increase of relative proliferation value of PAA-Sr coated surfaces. While on the day 1 cells on bare TiO2 have optical density of ~1.8 and TiO2-PAA -50-Sr ~ 1.6, on a day 8 proliferation of TiO2-PAA-50-Sr result in optical density of ~4.1, slightly higher than of bare titania with optical density of ~4. The TiO2-PAA-35-Sr proliferation is somewhat lower, resulting with optical density of ~ 3.8 after 8 days of culturing.

Even if there is no significant increase in proliferation for PAA-Sr samples in comparison to bare TiO_2, results are indicative of a high biocompatibility for the brush coated titania. Moreover, a positive trend is observed regarding the relative increase in proliferation of PAA-Sr samples in respect to TiO_2.

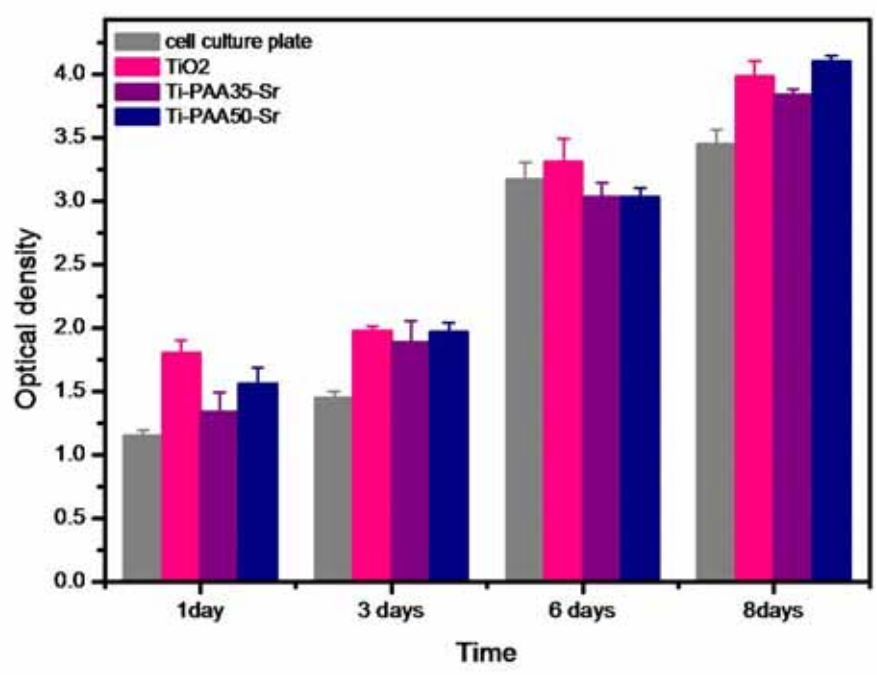

Figure 4.7. Osteoblast cell proliferation determined with the CCK-8 cell counter kit for 1, 3, 6 and 8 days after culturing in osteogenic medium on TiO_2 functionalized with PAA-35-Sr and PAA-50-Sr. Bare TiO_2 and cell culture plate well serve as a controls.

Furthermore, we have studied the initial osteoblast adhesion on the surfaces as a key regulator in cell migration, differentiation and mineralization. These cell functions further determine the fate of implant material in the body. Confocal Scanning Laser Microscopy images of cellular adhesion after 24 hours are shown in **Figure 4.8.** For the cells vinculin (green), F-actin (red) and the nucleus (blue) were stained. The three stainings are shown in the first, second and third panels, respectively, and the merged channels are shown in the last panel. For this experiment, cells were cultured on a bare titania, TiO_2-PAA-35-Sr, TiO_2-PAA-50-Sr and additionally on TiO_2-PAA-35. PAA brush on titanium without strontium serves here as a control to determine if strontium has actually an influence on cell behaviour and bioactivity.

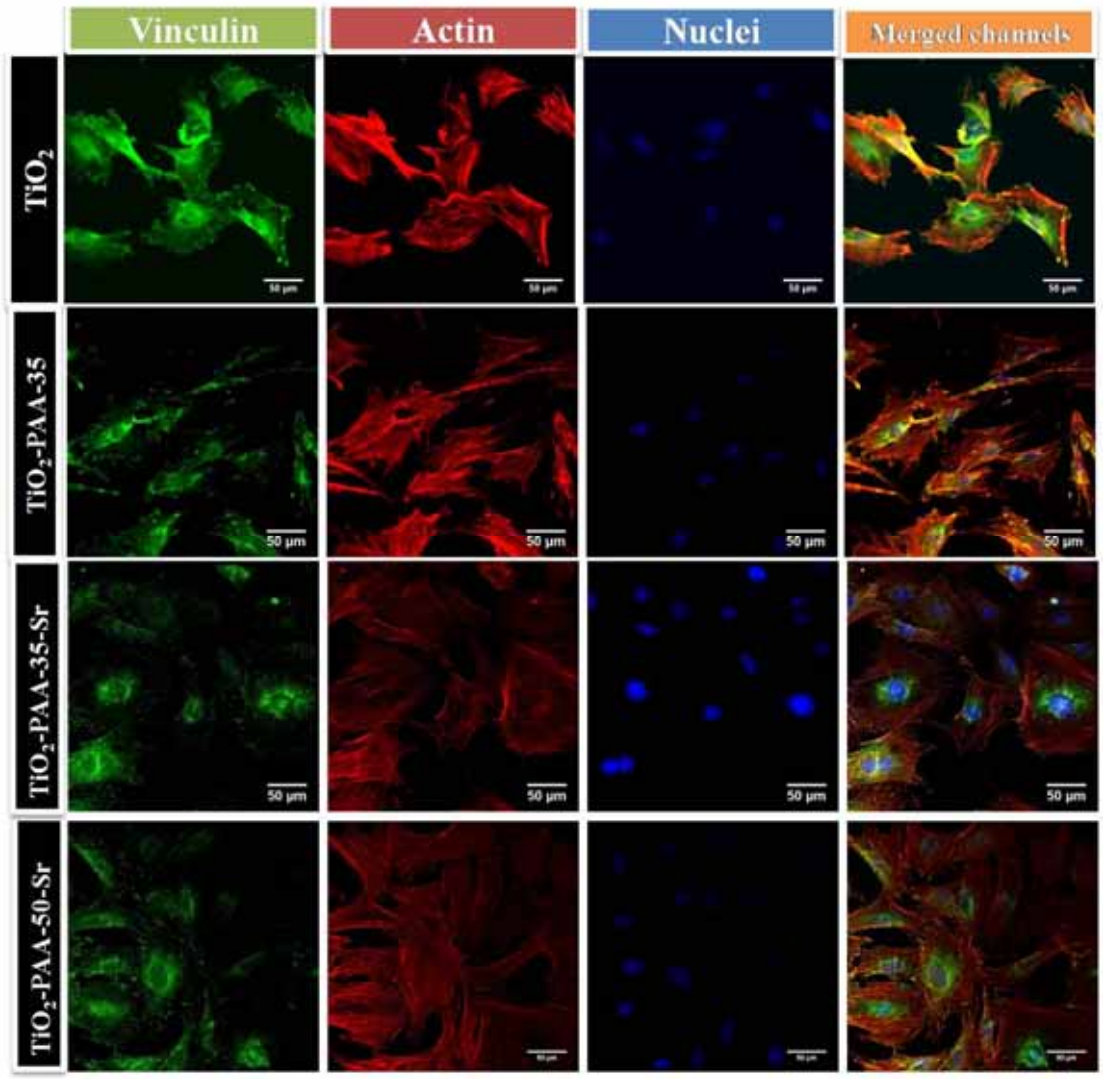

Figure 4.8. Osteoblast adhesion after 24 hours of culturing on bare TiO_2, titania functionalized with PAA-35, PAA-35-Sr and PAA-50-Sr. Green channel corresponds to vinculin staining, red to actin staining, blue to the nucleus staining and last panel are all channels merged into one. 40x magnification.

Osteoblast cells cultured on bare titania are smaller and less numerous than those cultured on PAA and PAA-Sr functionalized samples. In the images of vinculin staining we can first notice that there is significantly more bright green spots at the ends of stress fibres on PAA and PAA-Sr functionalized TiO_2 when compared to bare TiO_2. We can

also note the cytoskeleton with more stress fibres in the cytoplasm as observed in the images of F-actin staining. From the images of F-actin, in red channel, we appreciate that cells cultured on all the samples are larger in size compared to those cultured on bare titania. Additionally, they show a rearranged cytoskeleton with distinctive stress fibres inside the cytoplasm. These characteristics of an improved cell adhesion are more evident for the TiO_2-PAA-50-Sr sample. Comparing cell adhesion on TiO2-PAA-35 and TiO_2-PAA-35-Sr it can be concluded that strontium contributes to an enhanced cell activity as it is deduced from the presence of bigger cells adhering on strontium containing PAA, which also show more vinculin and more organised stress fibers.

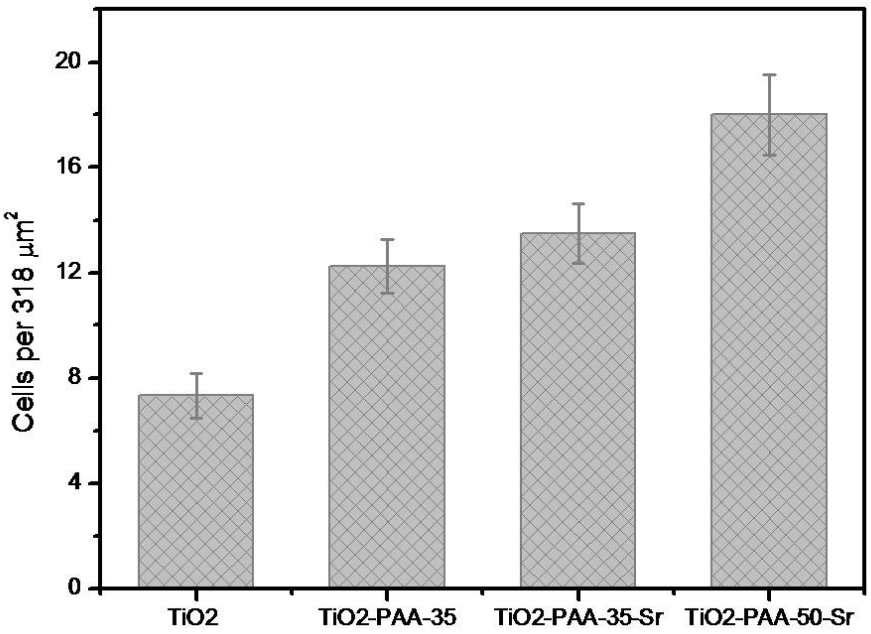

Figure 4.9. Average osteoblast cell number on TiO_2, titania functionalized with PAA-35, PAA-35-Sr and PAA-50-Sr resulting from minimum 3 samples on area of 318x318 µm and expressed as average value.

On average, the number of cells on TiO2-PAA-50-Sr is higher in respect to other samples as shown in **Figure 4.9.** Average cell number per 318 μm^2 for sample TiO2-

PAA-50-Sr is 18, higher in respect to 13 cells/318 μm^2 for TiO2-PAA-35-Sr and 12 per 318 μm^2 for TiO2-PAA-35. Here, we can also appreciate an improvement over the bare titania surface that resulted in an average cell number of 7 cells per 318 μm^2. In this case we can conclude that the strontium is contributing to an enhanced activity since the number of cells is somewhat higher on the brush with strontium than without as seen from comparison of TiO2-PAA-35-Sr and TiO2-PAA-Sr.

Finally, we have studied the impact of the PAA-Sr on the cells in regards to their capacity to deposit extracellular matrix components and further form a mineral tissue. Osteoblast mineralization is initial step in formation of new bone tissue and it determines bone ingrowth with implant substrate. Therefore, we have evaluated the alkaline phosphatase (ALP) activity of the differentiating osteoblast cells on the PAA-Sr functionalized titania with bare titania as control surface. ALP activity is a gene marker in the early stage of the osteogenic differentiation where cells deposit extracellular matrix components, mainly collagen and further mineralize this matrix into osteoid bone.

Figure 4.10 A displays the ALP activity expressed as stained surface area of alkaline phosphatase after osteoblasts are cultured in osteogenic medium for 12 days on the surfaces under study. It is clear that that same trend in ALP activity is observed as in evaluation of focal adhesion. This means that TiO_2-PAA-50-Sr sample shows highest ALP activity and titania lowest. Strontium is again found to have a positive influence on the cell activity, in this case in the matrix maturation and mineralization process, since the ALP activity is higher on a TiO_2-PAA-35-Sr sample than on same surface without incorporated strontium. Statistical analysis of ALP mean values shows significant

difference between bare titania and all the functionalized samples as shown in **Figure 4.10. B.** However, the statistically difference is nonsignificant between TiO_2-PAA-35 with and without strontium. The same statistically nonsignificant difference is observed when comparing TiO2-PAA35-Sr and TiO2-PAA-50-Sr. samples.

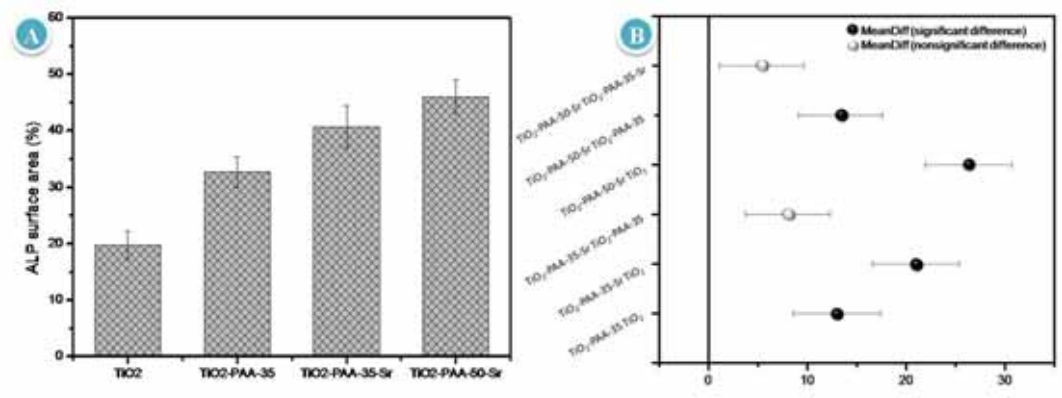

Figure 4.10. ALP activity after 12 days of osteoblast culturing expressed as stained surface area shown in A. Statistical comparison of mean values by Tukey is shown in B where black circles show significant differences between samples at a 0.05 level.

Despite this, the increase in activity is obvious as shown graph in **Figure 4.10 A**. This is appreciated as well from optical images of ALP stained area shown in **Figure 4.11**. Cells cultured on the functionalized titania after staining exhibit more area with dark blue- purple color, compared to osteoblast cells cultured on the bare TiO_2. These results indicate enhanced ALP activity in respect of higher strontium concentration as represented in **Figure 4.11. D.**

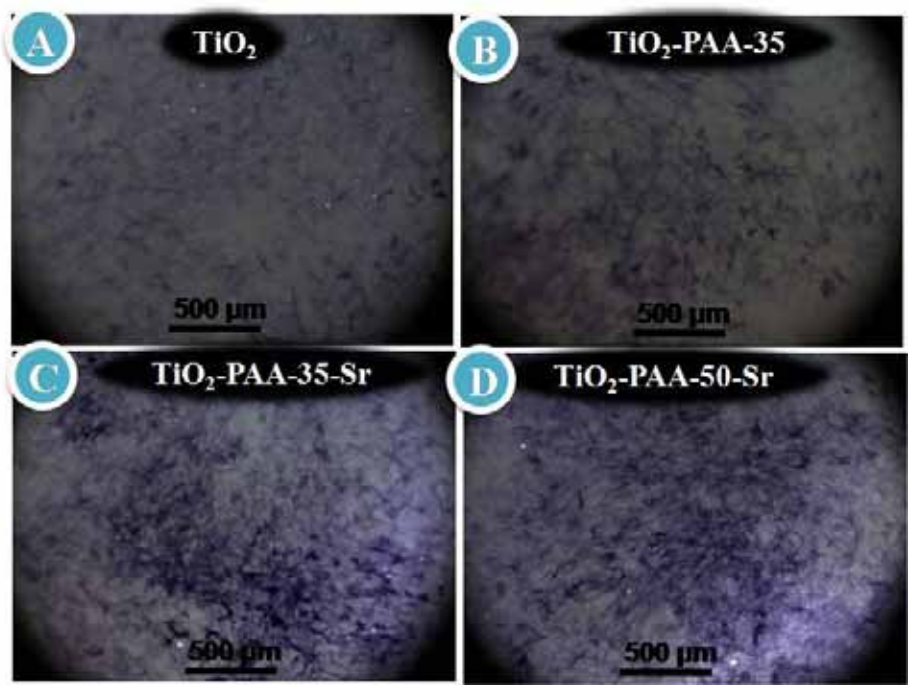

Figure 4.11. Optical images of ALP staining after 12 days of osteoblast culturing in osteogenic medium. Dark purple color is stained ALP that is used for calculation of ALP area in **Figure 4.10. A.**

These results support the hypothesis that strontium has a positive effect on a bone tissue formation and they lead to conclusion that increase in strontium influences rate of matrix maturation and mineralization as seen in improved activity of surface with denser PAA brush that contains more strontium.

Additionally, we have stained calcium from osteocalcin, a component of the mineralized extracellular matrix. Optical images of calcium staining with alizarin red shown in **Figure 4.12.** are of qualitative nature but they support the previous findings.

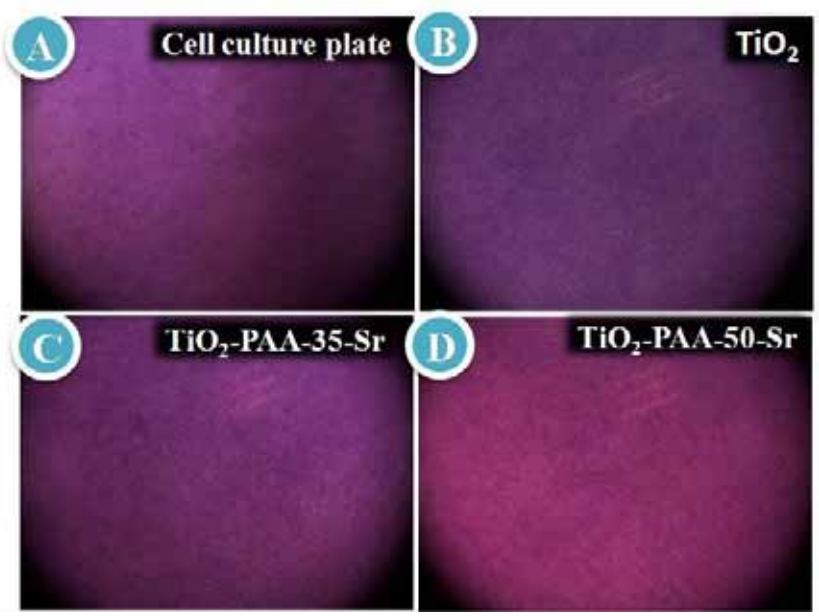

Figure 4.12. Alizarin red staining of calcium deposits from mineralized tissue after 12 days of culturing. More bright orange color indicates more of calcium deposited by osteoblast cells.

Since more bright- orange color results in a higher amount of calcium, TiO2.PAA-50-Sr displays the highest amount of osteocalcin deposited by osteoblast cells after 12 days of culturing. This observation is in good agreement with the other experiments on osteoblast activity and confirms that presence of strontium triggers faster deposition of ECM mineral components thus enhancing bone osseointegration.

4.4. Conclusions and perspectives

In this study, we have for the first time to our knowledge applied the coating of titania-polymer brushes entrapping strontium for enhanced osseoactivity of biomaterials. After careful preparation and characterization of the brush coating and of the strontium incorporated, we managed to vary the concentration of Sr^{2+} complexed to carboxylic groups in the brush. This is achieved trough varying grafting density of polyacrylic acid brushes since brushes with higher density of PAA chains offers more carboxyl groups and is consequently able of trapping more strontium.

Titania with PAA brushes entailing strontium display higher bioactivity and enhanced cell adhesion compared with bare TiO_2 with and without brushes. For the samples with higher chain density the effect of strontium is more pronounced. Moreover, these Sr-PAA coatings showed the ability to promote bone tissue mineralization and additionally accelerating the bone tissue mineralization at a higher strontium concentration. The positive mutual effect of polymer and osseoactive strontium is confirmed by the increased ALP activity and positive osteocalcin staining, main components of mineralized ECM.

These results show the potential of the modification of titania with brushes as a strategy to endow titanium based osseo- implants with strontium, especially for the purpose supporting the osteoporotic or broken bone.

Furthermore, by confining the action of strontium to the biomaterial interface this approach enables the enhancement of cellular activity reducing the negative side effects

of oral uptake of strontium. We envisage the design of denser brushes on titanium materials to gain control on the amount of strontium entrapped.

List of references

1. Hadjidakis DJ & Androulakis I (2006) Bone remodeling. *Annals of the New York Academy of Sciences* 1092:385-396.

2. Jonsson BY & Mjoberg B (2015) Porous titanium granules are better than autograft bone as a bone void filler in lateral tibial plateau fractures: A randomised trial. *The Bone & Joint Journal* 97-B(6):836-841.

3. Bonnelye E, Chabadel A, Saltel Fdr, & Jurdic P (2008) Dual effect of strontium ranelate: Stimulation of osteoblast differentiation and inhibition of osteoclast formation and resorption in vitro. *Bone* 42(1):129-138.

4. Buehler J, Chappuis P, Saffar JL, Tsouderos Y, & Vignery A (2001) Strontium ranelate inhibits bone resorption while maintaining bone formation in alveolar bone in monkeys (Macaca fascicularis). *Bone* 29(2):176-179.

5. Canalis E, Hott M, Deloffre P, Tsouderos Y, & Marie PJ (1996) The divalent strontium salt S12911 enhances bone cell replication and bone formation in vitro. *Bone* 18(6):517-523.

6. Takahashi N, Sasaki T, Tsouderos Y, & Suda T (2003) S 12911-2 Inhibits Osteoclastic Bone Resorption In Vitro. *Journal of Bone and Mineral Research* 18(6):1082-1087.

7. Boivin G, *et al.* (1996) Strontium distribution and interactions with bone mineral in monkey iliac bone after strontium salt (S 12911) administration. *Journal of Bone and Mineral Research* 11(9):1302-1311.

8. Brennan TC, *et al.* (2009) Osteoblasts play key roles in the mechanisms of action of strontium ranelate. *British Journal of Pharmacology* 157(7):1291-1300.

9. Fromigué O, *et al.* (2009) Calcium sensing receptor-dependent and receptor-independent activation of osteoblast replication and survival by strontium ranelate. *Journal of Cellular and Molecular Medicine* 13(8b):2189-2199.

10. Caverzasio J (2008) Strontium ranelate promotes osteoblastic cell replication through at least two different mechanisms. *Bone* 42(6):1131-1136.

11. Takaoka S, Yamaguchi T, Yano S, Yamauchi M, & Sugimoto T (2010) The Calcium-sensing Receptor (CaR) is Involved in Strontium Ranelate-induced Osteoblast Differentiation and Mineralization. *Horm Metab Res* 42(09):627-631.

12. Faure H, *et al.* (2009) Molecular determinants of non-competitive antagonist binding to the mouse GPRC6A receptor. *Cell Calcium* 46(5â€“6):323-332.

13. Liu AL-J, Shen P-W, & Chen P-J (2013) Strontium ranelate in fracture healing and joint pain improvement in a rheumatoid arthritis patient. *Clinical Cases in Mineral and Bone Metabolism* 10(3):206-209.

14. Zhu L-L, *et al.* (2007) Induction of a program gene expression during osteoblast differentiation with strontium ranelate. *Biochemical and Biophysical Research Communications* 355(2):307-311.

15. Hurtel-Lemaire AS, *et al.* (2009) The calcium-sensing receptor is involved in strontium ranelate-induced osteoclast apoptosis. New insights into the associated signaling pathways. *The Journal of Biological Chemistry* 284(1):575-584.

16. Li Y, *et al.* (2011) Effects of strontium ranelate on osseointegration of titanium implant in osteoporotic rats. *Clinical Oral Implants Research* 23(9):1038-1044.

17. Querido W, Farina M, & Anselme K (2015) Strontium ranelate improves the interaction of osteoblastic cells with titanium substrates: Increase in cell proliferation, differentiation and matrix mineralization. *Biomatter* 5(1):e1027847.

18. Maimoun L, *et al.* (2010) Strontium ranelate improves implant osseointegration. *Bone* 46(5):1436-1441.

19. EMA (2013) Recommendation to restrict the use of Protelos / Osseor (strontium ranelate). in http://www.ema.europa.eu/ema/, ed agency Em.

20. Morohashi T, Sano T, & Yamada S (1994) Effects of strontium on calcium metabolism in rats. I. A distinction between the pharmacological and toxic doses. *The Japanese Journal of Pharmacology* 64(3):155-162.

21. Cohen-Solal M (2002) Strontium overload and toxicity: impact on renal osteodystrophy. *Nephrology Dialysis Transplantation* 17(suppl 2):30-34.

22. Wu C, Ramaswamy Y, Kwik D, & Zreiqat H (2007) The effect of strontium incorporation into CaSiO3 ceramics on their physical and biological properties. *Biomaterials* 28(21):3171-3181.

23. Prucker O, *et al.* (2005) Photochemical Strategies for the Preparation and Microstructuring of Densely Grafted Polymer Brushes on Planar Surfaces. *Polymer Brushes*, (Wiley-VCH Verlag GmbH & Co. KGaA), pp 449-469.

24. Zhou F & Huck WTS (2006) Surface grafted polymer brushes as ideal building blocks for "smart" surfaces. *Physical Chemistry Chemical Physics* 8(33):3815-3823.

25. Tsortos A & Nancollas GH (2002) The Role of Polycarboxylic Acids in Calcium Phosphate Mineralization. *Journal of Colloid and Interface Science* 250(1):159-167.

26. Chen L, *et al.* (2013) Regeneration of biomimetic hydroxyapatite on etched human enamel by anionic PAMAM template in vitro. *Archives of Oral Biology* 58(8):975-980.

27. Liu DP, Majewski P, O'Neill BK, Ngothai Y, & Colby CB (2006) The optimal SAM surface functional group for producing a biomimetic HA coating on Ti. *Journal of Biomedical Materials Research Part A* 77A(4):763-772.

28. Mao C, *et al.* (1998) Oriented growth of hydroxyapatite on (0001) textured titanium with functionalized self-assembled silane monolayer as template. *Journal of Materials Chemistry* 8(12):2795-2801.

29. Darouiche RO (2004) Treatment of infections associated with surgical implants. *The New England Journal of Medicine* 350(14):1422-1429.

30. Weinstein RA & Darouiche RO (2001) Device-Associated Infections: A Macroproblem that Starts with Microadherence. *Clinical Infectious Diseases* 33(9):1567-1572.

31. Zimmerli W, Trampuz A, & Ochsner PE (2004) Prosthetic-joint infections. *The New England Journal of Medicine* 351(16):1645-1654.

32. Metwalli E, Haines D, Becker O, Conzone S, & Pantano CG (2006) Surface characterizations of mono-, di-, and tri-aminosilane treated glass substrates. *Journal of Colloid and Interface Science* 298(2):825-831.

33. Moulder JF, Stickle WF, Sobol PE, & Bomben K (1992) *Handbook of X-ray Photoelectron Spectroscop 2nd ed* (Physical Electronics USA, Inc.) 2nd Ed.

34. Wagner CD, *et al.* (2003) NIST Standard Reference Database 20, Version 3.4 (web version) (http:/srdata.nist.gov/xps/).

35. Young V & Otagawa T (1985) XPS studies on strontium compounds. *Applications of Surface Science* 20(3):228-248.

Chapter 5

Refining the surface topography of titanium: A chemical approach

5.1. Motivation

Titanium osseointegration, the bone- implant binding process, largely depends on the texture of titanium surface. Early work of Albrektsson from 1983 showed that osseointegration at the interface between titanium and bone is influenced by both the biochemical and physical features of the interface.(1) The macroscopic, microscopic, as well as molecular characteristics of the interface have been shown to influence on the osseointegration process. The presence of proper chemical and biophysical characteristics at the implant interface may however not be determinant for the osseointegration if the interface lacks the required roughness.(2) The bonding between titanium and bone is biomechanical. Rougher surfaces provide more surface area for the cells to adhere and stretch favoring in this way ossointegration.(2, 3) Examples of osteoblast cells adhering on smooth, as received titanium alloy and rougher, sandblasted titanium surfaces are shown in **Figure 5.1.** It can be seen in the figure that cells exhibit distinct morphologies in each case. They are flattened in both cases, but cells on sandblasted titanium alloy have more filopodia, communicating with neighboring cells extending over cavities and cues.

Osseointegration results from a rough surface interlocking with bone tissue that grows with direct contact with titanium, in cavities of the nanotopography of substrate. The success of osseointegration and consequently of the implant surgeries correlates with an increasing roughness of the implant surface(4, 5)

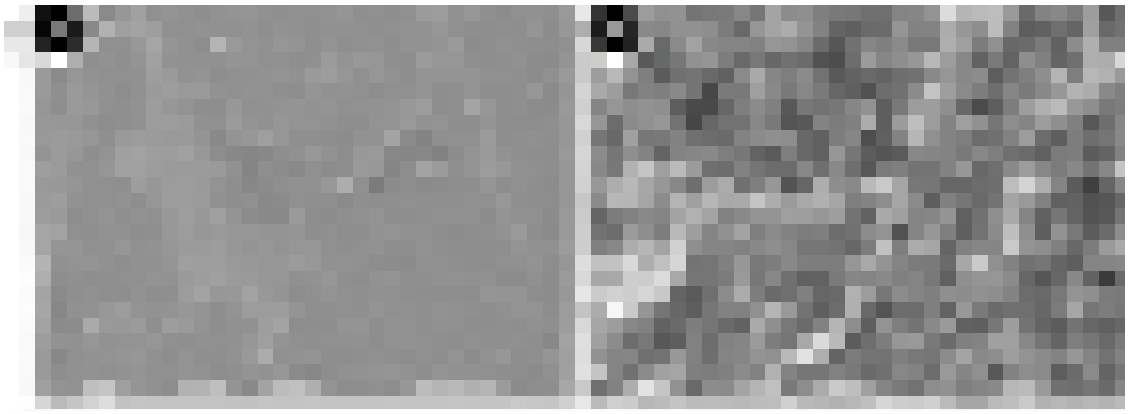

Figure 5.1. Osteoblast adhesion after 14 hours as viewed by SEM on A as received, smooth titanium alloy and B on rougher, sandblasted titanium alloy.

Sand-blasting, acid and alkali etching, plasma spraying, electropolishing and anodic oxidation are commonly used techniques to obtain controlled nano and micro scale features on the surface of titanium.(6-9) The endogenous formations techniques are commonly used for in situ generation of nanotopographical features without altering the original surface chemistry. Chemical etching is a tightly controlled corrosion process using baths of etching chemicals to remove material and create features with a desired shape. Chemical methods that consider etching of surfaces are simple and cost-effective, showing an attractive practicality. Yet, the drawback of traditional chemical methods is that the use of strong acids and strong bases inevitably raise safety and eco concerns. More important, residual acids or bases on the surface are harmful for cells and tissue and

may lead to an immunogenic response of the body. Because of this it is of great importance to develop more applicable and safer chemical methods for fabrication of nanotopographical features on titanium surfaces.

One of the endogenous approaches for surface modification is alkaline etching. It is a simple way to alter titanium topography and it has already been shown to cause irregular features on the titanium surface under increased temperature (600 ºC).(11) It is worth to note that alkaline etching with NaOH forms sodium titanate ($Na_2Ti_6O_{13}$) offering the possibility to further chemically modify the surface by exchanging the Na ions during post treatment. Post treatments can be used to remove the remains of base from the surface. An interesting component that can be used for post treatment is strontium (Sr^{+2}) that can be easily exchanged with Na^+ but it has additionally favorable effects on bone osseointegration. Strontium is proven to have a beneficial effect on the normal bone metabolism, where it modulates the development of bone tissue by stimulating new bone formation and inhibiting bone resorption.(12) Several drawbacks of oral strontium intake are already detailed in the previous chapter. Since it is known that strontium has a positive effect on ossointegration,(13-15) in this chapter we will focus on finding optimal conditions for achieving the titanium surface with a high content of strontium.

The implementation of the strontium into roughened titanium implants brings an extra component in mimicking the bone extracellular environment since strontium is naturally found in apatite crystals of the bone.(16) Additionally, the concentration of strontium doped into the implant surface can be regulated trough modulation of specific surface of titanium nanotopographhy.

Work in this chapter includes the alkaline etching of titanium alloys to refine their surface texture obtaining defined micro and nanotopographical cues. Our intention is to manipulate with number and dimensions of surface cues and cavities by changing parameters of treatment. Two kinds of titanium alloys are used for alkaline etching and strontium implementation; sandblasted Ti alloys and as received Ti alloys. The two samples differ in their topography, with the sandblasted alloy having rougher surface in comparison to the as received alloy, whose surface is relatively smooth. Alkaline treatment on these two alloys will demonstrate the influence of the initial material morphology on the resulting micro and nanotopography and consequently how the morphology affects the binding of the strontium as well.

Chemical treatment with NaOH is conducted by varying NaOH concentration, pH and the time of treatment. Through the variation of these parameters, distinct morphologies are obtained regarding the size and extent of topographical features, their degree of coverage and the three dimensional structure of the topographical cues. Besides altering topography, NaOH chemical etching changes the chemistry of the TiO_2, resulting in a layer of sodium titanate covering the implant surface. The presence of Na^+ on the surface is used to incorporate strontium in the TiO_2 surface via ion exchange of sodium by strontium. The strontium exchange is discussed in relation to the topography of the nanostructured titanium alloys and how this promotes strontium binding.

5.2. Experimental approach

5.2.1. Chemical etching

Titanium alloys (Ti-6Al-4V) are etched with sodium hydroxide (NaOH) changing the structure and surface chemistry of the alloy. The top layer of titanium is changed to titanate. **Equation 5.1** shows one of the possible reactions:

$$6Ti+2NaOH+11H_2O=Na_2Ti_6O_{13}+12H_2 \qquad \textbf{Equation (5.1.)}$$

Equation 5.1. Reaction of NaOH with Ti-6Al-4V alloy resulting in a layer of sodium titanate, $Na_2Ti_6O_{13}$ and water.

Two kinds of titanium alloy discs are used for the study: as-received (relatively smooth) and sandblasted (slightly roughened). Substrates are first acid-washed with a water mixture of 69 % HNO_3 and 49% HF in ratio of 3.3:1 (H_2O: HNO_3+HF). After acid washing, substrates are subjected to treatment with NaOH solutions of different ionic strength, 1 M and 3 M. The samples are treated at 180°C temperature for 3 and 6 hours in a teflon-lined stainless steel hydrothermal reactor. Samples are finally washed with mili-Q water and dried. Changes of surface chemistry are first determined by X-ray photoelectron spectroscopy (XPS) and sample topography is further characterized by scanning electron microscopy (SEM)

5.2.2. Strontium incorporation

Strontium is incorporated into modified titanium by ion exchange between Na^+ and Sr^{2+} ions on $Na_2Ti_6O_{13}$ formed after NaOH etching. A 250 mM strontium chloride ($SrCl_2$)

solution is adjusted to pH values 6, 9 and 12. The samples are immersed overnight in $SrCl_2$ and afterwards washed with mili-Q water. Elemental composition of the surfaces was revealed with XPS with an Mg Kα source having 1250 keV energy. Survey scans are obtained with pas energy of 30 eV and detail regions of C 1s, O 1s, Ti 2p, Sr 3d and Na 1s are taken with 15 eV pass energy. Strontium to titanium (Sr/Ti) ratio was as well determined with Energy-dispersive X-ray spectroscopy (EDXS) present in the SEM microscope, simultaneously revealing topography and quantifying strontium on the surfaces.

3.2.3. Biocompatibility

After chemistry and morphology were examined, substrates were preliminary evaluated for their biocompatibility. Cell proliferation was evaluated with MC3T3-E1 osteoblast precursor cells to assess the bioactivity of the etched alloys in comparison with bare titanium surface. Cell culture plates were used as a control group. Cells were cultured using α-MEM supplemented with 10% fetal bovine serum and 1% penicillin/streptomycin at 37 °C in an atmosphere of 5% CO_2. The culture medium was refreshed every 3 days. When the cells reached 80% confluence, they were trypsinized and resuspended in fresh medium to make a cell suspension with a final cell density of 3 × 10^4 cells/mL. 1 mL of cell suspension was added into each well of 24-well cell culture plates with Ti alloy samples inside. After incubation for 14 days, the medium is aspirated and wells are refilled with 400 µl of cell culture medium containing 50µl CCK-8. After 2 hours of further incubation in the 37 °C incubator, a 100 µl solution from each well is

transferred into 96 well plates for reading the optical density. The wavelength used for plate reading is 450 nm.

5.3 Results and discussion

5.3.1. Surface etching

Treatment of Ti alloys with NaOH resulted in distinct surface morphologies that depend on the conditions used for chemical treatment. In **Figure 5.2.** we can observe two sandblasted titanium alloys treated with two different etching time. The sample treated for 3 hours (**Figure 5.2. A**) exhibits a significantly softer and more regular surface topography compared to the Ti alloy treated for 6 hours (**Figure 5.2. B**), which shows surface with more irregular features in shapes of sharp flakes. This implies that under same pH, NaOH concentration and temperature, a longer time of NaOH surface etching will result in deeper and more defined topographical features.

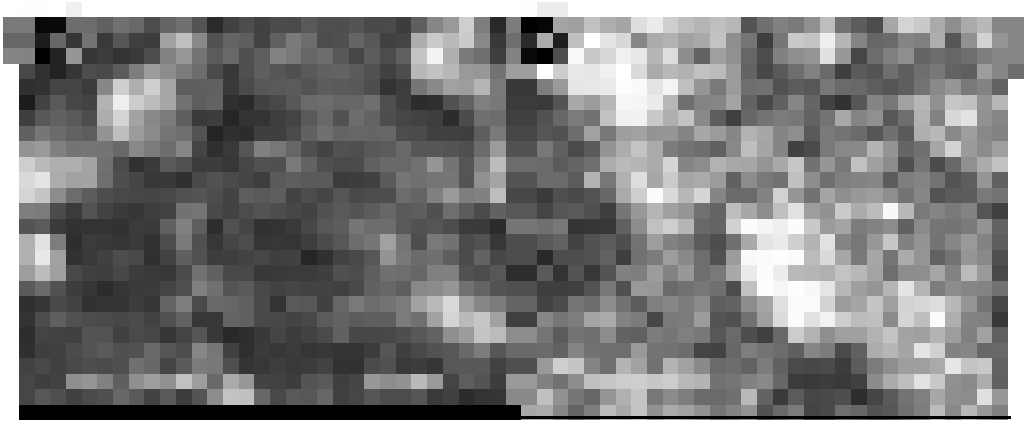

Figure 5.2. Topography of NaOH etched titanium alloys revealed by SEM at a 15000 X magnification. Both samples are sandblasted titanium alloys (Ti-6Al-4V) discs treated for **(A)** 3 hours and **(B)** 6 hours at 180°C with 1M NaOH solution.

Surface etching caused the appearance of flower like islands with star like arms extending radially from the centre. The flowers like islands are in the micron range. The islands increase their size and display sharper features with longer etching treatments.

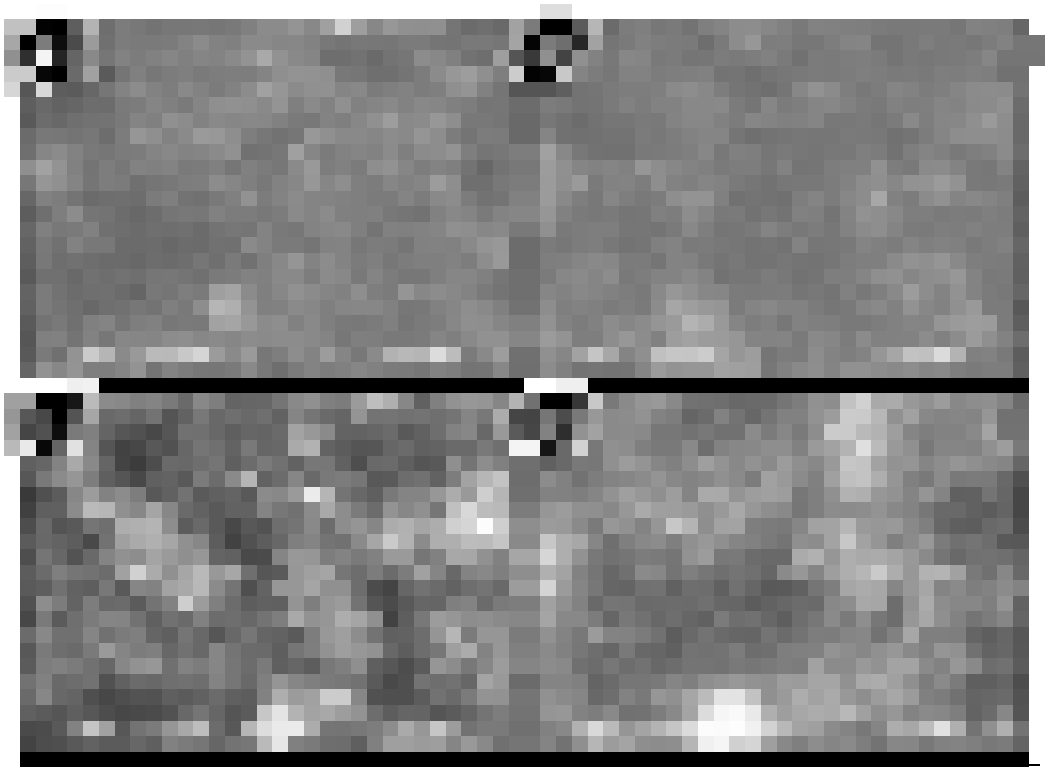

Figure 5.3. SEM images of as received (A and B) and sandblasted (C and D) titanium alloy (Ti-6Al-4V) samples after 3 hours of treatment at 180°C in 1M (**A** and **C**) and 3M (**B** and **D**) NaOH solution, shown at a magnification of 15000x.

Sandblasted and as received titanium alloys are treated at different NaOH concentrations, shown in **Figure 5.3.** The surface of as received alloys is smoother than of the sandblasted for both 1M and 3M NaOH. The surface edges of sandblasted titanium (**Figure 5.3. A** and **C**) are sharp whereas the as received alloys (**Figure 5.3. B** and **D**) display softer edges.

Regarding the effect of the NaOH concentration on titanium topography, the surface of the alloys that are etched with 1 M NaOH is less degraded (**Figure 5.3. A** and **B**) than the surface of the alloys treated with 3 M NaOH. As shown in **Figure 5.3. C** and **D,** treatment with 3 M NaOH resulted in more pronounced and deeper surface features. Since the time of treatment is kept the same for all samples, this draws the conclusion that more concentrated NaOH solution will give a rougher surface with more prominent topographical cues viewed as clear star like features.

In the case of smoother initial morphology, the as received alloys, the features are being more interconnected after the NaOH treatment while the sandblasted alloys result in sharper and more pronounced stars and flower like islands.

5.3.2. Strontium incorporation

Incorporation of strontium in the surface chemical composition is done by immersing the titanium alloys after etching $SrCl_2x6H_2O$ solution. The surface chemistry is than evaluated with XPS.

Figure 5.4. shows the difference in surface chemical compositions before and after treatment with strontium. The spectrum in black represents the surface chemistry of sandblasted titanium alloy that is treated with 3 M NaOH.

We can observe the presence of Na at binding energy of 1071 eV. Then, after the alloy is immersed in strontium solution, this peak completely disappears, as shown in the red

spectra. We can also observe the appearance of new peaks that belong to strontium in the spectra.

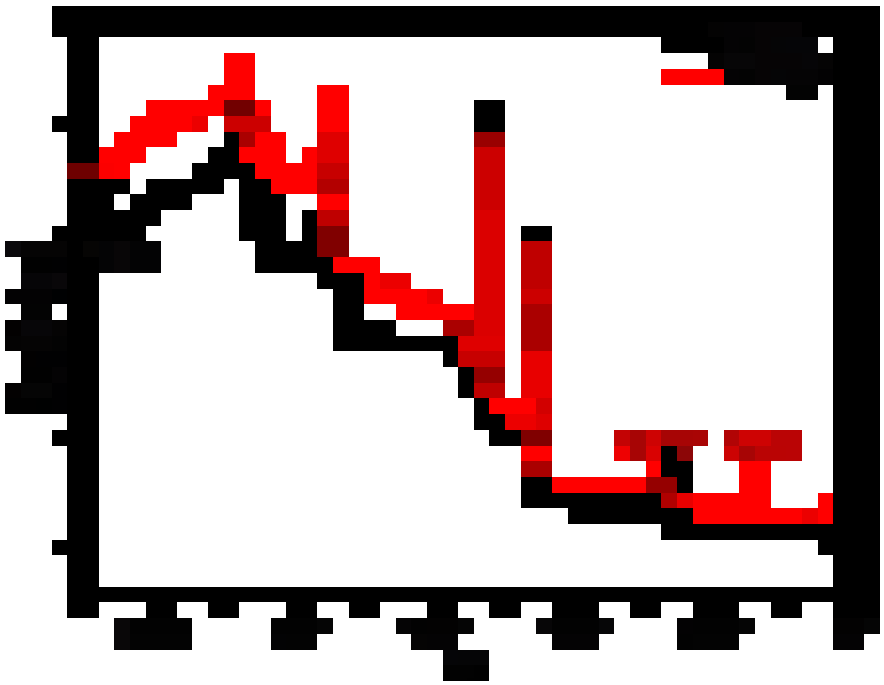

Figure 5.4. XPS Survey scans of sandblasted Ti alloys and modified with 3 M NaOH before (in black) and after (in red) of strontium incorporation.

The fact that the Na signal completely disappears suggests total exchange of sodium by strontium. Strontium 3d 5/3 peak is found at a BE of 138.4 eV and is assigned to strontium oxide, SrO. (17, 18)

A typical high resolution XPS spectrum of strontium core level is shown in **Figure 5.5 A.**

Figure 5.5. B shows a detail scan of the carbon region used for spectral calibration where 3p 3/2 spin orbit couple of strontium partially overlaps with C 1s region. Highest energy

peak at 285 eV correspond to aliphatic carbon, while 266.7 eV and 288.9 eV peaks are assigned to C-O and C=O, respectively.

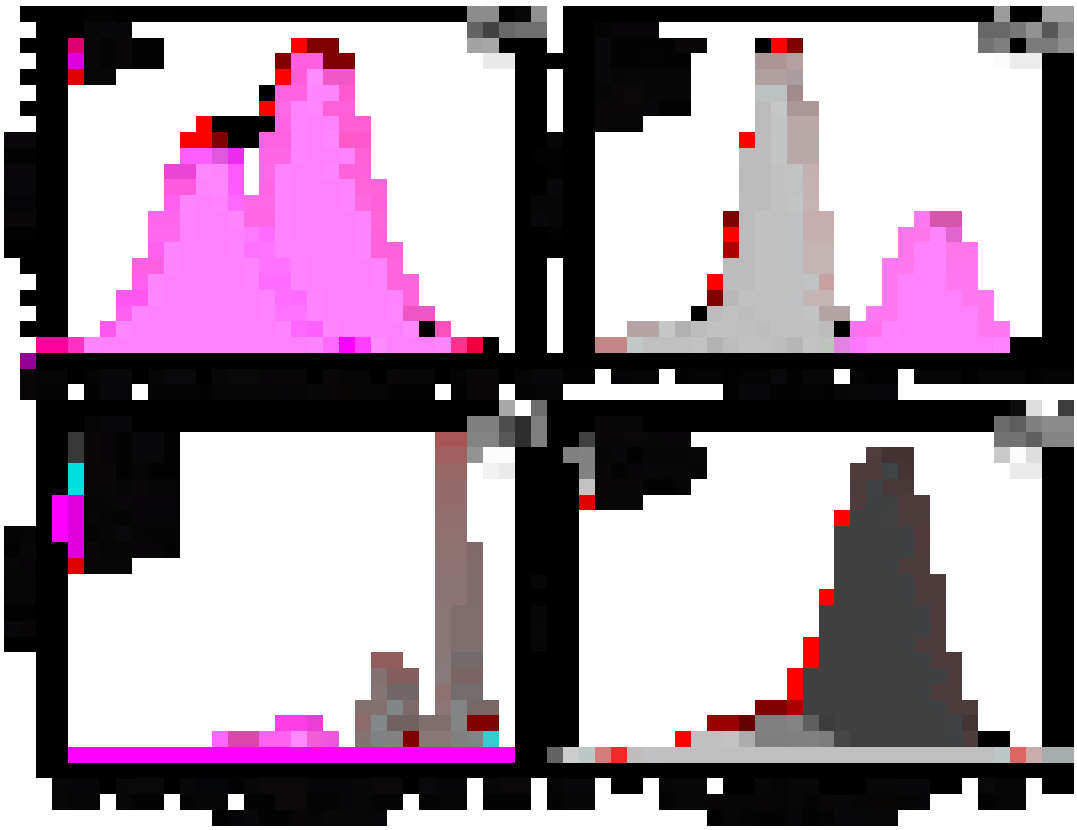

Figure 5.5. Typical XPS detail spectra of core electrons for A strontium, B carbon, C titanium and D oxygen after satellite removal, Shirley background subtraction and calibration of CC/CH to 285 eV. Regions are fitted to components as shown in each figure and assigned according to their binding energies at peak maxima.

In **Figure 5.5. C** the XPS spectra of titanium is shown with assignments to oxides of Ti IV at 458.5 eV and to Ti III at 456.3 eV for their 2p 3/2 spin orbit pairs. The ratio of Ti IV and Ti III is 95/5, typical for the surface of native titania. Oxygen peak in **Figure 5.5. D** is assigned to lattice oxygen at 530.2 eV. C-O and C=O species are found at 531.9 and

533.1 eV, respectively and they are resulting from adventitious carbon. These bonds are also observed in C 1s region. (17-19)

At a core level of strontium, Sr 3d, main peak at 133.4 eV is assigned to SrO. However, in XPS analysis one should take into account spectrophotometer resolution that is in our case 1 eV and we have to consider assignments of +/- 0.5 eV from our main peaks. Given the fact that strontium hydroxide, $Sr(OH)_2x8H_2O$ can also be found at 133.0 eV we have to consider the possibility that some strontium is adsorbed on the surface with water bound molecules. Therefore, we have done a depth profiling of surface with XPS where argon ions are employed to etch the surface so we are allowed to measure its chemistry at different depths and determine the presence of strontium within the profile. A depth profile showing changes in surface chemistry is shown in **Figure 5.6.**

As it can be seen, after the adventitious carbon layer is removed, the relative amount of strontium increases slightly and becomes constant as oxygen and titanium do, confirming the presence of strontium in the deeper parts of surface nanostructures. According to estimations for argon sputtering on our spectrometer, 1 nm layer is removed after 100 seconds of argon etching, what means that at point of 7000 seconds around 70 nm of top surface is removed and we observe presence of strontium.

Figure 5.6. XPS depth profile of sandblasted titanium alloy treated with 3M NaOH and immersed in strontium chloride solution. XPS spectra are taken after continuing argon sputtering at 5 times intervals. The initial point corresponding the to the composition of the surface previous to argon sputtering

The constant presence of oxygen at this depth also implies TiO_2 presence at depths of at least 70 nm thus covering homogeneously nanotopographical features because natively formed titania is taking up to 4 to 7 nm of the surface depth. (20) This shows that etching results in removal of 70 nm from the surface, a thickness 10 times the thickness of the naturally formed titania layer.

Next we have evaluated capacity of alloys with different topography that resulted from treatment with 3 M NaOH to bind strontium. The titanium alloys showed differences in total incorporated strontium regarding their starting structure.

More strontium is bound in rougher, initially sandblasted alloys than into the smoother surface, initial as received alloy as shown in **Figure 5.7.** This is related to the initial morphology, but also to more micro and nanotopographical features formed after the NaOH treatment, as previously revealed by SEM and shown in **Figure 5.3.**

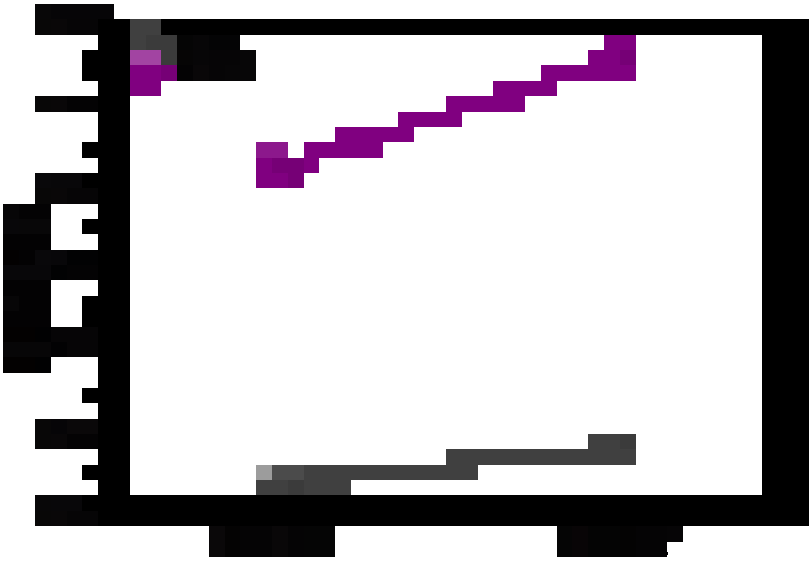

Figure 5.7. Increase of strontium incorporated in 3 M NaOH treated sandblasted alloy in comparison with as received alloy treated with 3 M NaOH as well, expressed as relative ratio to titanium (Ti) and to Oxygen (O).

The influence of the pH of the strontium solution is investigated in relation of the ion exchange capacity between strontium and sodium but also to evaluate how changes in the pH influence surface morphology.

Chemistry and morphology of strontium treated alloys is further investigated by SEM and Energy-dispersive X-ray spectroscopy (EDXS). EDXS is a spectroscopy implemented in SEM microscope and thus enabled us imaging of the topography and quantitative elemental analysis without need to remove the sample from the microscope.

A typical EDX spectrum for strontium treated titanium is shown in **Figure 5.8. A**. **Figure 5.8. B** represents typical EDX spectrum for sample that contains no strontium.

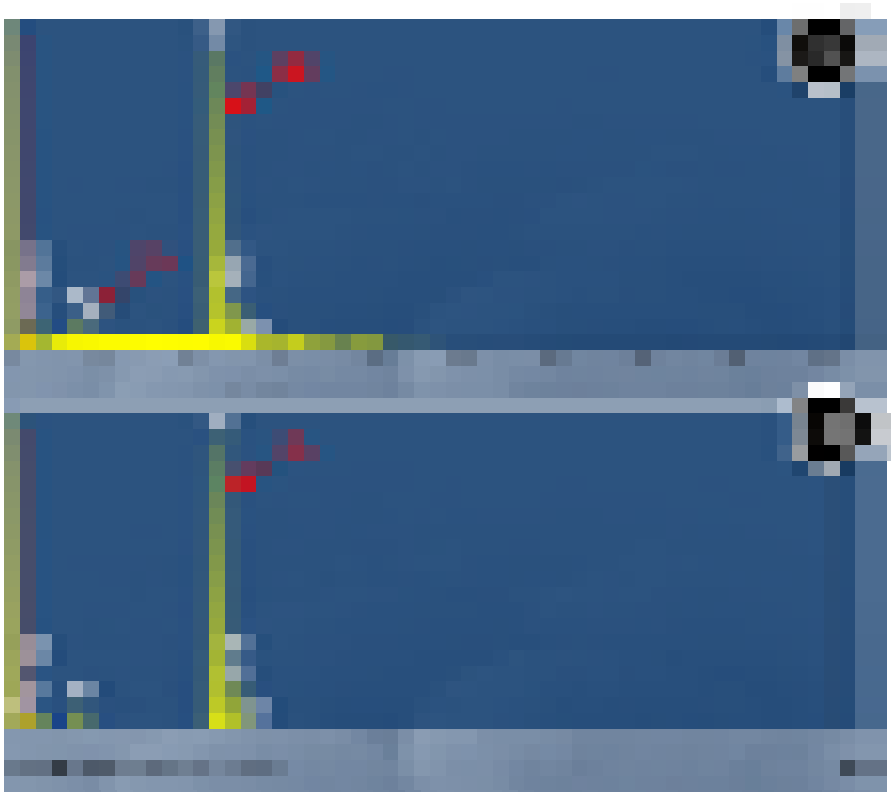

Figure 5.8. Elemental analysis by EDX used for quantification of relative strontium incorporated into the titanium surfaces. In **A** is shown typical EDX spectra with titanium signal at 4.5 keV and strontium signal at 1.8 keV, used for calculation for Ti/Sr. In **B** is a typical spectrum that shows no strontium into the surface chemical composition.

Sandblasted titanium alloys after the alkaline treatment with three molar NaOH are subjected to ion exchange experiments with strontium at a pH 6, 9 and 12. In **Figure 5.9.** are shown four sandblasted titanium alloy surfaces after alkaline treatment and three of them (**Figure 5.9. B**, **C** and **D**) are immersed in 250 mM strontium chloride solution. As revealed by SEM, the pH of the $SrCl_2$ solution has a significant influence on the topography of the samples: an increase in pH results in a rougher surface morphology of alloys and more pronounced surface features, as observed in **Figure 5.9. B, C** and **D,** where samples incubated with $SrCl_2$ adjusted to pH of 6, 9 and 12, respectively are shown.

Star like features cover the surface in all cases, while flower like islands are highly expressed when surfaces are incubated with strontium solution of pH 6 as seen in **Figure 5.9.B.** A higher pH in the strontium solution leads to bigger diameter of islands that are almost completely interconnected at a pH 9, shown in **Figure 5.9.C**. At a pH 12 it is difficult to distinguish between separate islands and the surface is covered with sharp branch like features with spiky characteristics as seen in **Figure 5.9.D**. The smoothest surface presented in **Figure 5.9. A,** corresponds to a control sample treated only with 3 M NaOH but without incubation in strontium chloride.

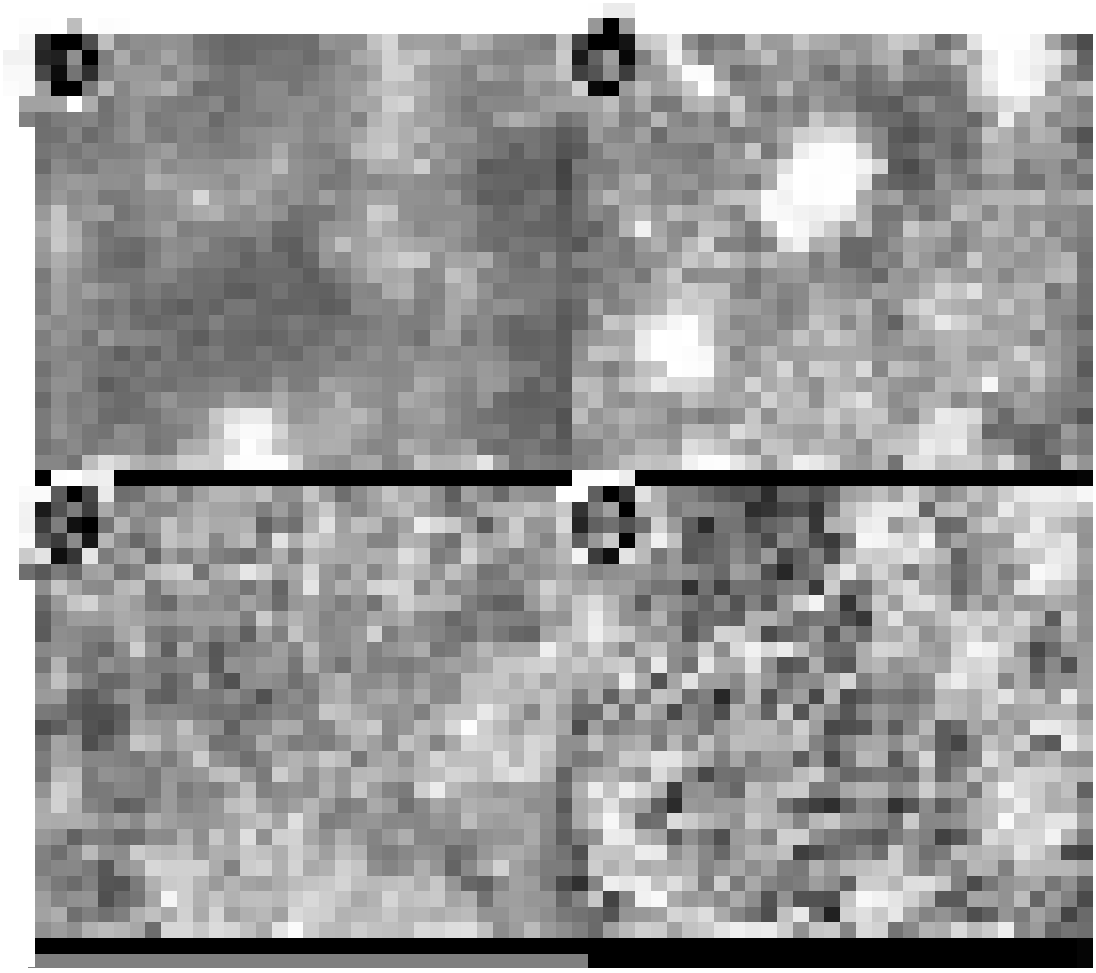

Figure 5.9. 15000 x magnification SEM images of sandblasted titanium alloys after 3 hours of alkaline treatment at 180 °C with 3 M NaOH solution (**A**). Titanium alloys after alkaline treatment immersed in 250 mM $SrCl_2$ solution at different ph values: (**B**) pH 6, (**C**) pH 9 and (**D**) pH 12.

From the examples shown, it is clear that etching of the substrates with NaOH alters the topography in a distinct manner depending on the process parameters. From the obtained results we can conclude that we are able to tailor titanium with desired topographical features by etching to produce topographies that mimic the ECM of the bone by changing the pH, ionic strength of NaOH, as well time of the alkaline treatment.

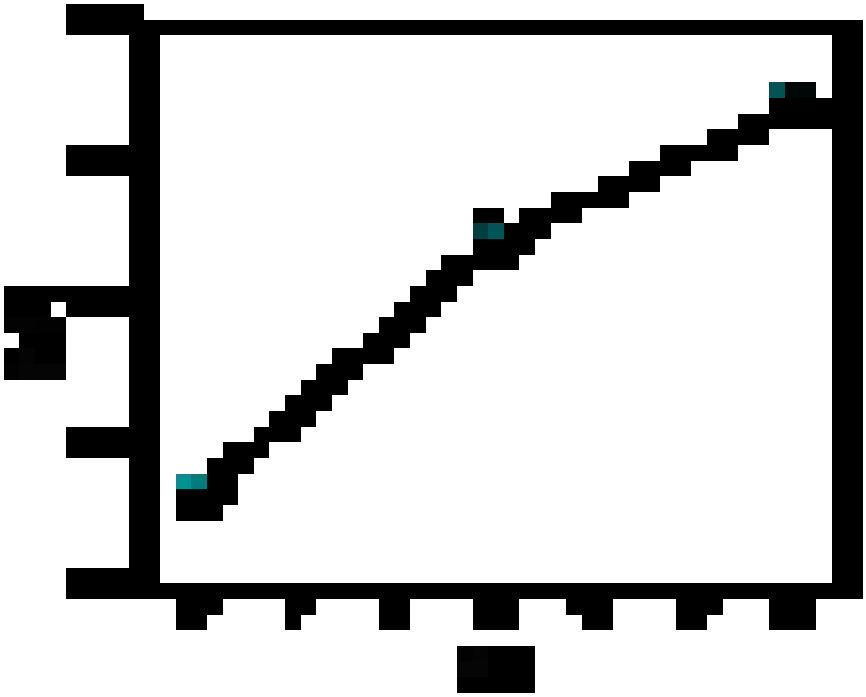

Figure 5.10. Increase in the strontium incorporated into titanium alloy in relation with increase of the $SrCl_2$ solution pH. Relative amount of strontium is expressed as Sr/Ti ratio resulting from EDX experiments.

As shown in **Figure 5.10.**, strontium in the surface of titanium alloy increases linearly with the increase of the pH of the $SrCl_2$ solution. Besides the pH of strontium solution, the time of incubation influences as well the final amount of Sr^{2+} incorporated into the surface chemical composition of titanium alloy as can be seen from **Figure 5.11.**

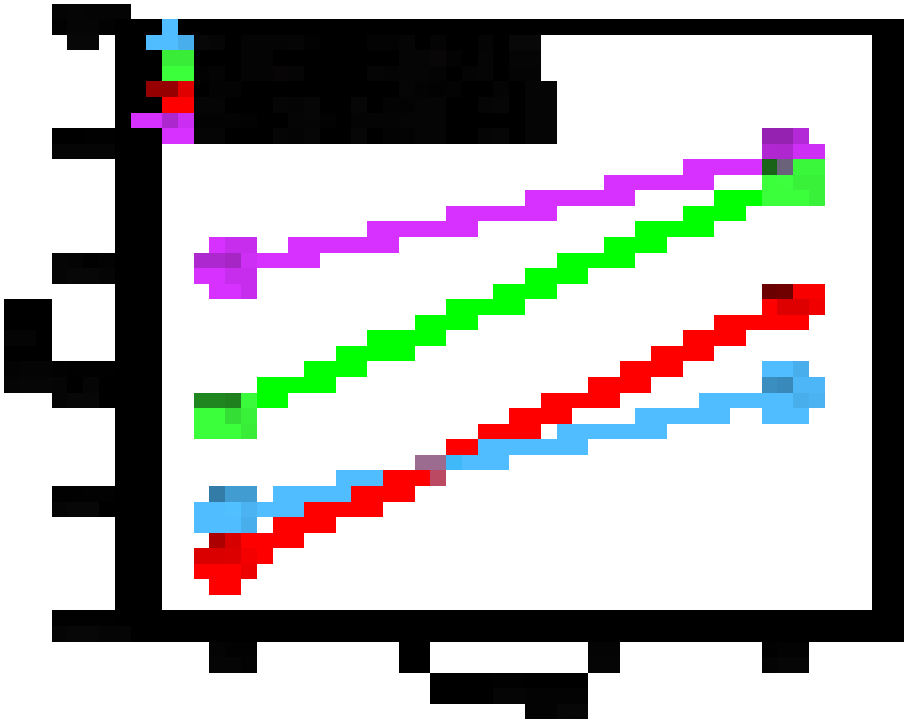

Figure 5.11. Influence of the incubation time with strontium chloride on total Sr incorporated into the as received and sandblasted Ti alloy substrates. pH value of 250 mM $SrCl_2$ solution used for this experiment is adjusted to 12. Relative amount of strontium is expressed as Sr/Ti ratio resulting from EDX experiments

In **Figure 5.11.** it is shown that the time dependent increase of incorporated Sr^{2+} for the alloys treated with a 3 M NaOH is faster in relation to samples treated with 1 M NaOH This means that alloys initially etched with 3 M NaOH have higher capacity for strontium incorporation. This is an outcome of two simultaneous scenarios. First, the alkaline treatment with higher concentration of NaOH will result in a titanium alloy surface containing more Na ions coming from the layer of $NaTiO_3$. Second, a surface with more cavities will provide more of the specific surface for formation of $NaTiO_3$ and thus more regions for ion exchange. This phenomenon also occurs when higher pH value of $SrCl_2$

solution is used for ion exchange of Sr^{2+} and Na^{+}, as shown in **Figure 5.10**. In this case as well we can see that alloys incubated in strontium solution of higher pH will exhibit rougher nano and micro topography, as seen in **Figure 5.9. B, C** and **D.**

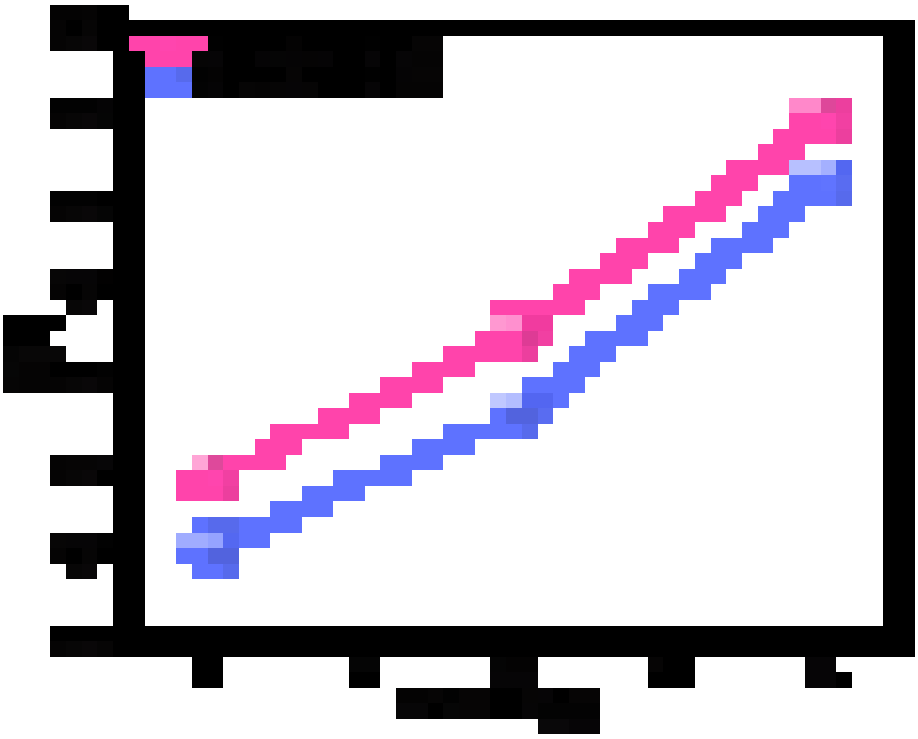

Figure 5.12. Influence of NaOH concentration on final incorporated amount of strontium into the surface of sandblasted and as received titanium alloys. The pH value of 250 mM $SrCl_2$ solution used for this experiment is adjusted to 12

The influence of NaOH concentration used for surface etching on total incorporated strontium is shown in **Figure 5.12.** In case of both, normal and sandblasted alloys, there is an increase in the strontium content with an increase of NaOH concentration following the same trend. The difference between these two is that more strontium is bound to the

sandblasted discs than to normal ones. This confirms the hypothesis that rougher samples will bind more ions since the sandblasted alloys initially present more irregular features on surface.

5.3.3. Biocompatibility and bioactivity

Preosteoblast cells are seeded and cultured on as received and sandblasted titanium alloys and sandblasted titanium alloys. Biocompatibility of the samples is evaluated with cell proliferation on as received and sandblasted titanium alloys that were additionally etched in one and three molar NaOH. Preosteoblast proliferation after 14 days is shown in **Figure 5.13** and as it can be seen no significant difference in proliferation was observed.

Figure 5.13. Proliferation of cells cultured on the Ti alloys samples with and without post-treatment; **A** as-received Ti alloy (1M NaOH), **B** as-received Ti alloy (3M NaOH), **C** as-received Ti alloy, **D** sand-blasted Ti alloy, **Control** cell culture plate.

However, from this data we can conclude that samples treated with sodium hydroxide are possessing good biocompatibility. Therefore, treatment with NaOH did not left toxic effects on the substrates and moreover a slightly increased proliferation is observed for 3 M NaOH treated samples. Experiments conducted with cells in this study are only preliminary, and bioactivity of the surfaces is to be evaluated in more details regarding different nanotopographies. Also we intend to evaluate the effect of the strontium implemented in these substrates on enhanced cell activity.

5.4. Conclusions and perspectives

In this study, a chemical method was utilized to change the surface chemistry and topography of the Ti alloys in order to improve the biological performance of the currently used Ti based implants. Results indicate that the generation of nano and micro structures on Ti alloys can be controlled by the adjustment of the ionic strength of the NaOH solution and the treatment time. To endow the implant with "bioactive" strontium ions in the biological fluid, ion exchange experiments using a strontium- containing buffer solution were done on the modified Ti alloy.

The findings of this study regarding altering the topography and chemistry are as follows; longer time of alkali treatment results in rougher and more irregular topographic features. Treatment with high concentration of NaOH, over 3 M, gives a rougher surface topography. Post treatment ion exchange between Na+ and Sr^{2+} is favored by alkaline pH around 12, which results in higher amount of Sr incorporated in the surface of the modified Ti alloys. An increase in the incubation time of alloys in $SrCl_2$ solution results in increase of incorporated strontium. The morphology of Ti alloys influences as well the final Sr^{2+} in surface; sandblasted Ti alloy has higher capacity for uptaking Sr, as they can react more intensely with NaOH, providing more exposed surface areas for ion exchange. Preliminary data confirm biocompatibility of chemically modified Ti alloys.

To conclude, the aim of this study was to show a way to modify titanium surface and obtain different nanostructures by simply changing basic parameters in chemical etching.

Additionally, we have shown how titanium alloys with more topographical features are able to bind more of strontium due to their larger specific surface

Further work in this project will focus on the detailed biological evaluation of the etched surfaces with osteoblast cells first to conclude which is the most appropriate nanostructure surface for cell adhesion and proliferation. Moreover, the surfaces with implemented strontium will be evaluated on long- term osseointegration by testing the mineralized tissue on the surfaces via calcium and phosphates staining. In conclusion, after the biological evaluation of most suitable implant surface, this work may bring novelty to tissue engineering and implant biomedicine as a cost-effective and efficient method for titanium implant modifications.

List of references

1. Albrektsson T*, et al.* (1983) The interface zone of inorganic implantsIn vivo: Titanium implants in bone. *Annals of Biomedical Engineering* 11(1):1-27.

2. Albrektsson T, Berglundh T, & Lindhe J (2003) Osseointegration: Historic background and current concepts. *Clinical Periodontology and Implant Dentistry, 4th edition* Blackwell Munksgaard, Oxford:809-820.

3. Alla RK*, et al.* (2011) Surface Roughness of Implants: A Review. *Trends in Biomaterials and Artificial Organs* 25(3):112-118.

4. Buser D*, et al.* (1991) Influence of surface characteristics on bone integration of titanium implants. A histomorphometric study in miniature pigs. *Journal of Biomedical Materials Research* 25(7):889-902.

5. Cochran DL (1999) A comparison of endosseous dental implant surfaces. *Journal of Periodontology* 70(12):1523-1539.

6. Gintaras J, Marija S, Ann W, & Tomas B (2007) Titanium Dental Implant Surface Micromorphology Optimization. *Journal of Oral Implantology* 33(4):177-185.

7. Kim HM, Kokubo T, Fujibayashi S, Nishiguchi S, & Nakamura T (2000) Bioactive macroporous titanium surface layer on titanium substrate. *Journal of Biomedical Materials Research* 52(3):553-557.

8. Vercaigne S, Wolke JG, Naert I, & Jansen JA (1998) Bone healing capacity of titanium plasma-sprayed and hydroxylapatite-coated oral implants. *Clinical Oral Implants Research* 9(4):261-271.

9. Harris LG, Meredith DO, Eschbach L, & Richards RG (2007) Staphylococcus aureus adhesion to standard micro-rough and electropolished implant materials. *Journal of Materials Science: Materials in Medicine* 18(6):1151-1156.

11. Wen HB, Liu Q, De Wijn JR, De Groot K, & Cui FZ (1998) Preparation of bioactive microporous titanium surface by a new two-step chemical treatment. *Journal of Materials Science: Materials in Medicine* 9(3):121-128.

12. Marie PJ, Ammann P, Boivin G, & Rey C (2001) Mechanisms of Action and Therapeutic Potential of Strontium in Bone. *Calcified Tissue International* 69(3):121-129.

13. Liu AL-J, Shen P-W, & Chen P-J (2013) Strontium ranelate in fracture healing and joint pain improvement in a rheumatoid arthritis patient. *Clinical Cases in Mineral and Bone Metabolism* 10(3):206-209.

14. Maimoun L*, et al.* (2010) Strontium ranelate improves implant osseointegration. *Bone* 46(5):1436-1441.

15. Wu C, Ramaswamy Y, Kwik D, & Zreiqat H (2007) The effect of strontium incorporation into CaSiO3 ceramics on their physical and biological properties. *Biomaterials* 28(21):3171-3181.

16. Boivin G*, et al.* (1996) Strontium distribution and interactions with bone mineral in monkey iliac bone after strontium salt (S 12911) administration. *Journal of Bone and Mineral Research* 11(9):1302-1311.

17. Moulder JF, Stickle WF, Sobol PE, & Bomben K (1992) *Handbook of X-ray Photoelectron Spectroscop 2nd ed* (Physical Electronics USA, Inc.) 2nd Ed.

18. Wagner CD*, et al.* (2003) NIST Standard Reference Database 20, Version 3.4 (web version) (http:/srdata.nist.gov/xps/).

19. Young V & Otagawa T (1985) XPS studies on strontium compounds. *Applications of Surface Science* 20(3):228-248.

20. Textor M, Sittig C, Frauchiger V, Tosatti S, & Brunette D (2001) Properties and Biological Significance of Natural Oxide Films on Titanium and Its Alloys. *Titanium in Medicine,* Engineering Materials, (Springer Berlin Heidelberg), pp 171-230.

Summary and conclusions of the thesis

Titanium, a material with excellent biocompatibility and widely used as dental or orthopaedic implant, displays on average a poor osseointegration with the forming bones. This is mainly a result of the suboptimal surface properties of titanium since the bone- implant binding occurs at the implant surface.

Work in this PhD thesis presented four different approaches to endow the surface titanium with characteristics that led to the advanced surface bioactivity and resulted in an enhancement of the cellular functions of osteoblast.

In the work presented in the second chapter of the thesis, niobium (Nb) is incorporated into carbon films with the goal to enhance the bioactivity of the bionert carbon coatings for titanium based orthopedic implants. Carbon coatings displayed a relatively smooth morphology but with addition of Nb surface roughness increases. Simultaneously, Nb-doped carbon films have increased mechanical properties in respect to carbon film. *In vitro* experiments with pre-osteoblast cells show that on Nb- carbon coatings cells exhibit better focal adhesion and a better alkaline phosphatase expression, which are both important regulators in cellular differentiation, migration and mineralization processes.

Chapter three described an approach to develop stabile collagen- alginate biopolymer coatings on titania. Upon crosslinking this multilayer system matches mechanical and topographical properties of the extracellular matrix regarding Young's modulus and topographic features, displaying a fibrilar structure. Due to presence of collagen, the

coating mimics the natural environment of osteoblast cells. These coatings showed high stability in cell culture medium and improved bioactivity compared to non coated TiO_2 surfaces. A superior bioactivity and mineralization potential is observed when the multilayer terminates with an alginate layer, in terms of osteoblast adhesion and expression of early stage mineralization marker, alkaline phosphatase.

The study on the strontium complexed in polyacrylic acid (PAA) brushes presented in the fourth chapter of this thesis proved a remarkable positive effect of Sr^{+2} on the osteoblast cells. This approach has the potential to overcome the drawbacks of strontium oral intake by controlling Sr^{+2} concentration and restricting the presence of the ion to the titania surface since the Sr^{+2} will be encapsulated in the PAA brush. Denser brushes with more polymer chains provide a larger number of carboxylic groups for strontium binding. Strontium concentration can be regulated trough the brush density increasing as well the rate of the bone tissue mineralization. Dense brushes with high concentration of entrapped Sr^{+2} display superior osseoactivity compared to the bare titana.

The findings in the study presented in chapter five of this thesis described a cost effective and elegant method for altering the topography and chemistry of titanium by use of alkaline etching. Nano and micro features are dependent on the time of alkaline processing as well as the concentration of NaOH. By increasing these two factors, the number and extent of the topographical cues displaying topography of flower or star like islands increase. These nanostructured surfaces are capable to bind strontium trough ion exchange with the Na^+ present in the $Na_2Ti_6O_{13}$ produced by the etching where additionally increase in pH value of strontium solution increases the number of surface

features. The exchange of Na^{+} by Sr^{+2} is favored by using slightly basic pH. The amount of total incorporated strontium largely depends on the surface morphology, with rougher surfaces offering more active sites for strontium binding.

List of Publications

2016

22. Xiang Liu, Joseba Irigoyen, **Danijela Gregurec**, Sergio Moya, Roberto Ciganda, Changlong Wang, Maria Echeverria, Philippe Hermange, Jaime Ruiz, Didier Astruc, *Precise Localization of Cu, Ag and Au Nanoparticles in Dendrimer Nanosnakes or Inner Periphery and Consequences in Catalysis*, Manuscript in preparation

21. Eleftheria Diamanti, **Danijela Gregurec**, María José Rodríguez-Presa, Claudio Gervasi, Omar Azzaroni, Sergio E. Moya, *Electrochemical characterization of a lipid bilayer supported on polyelectrolyte multilayers*, Manuscript in preparation

20. Guocheng Wang, **Danjela Gregurec**, Elena Rojas, Luis Yate, Sergio E. Moya**,** *Strontium implementation in nanostructured titanium alloys (Ti-6Al-V) for enhanced biological performance*, Manuscript in preparation

19. Danijela Gregurec, Nikolaos Politakos, Tanja Luedtke, Luis Yate, Marija Kosutic, Sergio E. Moya; *Superior osseo- activity on TiO_2 via polyacrylic acid brush- strontium system*, Manuscrtipt in preparation

18. Danijela Gregurec, Luis Vazquez, Sergio Moya, Fernando Lopez Gallego; *Force spectroscopy predicts thermal stability of immobilized proteins by measuring single-particle mechanics*, Submitted to Proceedings of the National American of Sciences (2016)

17. Nicolas Muzzio, **Danijela Gregurec**, Eleftheria Diamanti, Joseba Irigoyen, Miguel Pasquale, Omar Azzaroni, Sergio E. Moya; *Thermal Annealing of Polyelectrolyte Multilayers: a New Approach for the Enhancement of Cell Adhesion*, Submitted to Advanced Materials Interfaces (2016)

16. Roberto Ciganda, Ricardo Hernández,, Changlong Wang, Joseba Irigoyen, **Danijela Gregurec**, Sergio Moya, Jaime Ruiz, Didier Astruc; *From ferocenes to caralytically active gold nanoparticles*, Submitted to Angewandte Chemie International Edition (2016)

15. Danijela Gregurec, Guocheng Wang, Ricardo H. Pires, Marija Kosutic, Tanja Luedtke, Mihaela Delcea, Sergio E. Moya; *Bio inspired titanium coatings: Self-assembly of collagen- alginate films for enhanced osseointegration*, Journal of Materials Chemistry B (2016), DOI: 10.1039/C6TB00204H

14. Diamanti Eleftheria, Nicolas Muzzio, **Danijela Gregurec**, Joseba Irigoyen, Miquel Pasquale, Omar Azzaroni, Sergio Enrique Moya; *Impact of thermal annealing on wettability and antifouling characteristics of alginate poly – L – lysine polyelectrolyte multilayer films*, Submitted to Colloids and Surfaces B: Biointerfaces (2016)

13. Changlong Wang, Roberto Ciganda, Lionel Salmon, **Danijela Gregurec**, Joseba Iriroyen, Sergio Enrique Moya, Jaime Ruiz, Didier Astruc; *Extremely efficient transition metal nanoparticle catalysts in aqueous solutions*, Angewandte Chemie International Edition (2016), DOI: 10.1002/anie.201511305R1

2015

12. Nicolas Muzzio, Miquel Pasquale, **Danijela Gregurec**, Diamanti Eleftheria, Marija Kosutic, Omar Azzaroni, Sergio Moya; *Polyelectrolytes Multilayers to Modulate Cell Adhesion: A Study of the Influence of Film Composition and Polyelectrolyte Interdigitation on the Adhesion of the A549 Cell Line***,** Macromolecular Bioscience, (2015), DOI: 10.1002/mabi.201500275 **(cover)**

11. Haibin Gu, Roberto Ciganda, Patricia Castel, Amélie Vax, **Danijela Gregurec**, Joseba Irigoyen, Sergio Enrique Moya, Lionel Salmon, Pengxian Zhao, Jaime Ruiz, Ricardo Hernandez, Didier Astruc; *Redox-Robust Pentamethylferrocene Polymers and Supramolecular Polymers, and Controlled Self-Assembly of Pentamethylferricenium Polymer-Embedded Ag, AgI, and Au Nanoparticles*, Chemistry-A European Journal, (2015), 21 (50), pp 18177-18186

10. Waldemar A Marmisollé, **Danijela Gregurec,** Sergio Enrique Moya, and Omar Azzaroni; *Pendant amino polyanilines as tunable electrochemically active polymers at neutral pH*, Chemelectrochem (2015), 2 (12), pp 2011-2019

9. Marcus Levin, Elena Rojas, Esa Vanhala, Minnamari Vippola, Biase Liguor, Kirsten I Kling, Ismo K Koponen, Kristian Mølhave, Timo Tuomi, **Danijela Gregurec,** Sergio Enrique Moya, Keld A Jensen; *Influence of Relative Humidity and Physical Load During Storage on Dustiness of Inorganic Nanomaterials – Implications for Testing and Risk Assessment*, Journal of Nanoparticle Research (2015), 17 (8), pp 1-13

8. Eleftheria Diamanti, Luis Cuellar**, Danijela Gregurec**, Sergio Enrique Moya, Edwin Donath; *Role of Hydrogen Bonding and Polyanion Composition in the Formation of Lipid Bilayers on Top of Polyelectrolyte Multilayers*, Langmuir (2015), 31(31), pp 8623-8632

7. Eleftheria Diamanti, **Danijela Gregurec**, Gabriela Romero, Luis Cuellar, Edwin Donath, Sergio Enrique Moya; *Lipid Layers on Polyelectrolyte Multilayers: Understanding Lipid – Polyelectrolyte Interactions and Applications on the Surface*

Engineering of Nanomaterials, Accepted, Journal of Nanoscience and Nanotechnology (2015)

6. Waldemar A Marmisollé, Joseba Irigoyen, **Danijela Gregurec**, Sergio Enrique Moya and Omar Azzaroni; *Bioinspired supramolecular surface chemistry: Substrate-independent, phosphate-driven growth of polyamine-based multifunctional thin films;* Advanced Functional Materials, 2015, 25 (26), pp 4144-4152

5. Guocheng Wang, Sergio Enrique Moya, ZuFu Lu, **Danijela Gregurec,** Hala Zreiqat; *Enhancing orthopedic implant bioactivity: refining the nanotopography*; Nanomedicine (London), 2015, 10 (8), pp 1327-1341

4. Yuan Qiu, Elena Rojas,Richard A. Murray, Joseba Irigoyen, **Danijela Gregurec**, Pablo Castro-Hartman, Jana Fleddermann, Irina Estrela-Lopis, Edwin Donath, Sergio E. Moya; *Cell Uptake, Intracellular Distribution, Fate and Reactive Oxygen Species Generation of Polymer Brush Engineered CeO2-x NPs*; Nanoscale, 2015, 7, pp 6588–6598

3. Luis Yate, Luis Emerson Coy, **Danijela Gregurec,** Willian Aperador, Sergio Enrique Moya, Guocheng Wang; *Nb-C nanocomposite films with enhanced biocompatibility and mechanical properties for hard-tissue implant applications*; ACS Applied Materials & Interfaces, 2015, 7 (11), pp 6351–6358

2. Danijela Gregurec, Mateusz Olszyna, Nikolaos Politakos, Luis Yate, Lars Dahne, Sergio Enrique Moya; *Stability of polyelectrolyte multilayers in oxidizing media: a critical issue for the development of multilayer based membranes for nanofiltration*; Colloid and Polymer Science, 2015, 293, (2), pp 381-388

2013

1. Ling Zhu, **Danijela Gregurec**, Ilya Reviakine*; Nanoscale Departures: Excess Lipid Leaving the Surface during Supported Lipid Bilayer Formation*; *Langmuir*, 2013, 29 (49), pp 15283–15292